NTNU
Norwegian University of
Science and Technology

Battery Management System for a low-cost ROV

Knut Amund Knutsen
Gulsvik

Marine Technology
Submission date: June 2017
Supervisor: Roger Skjetne, IMT
Co-supervisor: Hans-Martin Heyn, IMT

Norwegian University of Science and Technology
Department of Marine Technology

Battery Management System for low-cost ROV application
Knut Amund Gulsvik

Supervisor:	Roger Skjetne, NTNU, Institute of Marine Technology
Co-advisor:	Hans-Martin Heyn, NTNU, Institute of Marine Technology
	Andreas Viggen Henriksen, BluEye Robotics AS
	Borja Serra, BluEye Robotics AS

Master's Thesis 2017
Department of Marine Technology
Norwegian University of Science and Technology
Otto Nielsens veg 10, Marinteknisk senter
Telephone +47 464 15 000

Typeset in LaTeX
Printed by NTNU Trykk
Trondheim, Norway 2017

NTNU Trondheim
Norwegian University of Science and Technology
Department of Marine Technology

MSC THESIS DESCRIPTION SHEET

Name of the candidate: Gulsvik, Knut Amund Knutsen
Field of study: Marine control engineering
Thesis title (Norwegian): Batteristyringssystem for lavkost ROV
Thesis title (English): Battery management control system for low-cost ROV

Background

Li-ion batteries have become the standard battery technology within a wide variety of applications, such as mobile equipment, electric vehicles, spacecraft power systems, and drones. This is due to its superior energy density, low self-discharge as well as close to no memory effect (aging).

However, Li-ion batteries need to be managed properly to ensure safety both for personal and equipment. Therefore, a robust and precise battery management system (BMS) is necessary to make sure that the battery does not operate outside of its Safe Operating Area.
Current, voltage, temperature, and pressure during charge/discharge are all parameters that are important to monitor. From these measurements, different techniques can be used to obtain useful information for the user, such as State of Health (SoH), State of Charge (SoC), etc. These techniques have different advantages and limitations in terms of operation, battery type, robustness, cost, etc.
However, there are no way of online measuring the SoC or SoH directly, and several challenges arises trying to obtain these important parameters:

- How to obtain a feasible model of the battery, which sufficiently represents battery dynamics for a variety of operating conditions.
- How to estimate the SoC, SoH, and other parameters based on measurements in a robust way. Inherent nonlinear phenomena in the batteries, sensor noise, sensor bias, aging, temperature, discharge rate, and SoC level all affect the battery response, and it is therefore important that the model/observer combination is representable for the most important factors.
- There is usually a trade-off between complexity, robustness, cost, and computational power. Finding the right combination between the vehicle operations and the power/energy needs is thus crucial.

Work description

1. Perform a background and literature review to provide information and relevant references on:
    - Relevant battery technologies.
    - Typical BMS functions for battery-powered vehicles. Clarify terms such as SoC, SoH, SoP, etc.
    - Battery models relevant for SoH and SoC estimation.
    - Estimator schemes for SoH, SoC, and SoP state parameters.

   Write a list with abbreviations and definitions of terms, explaining relevant concepts of the thesis.

2. Investigate ROV operations and related power/current/voltage profiles:
    - Identify requirements for battery management system for the ROV.

3. Conclude on a sufficiently detailed battery model based on requirements. Perform parameter estimation and verification of the identified model through simulation studies.

4. Identify a suitable SoC estimator method/algorithm. Perform verification and sensitivity analysis through simulations. Consider and discuss the need for sensor fault detection and handling of inaccurate/biased measurements.

5. Discuss how a SoH estimator theoretically and practically could be implemented for the BlueEye's ROV.

6. Conclude on a SoP estimation scheme and implement it. Explore the possibility of using SoP as a means for gradual load-shedding.

Tentatively:

7. Consider any other smart features, e.g. remaining battery time.

Specifications

The scope of work may prove to be larger than initially anticipated. By the approval from the supervisor, described topics may be deleted or reduced in extent without consequences with regard to grading.

The candidate shall present personal contribution to the resolution of problems within the scope of work. Theories and conclusions should be based on mathematical derivations and logic reasoning identifying the various steps in the deduction.

The report shall be organized in a logical structure to give a clear exposition of background, results, assessments, and conclusions. The text should be brief and to the point, with a clear language. Rigorous mathematical deductions and illustrating figures are preferred over lengthy textual descriptions. The report shall have font size 11 pts. It shall be written in English (preferably US) and contain the following elements: Title page, abstract, acknowledgements, thesis specification, list of symbols and acronyms, table of contents, introduction with objective, background, and scope and delimitations, main body with problem formulations, derivations/developments and results, conclusions with recommendations for further work, references, and optional appendices. All figures, tables, and equations shall be numerated. The original contribution of the candidate and material taken from other sources shall be clearly identified. Work from other sources shall be properly acknowledged using quotations and a Harvard citation style (e.g. *natbib* Latex package). The work is expected to be conducted in an honest and ethical manner, without any sort of plagiarism and misconduct. Such practice is taken very seriously by the university and will have consequences. NTNU can use the results freely in research and teaching by proper referencing, unless otherwise agreed upon.

The thesis shall be submitted with a printed and electronic copy to the main supervisor, with the printed copy signed by the candidate. The final revised version of this thesis description must be included. The report must be submitted according to NTNU procedures. Computer code, pictures, videos, data series, and a PDF version of the report shall be included electronically with all submitted versions.

Start date: 15 January, 2017 **Due date:** As specified by the administration.

Supervisor: Roger Skjetne
Co-advisor(s): Hans-Martin Heyn, Andreas Viggen Henriksen and Borja Serra (BluEye)

Trondheim,

Roger Skjetne
Supervisor

Preface

The thesis ”Battery management system for low-cost ROV-application” is written as to fulfill my graduation requirements for my master degree in the study of Marine Controls at the Norwegian University of Science and Technology (NTNU). The study was performed during the spring of 2017 from January to June. The project was undertaken by request of BluEye Robotics who desired to investigate the possibility of having more control of all the parts constituting their product, and thereof also the battery management system. To further enhance the user experience and to provide the user with a even more streamlined experience, the possibility of incorporating smart and user-friendly functionalities has been taken into considiration.

I did not have any prior knowledge on battery management systems nor batteries. To get insights into this new field and to use my acquired knowledge of Marine Controls in a new way has been very exciting. Some problems such as lack of proper battery testing facilities and malfunctions of the ROV has been challenging. However, overall, it ha been a great experience.

I would like to thank my supervisor Roger Skjetne for guiding me through my master thesis. A special gratitude goes to my co-supervisor Hans-Martin Heyn, who has showed great knowledge on the topic. Lastly, I would like to thank Joachim Arntzen, Andreas Viggen and the rest of the BluEye Robotics team for contributing with insight on how the ROV operates, facilitate test runs for data gathering and debugging of hardware/software of the drones.

Knut Amund Gulsvik, Trondheim, June 2017

Acknowledgements

I would like to thank my supervisor Roger Skjetne for guiding me through my master thesis. A special gratitude goes to my co-supervisor Hans-Martin Heyn, who has showed great knowledge on the topic. I would also like to thank Joachim Arntzen, Andreas Viggen and the rest of the BluEye Robotics team for contributing with insight on how the ROV operates, facilitate test runs for data gathering and debugging of hardware/software of the drones. Lastly, I would like to thank my sisters Kaia Gulsvik and Guro Gulsvik for being a great help with the correction of typographical errors.

Abstract

A combination of advanced State-of-charge (SoC), State-of-Health (SoH) and State-of-Power (SoP) estimation techniques have been combined into a novel scheme to ensure safe and efficient operation of a battery pack.

A battery model was chosen based on literature review and identified requirements for a BMS for a remotely-operated-vehicle (ROV) application. This revealed that a 2RC equivalent-electric-circuit (EEC) model provides the required level of accuracy, complexity of implementation and computational cost. Laboratory experiments where performed on a fresh cell in order to extract the parameters of the model. The relationship between open-circuit-voltage (OCV) and SoC was found by curve-fitting a custom function to the voltage data and measured SoC. A highly accurate OCV-SoC function $v_{oc}(soc)$ is found to be crucial to ensure converge to correct SoC and open-circuit voltage, as it is the foundation of the model. The RC parameters β is found through nonlinear greybox modelling using the Levenberg-Marquard algorithm. The model has problems fitting the data to 1RC model, so an extra RC-cicrcuit was added. The estimation results showed the parameters expected dependency on SoC. The effect of including this dependency and thereof also complexity was however not found necessary as the RMSE of output voltage only decreased $\approx$ 3.2mV.

The obtained battery model with the respective parameters showed good performance for cell measurement data obtained in the lab experiments. In order to maintain this performance for different operating conditions, a comparative study on different versions of Joint Extended Kalman Filters (JEKF) was performed.

All of the proposed JEKF's performed well in terms of SoC estimation, even for biased current measurements, decreasing total capacity and noise voltage measurements. For SoH estimation through total capacity estimation, a seperate Kalman filter running only at the end of a discharge cycle is suggested. Since total capacity is such a slowly varying process, there is no reason to estimate it every second.

A novel approach of using SoP as a model-predictive control law saturating maximum power of the battery has been explored. While the accuracy of the SoP estimates are not validated, the concept shows great potential and should be implemented regardless of the choice of SoC/SoH observer.

Keywords: ROV, BMS, Joint Extended Kalman Filter (JEKF), State-of-Charge (SoC), State-of-Health (SoH), State-of-Power (SoP)

Sammendrag

En kombinasjon av avanserte metoder for å finne tilgjengelig kapasitet (SoC), tilgjengelig effekt (SoP) og den overordnede helsetilstanden til et batteri(SoH) har blitt kombinert på en innovativ måte for å tilse trygg og effektiv bruk av et batteri.

Et litteraturstudie på relevante batterimodeler har blitt utført. Fra dette ble det funnet at en 2RC ekvivalent-elektrisk krets-model (EEC) ville gi den ønskede kombinasjon av presisjon, kompleksitet og nødvendig prososorkraft. Celletesting av nye battericeller har blitt utført for å finne parameterne til denne modellen. Forholdet mellom åpen kretspenning (OCV) og SoC ble funnet ved å tilpasse strøm og spenningsdata til en egendefinert åpen kretspenningsfunksjon V_{oc}(soc). Det ble funnet at det er høyst nødvendig at denne funksjonen er nøyaktig for å sikre konvergens av terminal spenning og ladningstilstands-estimat. Parameterne i ECC modellen ble funnet ved hjelp av en ulineaær minste kvadrats metode. Algoritmen hadde problemer med å tilpasse måledataene til en 1RC krets, så et ekstra RC krets ble lagt til. Parameternes avhengighet av ladningstilstand ble eksludert grunnet at avhengigheten hadde liten effekt på nøyaktigheten til modellen. RMSE for terminalspenning med måledataene gitt fra celletesting var 17.8mV.

Batterimodellen med de respektive parameterne viste generelt gode resultater for ideelle forhold. For å opprettholde denne nøyaktigheten for ulike operasjonstilstander ble forskjellige typer Kalman Filtere testet. Kombinert parameter- og tilstands estimering gjorde at modellen kan tilpasse seg den endrede dynamikken i batteriet.

Alle filterene viste god nøyaktighet i estimering av SoC, selv for støy i spenningsmålinger, bias i strømmålinger og en minskene total kapasitet. Kapasitetsestimatene ble brukt som en mål på helsetilstanden til batteriet. Det ble funnet at seperasjon av kapasitetsestimering er ønskelig slik at kapasitet bare blir oppdatert ved slutten av en ladningssyklus. Dette begrunnes i at endring i kapasitet er en svært langsom prosess, samt at det er en parameter som er lite observerbar gjennom spenningsmålinger.

En ny måte å bruke SoP estimatene for å be om gradvis reduksjon av effekten fra thrusterne har også blitt testet ut. Nøyaktigheten av disse estimatene har ikke blitt validert, men konseptet viste stort potensiale og burde bli vurdert implementert uavhengig av SoC/SoH estimator.

Contents

List of Figures

List of Tables

Abbreviations

Anode Electrode inside a cell which delivers electrons through external electric circuit to the cathode, upon disharge.

Balanced The state of a battery in which all the cells are at the same state of charge.

Battery A collection of cells in series.

Battery pack A collection of batteries coupled in series.

BEV Battery Electric Vehicle (fully electric power system)

BMS Battery Management System: A device or system whose purpose is to monitor, control, and/or optimize a battery.

Cathode Electrode inside a cell which recieves electrons through external electric circuit from the anode, upon disharge.

Cell The most basic element of a battery.

Current The flow of electrons through a conductor [A].

Cutoff voltage Upper or lower limit of voltage of which the cell should not be charged/discharged specified by manufacture.

C-rate A measure of the current going in or out of the battery. A battery charged/disharged from empty/full with 1c would be full/empty in 1 hour.

ECM Electro-chemical model: A more advanced battery model to capture voltage response by modeling physical process inside of each cell.

Electrolyte The chemical between the cell's electrodes.

HEV Hybrid-Electric vehicle

Leakage Current inside a cell that depletes it charge.

PCM Parallel-cell-module.

OCV Open circuit voltage: Voltage of a relaxed cell.

Resistance A measure of device inability of carrying current (R=V/I).

ROA Recommended Operating Area: A set of voltage and temperature limits of which the current is limited when these conditions are met.

SOA Safe Operating Area: A set of voltage, current and temperature values of which the battery can operate safely.

SOC State of Charge: Proportion of the charge in a cell or a battery, compared to its nominal capacity [%].

SOH State of Health: Arbitrary measure of a battery's condition with respect to its nominal condition[%].

SOP State of Power: An estimate of how quickly one can add or remove energy from a pack without violating design constraints.

Thermal runaway A self-accelerating cycle that results in high temperature or possible fire or exploitation.

Thevinin model A special electric equivalent model that consist of one resistor and one parallel RC-network.

Total capacity Quantity of charge removed from a cell as it is brought from fully charged state to fully discharged.

Unbalanced State of a battery in which the cells are not all at the same state of charge.

1

Introduction

1.0.1 Thesis motivation

Lithium-ion batteries have become the standard battery technology within a wide variety of applications, such as mobile equipment, electric vehicles, spacecraft power systems, and drones. This is due to its superior energy density, low self-discharge as well as close to no memory effect (aging).

However, lithium-ion batteries (LIB) need to be managed properly to ensure safety both for personal and equipment. Therefore, a robust and precise battery management system (BMS) is necessary to make sure that the battery is not abused. Current, voltage, and temperature during charge/discharge are all parameters that are important to monitor. From these measurements, different techniques can be used to obtain useful information for the user, such as State of Health (SoH), State of Charge (SoC) and State of Power (SoP). These techniques have different advantages and limitations in terms of operation, battery type, robustness, costs, etc.

SoC, SoH and SoP can not be measured directly, and several challenges arises trying to obtain these important parameters:

- How to obtain a feasible battery model which represents battery dynamics for a variety of operating conditions.
- How to estimate the SoC, SoH, SoP and other parameters based on measurements in a robust way. Inherent nonlinear phenomena in the batteries, sensor noise, sensor bias, aging, temperature, discharge rate, and SoC level, all affect the battery states, and it is therefore important that the combination of model and/or observer can accurately describe the states of the system.

There is usually a trade-off between complexity, robustness, cost, and computational power. Finding the right combination between the vehicle operations and the power/energy needs is thus essential, especially for low-cost application such as an ROV.

This thesis combines start-of-the-art methods for SoC, SoH, and SoP estimation. A novel approach of using SoP estimates for gradual load-shedding is also proposed.

1.0.2 Thesis Scope and Objectives

1. Perform a background and literature review to provide information and relevant references on:
    - Relevant battery technologies.
    - Typical BMS functions for battery-powered vehicles. Clarify terms such as SoC, SoH, SoP, etc.
    - Battery models relevant for SoH and SoC estimation.
    - Estimator schemes for SoH, SoC, and SoP state parameters.
    - Write a list with abbreviations and definitions of terms, explaining relevant concepts of the thesis.
2. Investigate ROV operations and related power/current/voltage profiles:
    - Identify requirements for battery management system for the ROV.
3. Conclude on a sufficiently detailed battery model based on requirements. Perform parameter estimation and verification of the identified model through simulation studies.
4. Identify a suitable SoC estimator method/algorithm. Perform verification and sensitivity analysis through simulations. Consider and discuss the need for sensor fault detection and handling of inaccurate/biased measurements.
5. Discuss how a SoH estimator theoretically and practically could be implemented for the BlueEye's ROV.
6. Conclude on a SoP estimation scheme and implement it. Explore the possibility of using SoP as a means for gradual load-shedding.

1.0.3 Thesis Organization

The structure of the thesis is as follows:

- **Chapter 2 Battery technologies**: Basic understanding of a battery, the operation of a battery cell, definition of relevant expressions and specifications for the battery onboard the ROV.
- **Chapter 3 The ROV**: Identification of the operational profile for the ROV with respect to current, voltage and temperatures.
- **Chapter 4 BMS**: Discussion of general BMS design and requirements for a BMS onboard the ROV.
- **Chapter 5 Battery models**: A literature review of relevant battery models and identification of suitable battery model. Parameter estimation, simulation and verification of the 2RC EEC model.
- **Chapter 6 SoC estimation**: Definition of SoC. Literature review of relevant SoC estimation techniques. Simulation and validation of dual EKF. Sensitivity to non-ideal sensors, temperature and aging.
- **Chapter 7 SoH estimation**: Definition of SoH. Literature review of relevant SoH estimation techniques. Theoretical discussion of choice of SoH estimator, and implementation on a theoretical level.
- **Chapter 8 SoP estimation**: Definition of SoP. Literature review on relevant SoP estimators. Simulation of SoP estimator. Exploration of SoP as a saturating control law for discharge power.
- **Chapter 9** Conclusion and future work.

2

Battery Technologies

There are a lot of different combinations of materials used in batteries today, depending on the application it is designed for. Material costs, safety concerns, power and voltage output are some of the factors that decides what battery type that are adequate for the application intended. In order to design a proper battery management system, some knowledge of the battery is required. This chapter will therefore briefly discuss different battery technologies, the electro-chemistry for a lithium-ion battery and the advantages/disadvantages related to this technology. At the highest

level, batteries can be divided into two groups: primary (non-rechareable) and secondary (rechargable) cells. In this paper we will focus on secondary cells, as that is what we are interested in. We will first see what are the most commercially popular battery technologies in todays market, then look more closely on lithium-ion batteries.

2.1 Lithium-Ion batteries

Within secondary cells, there are tens of different combinations of electrodes and electrolytes. The most common cells uses either lead, nickel or lithium as there anode, with various combinations of cathode composition.

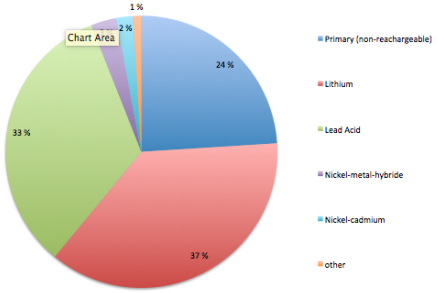

Figure 2.1: Marketshare for various battery technologies in terms of revenue.

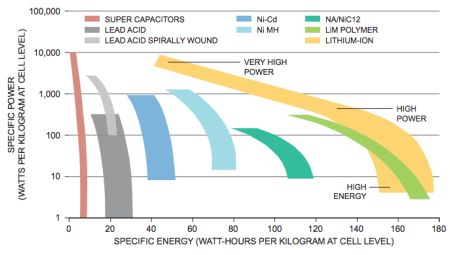

Figure 2.2: Specific power and specific energy ratios for different battery technologies.

According to Sullivan & Frost study from 2009 (Figure 2.1), LIB technology is the secondary cell that has the highest revenue world wide (37%), followed by Lead Acid(33%) and Nickel Cadmium

(5%) types. There has been a rapid development in battery technologies and the trend is that LIB market is only increasing, mostly due to the extended use in mobile phones and laptops.

Figure 2.2 shows different chemical combination in batteries, in reference to specific power and energy to weight ratios. Lead-acid battery has relative high power to weight ratio and low production costs, and is commonly used in cars to provide power for the starter. Since a car is heavy compared to the battery, lead-acids low energy-to-weight ratio is of no concern. Lithium-ion batteries on the other hand, scores high in both specific energy and power, and is therefore a preferable choice when space and weight is of concern, as it usually is with mobile devices. Table 2.1 summarizes the main advantages and disadvantages of a general Lithium-Ion battery.

Table 2.1: Advantages and disadvantages with a lithium-ion battery

Advantages	**Disadvantages**
High specific energy	Relative expensive
High rate and high power discharge capability	Degrades at high temperatures
Rapid charge capability	Need for protective circuitry
High power discharge capability	Capacity loss or thermal runaway when overcharged
Broad temperature range of operation	Possible thermal runaway
Long cycle life	
Sealed cells; no maintenance required	
Close to no memory effect	

In short, lithium-ion batteries are superior to other battery chemistries due the advantages listed in Table 2.1. However, the main disadvantages are related to safety and is an issue that can not be relaxed. The safety aspect will be addressed in Chapter 2.3.2, and is what enforces a functional and efficient battery management system for these types of batteries.

2.2 Formats

Within the family of lithium-ion batteries there are a wide variety of chemical combinations as well as structural designs. There are mainly three different cell designs; cylindrical, prismatic or pouch cell. Cylindrical cell design is most common due the to low production costs combined with mechanical stability. On the other hand, it is a heavier design with lower space efficiency in contrast to a prismatic or pouch design. The main advantages and limitations with each cell design is summarized in Table 2.2:

The battery installed on the ROV consist of cylindrical shaped cells wired together in parallel and series connections, physically stored together in a cubic format.

Table 2.2: Advantages and disadvantages with the different cell designs (Messina (2015), Battery University (2016)).

	Cylindrical	**Pouch**	**Prismatic**
Advantages	Low cost/easy to manufacture, Mechanically safe	Simple, high specific energy flexible and lightweight.	Thin and light design, more flexible installation possibilities
Disadvanteges	Low space efficiency	Swelling must be considered, exposing to humidity and high temperature can shorten life	Expensive, hard to do thermal management, sensitive to deformation

2.3 Operation of a cell

In this section, the basic understanding of the underlying physical phenomena that takes place within a battery cell is explained, as it is helpful to understand the responses that the battery gives. In general, the battery is composed by one or more electrochemical cells that converts the chemical energy contained in its active materials into electric energy. This is done by means of an oxidation-reduction (redox) reaction. The basic setup for a lithium-ion battery consist of 5 main parts:

- positive electrode (cathode)
- negative electrodes (anode)
- electrolyte
- separator
- current-collector plates

As the battery is fully charged, the anode structure is positively charged as most of the lithium is stored within the anode structure. During loading, a reduction - oxidation occurs when the trapped lithium particles start to diffuse toward the electrolyte, splitting lithium into ions and electrons. Li^+-ions transfer through the solution due to the potential difference while the electrons moves through the current collector. Reduction reaction takes place at the cathode where the traveling lithium-ions from the anode start to react with the electrode coming from the positive collector.

The seperator is a porous membrane, allowing the transfer of Li^+-ions only, thus serving as a barrier between electrodes preventing short-circuiting. When charged, the process is reversed.

Below is an example that shows this redox reaction for a LiCoO2-cell as well as graphical explanation.

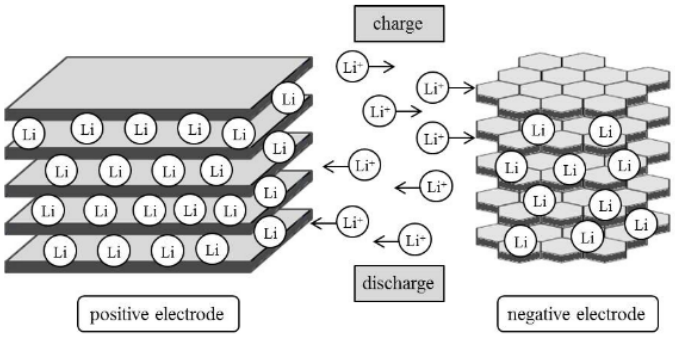

Figure 2.3: Graphical representation inside a lithium cell (Garche, J. et.al, 2009)

.

Li^+ are inserted or removed from the host material without major structural changes to the electrodes. This contributes to the long cycle life of lithium batteries (Linden and Reddy, 2002).

The material that acts as cathode and anode greatly influences the performance of the battery. To store most energy and obtain the highest voltage, it is beneficial to use two materials that are furthest from each other in the voltage table. The electrical voltage is the sum of the oxidation potential of the material that is oxidized and reduced potential for material reduced. However, on designing electrode materials, safety issues most also be addressed as some of the materials that are furthest apart on the voltage table can be become highly unstable under certain circumstances.

The commercially most popular LIB types consist of a graphite based anode. Graphite's unique lattice structure are ideal for capturing and storing lithium-ions, and are relatively cheap in production (Linden and Reddy, 2002).

For the cathode, there are more material variations, with the most popular being a layered type oxide (such as lithium cobalt oxide), a poly-anion (such as lithium iron phosphate) or a spinel (such as lithium manganese oxide) (Buchmann, 2011). As we shall see in Section 2.4, a combination of the previous anodes are often used to utilize the strengths of each metal, which is the case for the battery on board the ROV.

2.3.1 Battery concepts and definitions

The most important definitions used throughout this thesis regarding a battery cell is listed below:

A cell is *fully discharged* when its open-circuit voltage reaches lower cutoff voltage specified

by manufacture.

A cell is *fully charged* when its open-circuit voltage reaches upper cutoff voltage specified by manufacture.

Total capacity Q_{tot} is the quantity of charge removed from a cell as it is brought from a fully charged to fully discharged state[Ah].

Q_{tot} degrades slowly with time because of aging effects.

Discharge capacity Q_{rate} is the quantity of charge removed from a cell as it is discharged at a constant rate from a fully charged state until its loaded terminal voltage reaches lower cutoff limit specified by manufacture. Q_{rate} varies with temperature and discharge rate.

Nominal capacity Q_{nom} of a cell is a manufacturer-specified quantity that indicates the amount of charge that the cell is rated to hold. Q_{nom} is a constant value.

Residual capacity is the quantity of charge that would be removed from a cell were it brought from its present state to a fully discharged state.

State of charge (SoC) is the ratio of its residual capacity to its total capacity.

State of Health (SoH) is a measure of a cells performance degradation. Usually as a ratio of Q_{tot} over Q_{nom}.

State of Power (SoP) is a measure of a cells performance degradation.

2.3.2 Safety of Lithium-ion batteries

Lithium-ion cells are rather unforgiving if operated outside its Safe Operating Area (SOA), with consequences ranging from the annoying to extremely dangerous. In most cases the only effect is simply that the life of the cell is reduced, or that the cells are damaged, with no hazardous results. However, abusing a lithium-ion cell in particular ways can be extremely dangerous and can result in physical damage and/or overheating (from over-voltage, over-current, or external heat). This can develop into a thermal runaway, an uncontrolled exothermic reaction of the active material of a battery cell with its electrolyte. Also, under-and overcharge makes the battery cells expand possibly causing rupture of the battery pack casing. The SOA for a lithium-ion battery is bounded by three parameters; current, temperature and voltage. Figure 2.4 shows the SOA for the battery

currently installed on the ROV, with SOA for charge and discharge in blue and orange respectively.

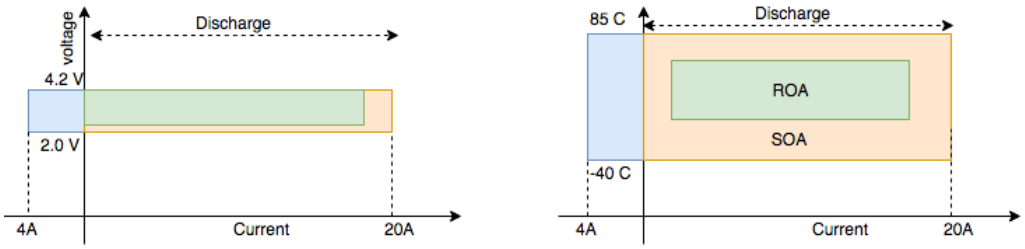

Figure 2.4: Illustration of SOA and possible ROA for the lithium-ion battery installed on the ROV

Less extreme design limits can be set defined by the Recommended Operating Area (ROA), which is a subset of the SOA of which the BMS designer can set limits on current, voltage and temperature to ensure a safety buffer against the limits of SOA. Operating the battery on the limits of SOA will lead to a more rapid decay battery performance, so by introducing a ROA the designer can balance the tradeoff of using the battery aggressively (over whole SOA), or ROA to ensure longer life expectancy.

Further on, the lifetime of these cells will be drastically reduced if discharged/charged outside a certain temperature range. The cells might even experience a thermal runaway and ignite if allowed to exceed a safe temperature. The lifetime will also be reduced if discharged at too high a current, or charged too fast, setting a limit on the discharge/charge rate to ensure long lifespan. All of these events, external and internal, must be prohibited and therefore arises the necessity of a functional battery management system that can monitor, control and take actions to ensure operation within SOA.

2.3.3 Efficiency of Lithium-Ion battery

The inner resistance in a lithium-ion battery is quite low compared to other battery cells, making it highly efficient compared to other battery technologies. Though small, the resistance is still present and is depended on a number of variables, such as current draw, capacity left,cycles and temperature. It is important to remember that either one of the mentioned variables effect the resistance, which in turn effect the other variables. Figure 2.5 is adapted from Andrea (2010), which illustrates the resistance dependence's in these variables.
Taken from the LG's technical specification sheet for the battery currently installed on the ROV, this relationship can be seen. Figure 2.7 shows the cell voltage against effective capacity for different discharge currents. Here, the battery has been discharged with different constant currents until it the battery terminal voltage has reached the lower limit set at 2.5V, and the charge that has been taken out is the capacity plotted on the x-axis. It is important to understand this graph,

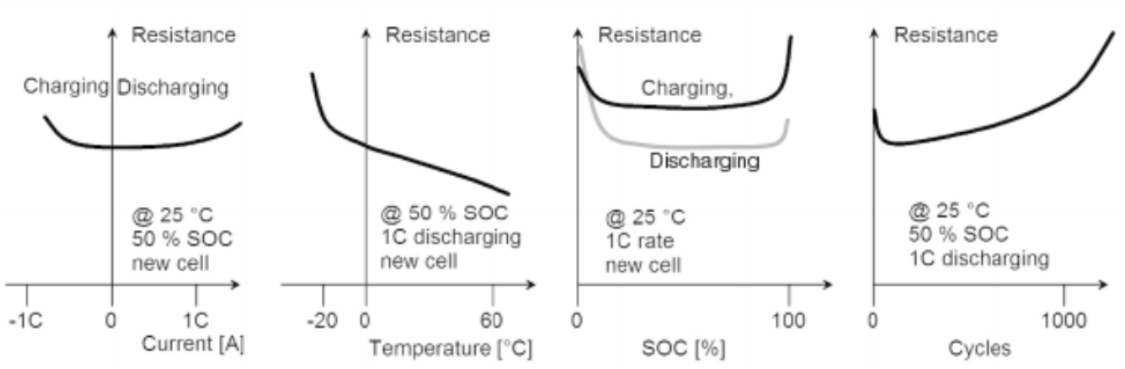

Figure 2.5: Cell resistance versus various variables; current, temperature, SoC, and cycles. Adapted from Andrea (2010).

because it plays a vital part for modeling later on. What it noticeable, is that it looks like the capacity of the cell is depended on the discharge current. This is however not true, as a new lithium-ion battery is from a charge point of view 100% efficient over a full charge/discharge cycle. That is, all charge that is put into the battery is extractable when the battery goes from fully charged to fully discharged regardless of the discharge current. The effective discharge capacity though, that is the charge that can be extracted by keeping the same constant current until the lower terminal voltage limit is met, is depended on discharge current. If the battery was discharged with high constant current until lower voltage limit is met, the battery is not fully discharged and it would still be possible to extract the last charge in the battery. For some applications it is crucial that the battery delivers high power until lower voltage limit is met(such as backup power), and can therefore not utilize the whole capacity without damaging the battery. Other applications, like the ROV, the remaining capacity can be exploited by requesting power reduction to the control board. This is what is called a "limp home" or "valet" mode or function.

	0.2C	3A	5A	10A	15A	20A	25A	30A
Capacity (mAh)	3000	2886	2884	2925	2913	2873	2802	2702
% C_N	100	96	96	98	97	96	93	90
Energy (Wh)	11.0	10.3	10.1	9.8	9.5	9.2	8.7	8.2
% W_N	102	95	94	91	88	85	81	76

Figure 2.6: Energy efficiency W_n and effective capacity C_n for increasing constant currents (LG chem: Mobile battery division, 2016).

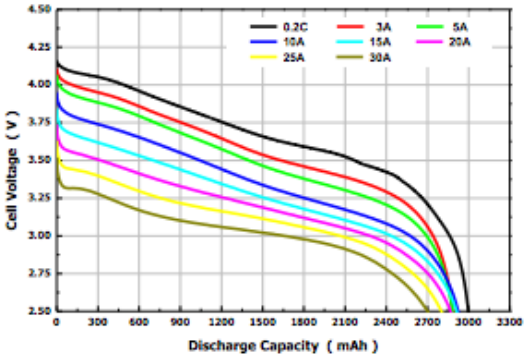

Figure 2.7: Non-linear relation between useful capacity and voltage for different discharge currents (LG chem: Mobile battery division, 2016).

In terms of energy, the lithium battery is not 100% efficient. This is due to the internal resistance within the cell itself, where energy is converted into heat. The internal resistance in the battery increases with increased current, which reflects itself in the Table 2.6. The energy efficiency W_n decreases more than the effective capacity efficiency C_n as the energy E_t left in the cell at time t is

$$E_t = C_t \cdot V_t(C_t) \tag{2.1}$$

where voltage $V_t(C_t)$ is depended on the discharge current (Fig. 2.7). The reason this graph is so important for the design of a functional battery management system, is that it can give us a relationship between the *Open Circuit Voltage (OCV)* and *State-of-Charge (SoC)*. These terms will be further discussed in chapters to come, but it is useful to briefly introduce these two definitions already now. The OCV is according to (Andrea, 2010) defined as the battery voltage under the equilibrium conditions, i.e. the theoretical voltage when no current is flowing in or out of the battery, and, hence no reactions occur inside the battery. This voltage is normally a function of the SoC.

2.4 Battery onboard the ROV

The battery currently used on board the ROV is a 32 cell 4S8P Lithium Nickel Manganese Cobalt Oxide (NMC) developed by LG. The anode is graphite and silicon monoxide (SiO/C) composite, and the anode is a composite consisting of Nickel(Na), Cadmium(Ca) and Maganese(Mg). Nickel is known for its high specific energy but low stability. Manganese has the benefit of forming a spinel structure to achieve very low internal resistance but offers a low specific energy. The optimal composition of each material therefore depends on the safety and power requirements of the battery. It is composed of 8 cells wired in parallel, each with a nominal capacity of 3Ah and nominal voltage at 3.6 V. These parallel blocks, referred to as parallel-connected cell modules(PCMs), are coupled together in four series (4S). This configuration yields a capacity of Q_{nom} = 3 Ah $\cdot$ 8 = 24 Ah and nominal voltage at V_{nom} = 14.4 V for the battery pack as a whole. Table 2.3 shows the characteristics the cells and pack currently used on the ROV. As we saw in last section, the inner resistance of the battery depend on both current, temperature, number of cycles and SoC. These effects can be seen in the manufactures documentation plots (Fig. 2.7-2.11). By evaluating these plots, and combining what is known about the ambient environment and operation for the battery on board the ROV, the necessary complexity of the BMS system can be evaluated.

Figure 2.8 and 2.9 show how current effects the temperature in the battery. From this it can be seen that a higher current leads to temperature rise due to more generated heat because of higher inner resistance. In fact, the temperature over one cycle increases with $25C^o$ for 10A constant current and $55C^o$ for 20A.

Table 2.3: Specifications of the current battery onboard the ROV given by LG chem: Mobile battery division (2016).

	Battery currently in use [LiNiMnCoO2]	
Parameter	**Nominal value**	**Operating range/comment**
Capacity	3.6V	Min: 2-3.4V Max = 3.6-4.2V
Specific energy	240 Wh/kg	
Nominal capacity	3 Ah	(at 0.2C)
Charge rate (c-rate)	0.5 C (1.5A)	Fastcharge: 1.67C (4.5A)
Discharge rate (c-rate) Ah		0-6.67C (0-20.0A)
Weight	1.504Kg	
Operating temperature	Charge	0-45 C^o
-	Discharge	-20-60 C^o

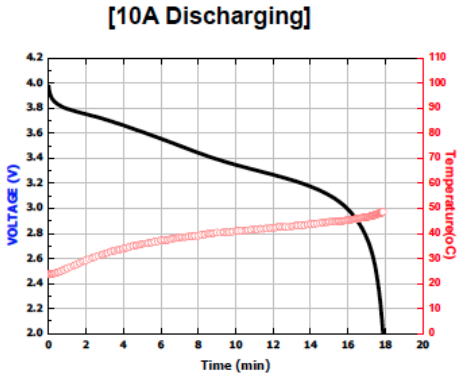

Figure 2.8: Effect of constant medium constant current (10A) on temperature for a full discharge cycle.

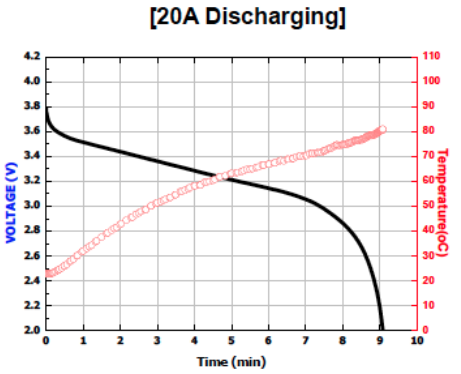

Figure 2.9: Effect of constant high constant current (20A) on temperature for a full discharge cycle.

In Figure 2.10 the effect of constant low temperature can be seen. It is clear that the lower the temperature, the lower the discharge curve. This is as expected. Looking at this with the ROV application in mind, the ROV is operating under water where temperature will most likely range from $4 - 30C^o$, depending on which part of the world the ROV is used. Having in this in mind, the effects of extreme low ambient temperature is not that critical for this application as it is for a HEV or BEV. Even so, the ROV might be in colder climates such as Norway, or even for arctic exploration, where the temperature prior to operation might go down to $-30C^o$. As the ROV is submerged and the ROV starts draw power, the ambient temperature will rise to above 0 conditions and the battery will heat up to more friendly temperatures.

Figure 2.11 shows the aging effect of the battery displayed as the decrease in capacity over number of cycles. The test was performed with a periodic current draw of 5s with 20A and 1s off until cutoff voltage at 2.5V or temperature cutoff at $90C^0$. The capacity drops 77% for 500 cycles, which at a constant current will lead to averaged 23% decrease in operation time. A battery is said to met its lifecycle when the total capacity of the pack has reached 20% of its nominal value. It is clear that the aging effect has to be taken into account for and somehow be estimated. However, assuming that the ROV is being used one time a week for a whole charge/discharge cycle, the battery would experience 500 cycles in 10 years.

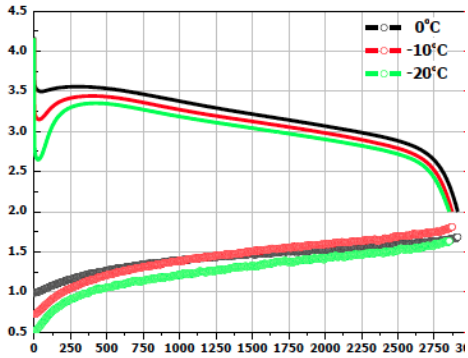

Figure 2.10: Low temperature effect on voltage with constant current of 10A.

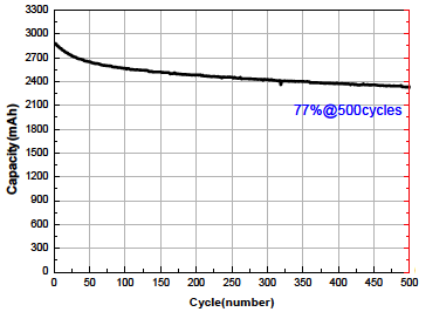

Figure 2.11: Aging effect on capacity for a dynamic discharge cycle with cut-off at v = 2.5V or temperature = $90C^o$.

3

The ROV: Pioneer 1

The Pioneer 1 is the first iteration of a remotely operated vehicle (ROV) developed by Blueye Robotics. It has a goal of providing world-class performance at the same level as larger and more expensive ROV, while at the same time targeting the commercial market. That puts in general high requirements on production costs, while still maintaining high performance. That goes for the battery and BMS solution as well. In the light of a BMS solution, it must provide a trade-off between fidelity and computational costs. Expensive and accurate sensors give less demand on software solution, and thereof also computational power. On the other hand, cheap and less accurate sensors demand smarter software algorithms in order to maintain a satisfactory level of accuracy. This usually goes at the expense of more costly microprocessors.

Developing a custom battery management systems that, in total is cheap in production, while giving satisfactory results for all operating conditions, is a challenging task. A natural place to start is to map power consumption profile, current battery specifications as well as the ambient environment in which the battery will operate.

3.1 Power consumers

The current ROV model operates on a nominal voltage of 14.4 V with a max current draw of around around 40 A. The electric consumers can be broken down into two main parts; the more or less static current draw due to electric boards, light, video camera etc. and the dynamic part i.e the thrusters. The former were measured to be around 0.8 A, while the latter naturally depends on how the ROV is operated. To get an idea of the power consumption of the thrusters, current and voltages was measured using the current BMS on board with a sampling frequency of 0.84 Hz. Two different field tests where performed. Because of drone and sensor malfunctions, neither of the data sets are complete. Table 3.1 summarizes key information of the field tests:

Table 3.1: Key information for field tests.

-	Location	Time	Ambient Temperature	Note
1	Nidelva	01.05.17	12 / 6	No extra current sensors on thrusters, possible 3 temperature sensors malfunctioning
2	Nidelva	25.10.16	-5 / 4	Drone malfunction, small SoC-range

3.1.1 Data from test1

This test was done without the lateral truster in use, as Blueye has moved away from using a lateral thruster. Figure 3.1-3.2 shows the measured pack current, PCM voltages and PCM temperatures for field test 1, provided by the BMS. The profile is categorized as "playfull", driving with full

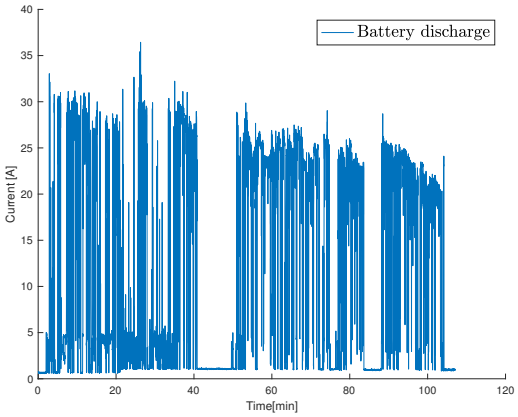

Figure 3.1: 1.Measured current from battery during drone operation in Nidelva.

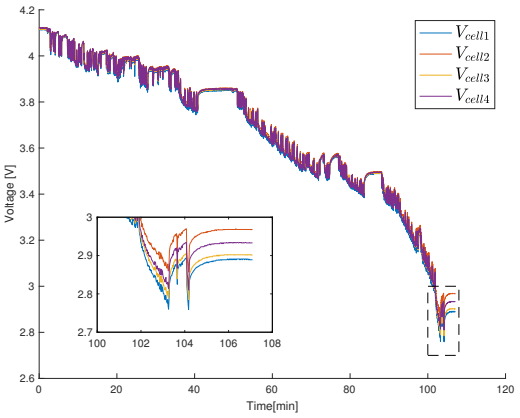

Figure 3.2: 1.Measured voltage on each parallel connection during drone operation in Nidelva.

throttle most of the time. This can be seen by the longer periods of high pack discharge current, where the thrust boost-function is enabled (Fig. 3.1). For the shorter periods at discharge current around 5A, the boost was turned off. This was approximated the same force as the drag of the cable and the ROV in the high current river Nidelva. Discharge current of approximate 5-10A can therefore be expected that for inspection and other application that demands steady video feed.

The usage history of the battery pack is unclear. It has been disassembled and recharged on a cell level because of misuse(under-discharge). This can be the cause of the difference in voltage level that the parallel connections converge to at the very end of operation. That is, the difference in open-circuit voltage (OCV) for the different parallel connections. However, it is more likely that this difference is due to imbalance of the battery pack.

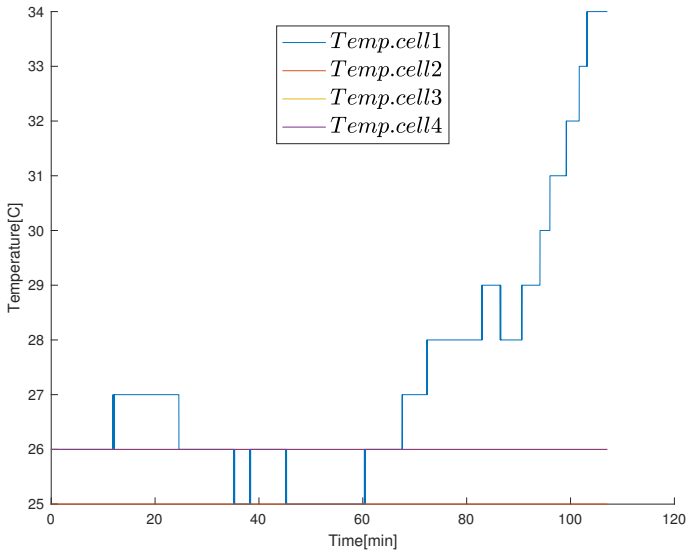

Figure 3.3: Temperature of the four cells during test run in Nidelva.

3.1.2 Data from test2

Figure 3.4-3.5 shows the measured pack current, PCM voltages and PCM temperatures for field test 2. Figure3.7-3.10 shows the measured current at each individual thruster. In this profile, all

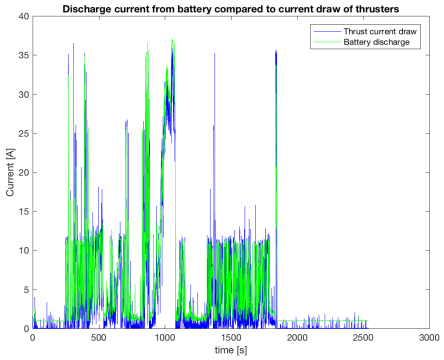

Figure 3.4: 2. Measured current from battery during drone operation in Nidelva.

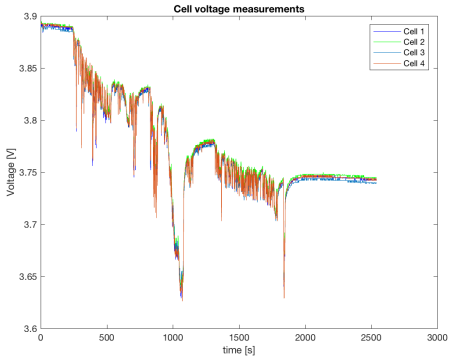

Figure 3.5: 2. Measured voltage on each parallel connection during drone operation in Nidelva.

four thrusters were enabled. The overall current draw is less than for the other profile (Fig. 3.4). The operator used the video feed for seabed discovery, so little manoeuvring was necessary. The stern thrusters are the main contributors to the battery discharge current. The high peaks comes from the vertical thruster on submergence and resurface.

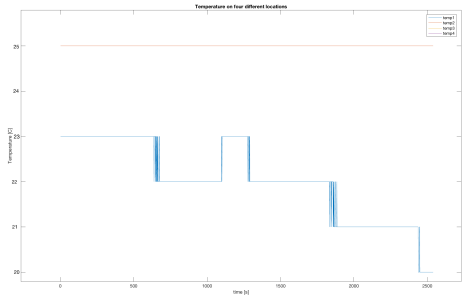

Figure 3.6: Temperature of the four cells during test run in Nidelva.

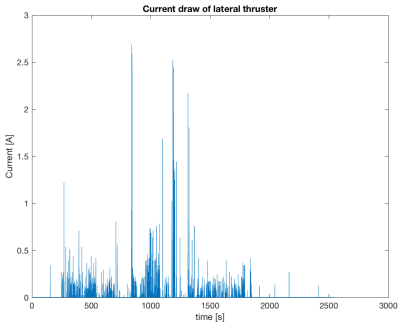

Figure 3.7: Current draw from lateral thruster.

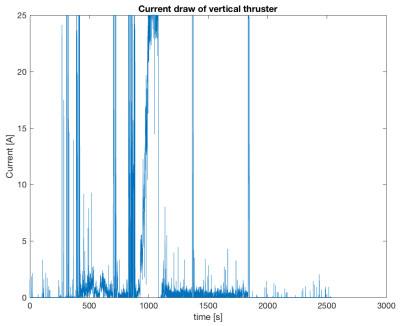

Figure 3.8: Current draw from vertical thruster.

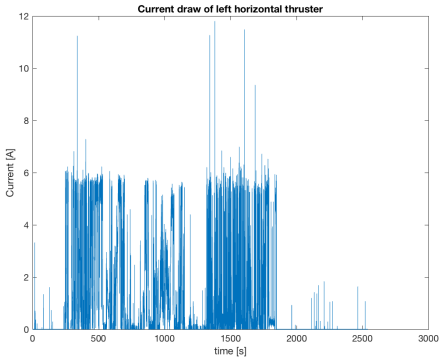

Figure 3.9: Current draw from stern thruster.

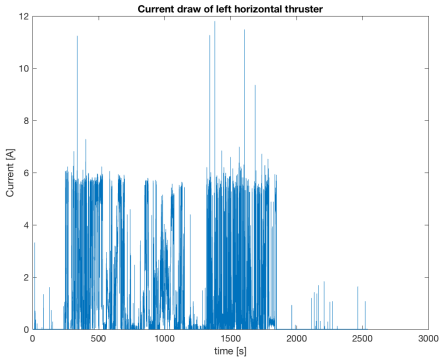

Figure 3.10: Current from right stern thruster.

3.2 Summary

In summary, it has a highly dynamic highly dynamic current profile. Charge and discharge cycles are naturally separated, in contrast to HEV/BEV's, which has regenerative abilities. The maximum theoretical pack current with three thrusters is $3 \cdot 22A + 1A$ = 67A. Maximum observed thrust is 39.6A. The temperature within the battery pack stays rather constant for arctic operations, given that the temperature measurements can be trusted. According to the data, the temperature rise from internal resistance equalizes the net heat dissipation due to low ambient temperature. This is

naturally not the case for warmer climates, nor different operating profiles. Table 3.2 summarizes the key findings of the operational environment of the ROV compared to that of HEV's, BEV's and PE.

Table 3.2: Operational environment for different applications.

Characteristics	HEV	BEV	PE	ROV
Max rate	20C	5C	3C	2.5C
Rate profile	Very dynamic	Moderate	Piecewise constant	Moderate/high
Life time	10-15 years	10-15 years	$<$ 5 years	10 years
Ambient temperature	-30 - 50	-30-50	-30-50	4-30

4

Battery Management System

4.1 Purpose of battery management systems

A BMS is an electronic regulator that controls and monitors the charging and discharging cycle for a rechargeable battery. The safety and control requirements of a battery require the use of a BMS to ensure that the battery operates within acceptable limits. The battery management system consist of both hardware and software in order to measure the properties of the battery and its ambient environment. It then displays the necessary information to the operator enabling him to plan an operation safely and effectively. Its main purposes for a general applications are to:

- **Ensure safe operation of the battery, during both charge and discharge.** Batteries are composed of highly reacting chemicals. If the battery are exposed to conditions that are outside of its Safe Operating Area, destructive and irreversible chemical processes might occur. Depending on the type of condition that is violated, this can not only lead to lost efficiency and capacity of the battery, but also cause failure for battery and electrically connected components. Since a battery usually is the last, if not only, power source for the application, it is crucial that this do not fail. Worst case scenarios happens when there is a thermal runaway where an uncontrollable chemical reaction takes place, making the battery catch fire. These types of failures can spread throughout the entire battery pack and eventually to the host. This can cause a direct threat for applications where the user are in close proximity of the battery itself, such as mobile phones,electric vehicles etc. However, a battery failure might indirectly be even more fatal if applications that are depended on the battery power supply does not get its power, such as back-up systems on ships, hospitals etc. Safety is therefore of the out most concern for a BMS.

- **Efficient operation of battery.** Operating within its SOA is not only a matter of safety, but also efficiency. Cell balancing to prevent local under-or over-charge is an example of this. The battery effective capacity is dependent on the discharge rate, that is less charge can be extracted from a battery on a mission that requires high power for acceleration or advanced maneuvering than for less damning missions. Temperature also affects the effective capac-

ity, with colder temperatures limiting the amount of energy that can be obtained form the battery. It is necessary to predict the battery's ever-changing storage capacity so that a user can optimally plan a mission within the battery's capabilities.

In order to achieve these objectives, the BMS must first measure the internal states of the batteries (Andrea, 2010). From these measurements, different management functions are implemented and derived properties of the battery are calculated and evaluated. Lastly, the necessary information is communicated to the external system, as well as operator.

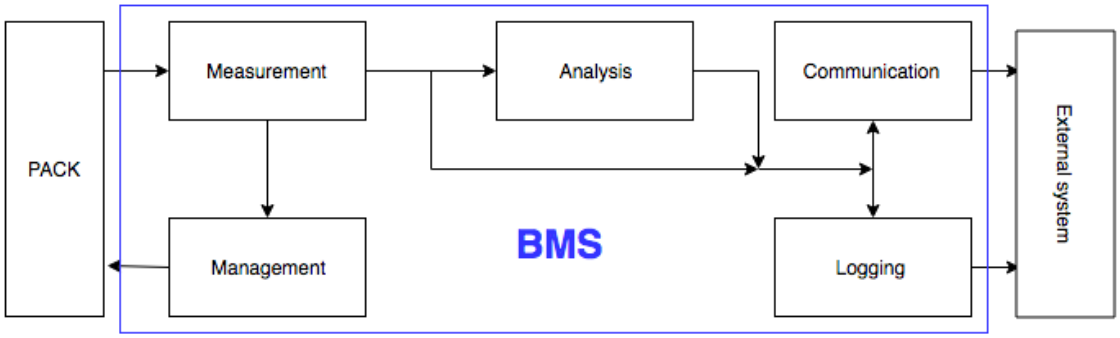

Figure 4.1: BMS function Andrea (2010)

4.2 Measurements

A classic BMS needs to measure and monitor the following states of the battery (Andrea, 2010).:

- Cell Voltage
- Pack Temperature
- Pack Current

This is an absolute minimum in order to have a sufficient BMS (Andrea, 2010). For battery packs consisting of multiple cells connected in parallel, voltage measurements at each parallel connections is sufficient. That is because battery cells connected in parallel self-equalize in voltage. Temperature monitoring is necessary to ensure that the battery operates within its SOA, both of security reasons but also because the battery parameters change at extreme temperatures. If the battery is small i.e. few cells, measuring temperature at different locations will not be necessary. The BMS currently installed on the ROV has four temperature sensors, and from tests we see that the temperature varies only with a 2-3 C^o between the cells during those operation. Normally, this difference in temperature comes from manufacturing differences, where some cells have higher

inner resistance than others. It can also be that the cells that are located in the middle of the pack experience higher temperature because of less heat dissipation. If you consider an EV where the cells are distributed throughout the length of the car, the individual cells are subject to a range of ambient temperatures, whether the cell is located underneath the cabin, motor, trunk etc. For these applications, monitoring temperature throughout the pack is important.

The rate of measurements are depended on the application. For application where current varies rapidly, such as for the ROV, a sampling rate of 1 Hz for current and voltage is accourding to Andrea (2010) sufficient in order to catch the dynamics. Temperature however, does not vary that rapidly and does not need to be sampled that often. In order to estimate the SoC based on OCV, an accuracy of 10mV or better is required. This is due to the close to constant relation between SoC and OCV at specific regions (80-90%) of the OCV-SoC curve (Andrea, 2010).

4.3 Management

A BMS most critical task is to protect the battery and its host from abusive conditions that could lead to battery failure and thermal runaway. Apart from the inconvenience and material cost of battery failure, it can also provide a direct threat to personnel, especially for high power lithium cells. Cell protection is therefore indispensable for these kind of batteries. A general BMS manages a pack in three different ways (Andrea, 2010):

- Protection: Not allow battery operate outside of SOA
- Balancing: maximize capacity of the pack
- Thermal: actively bring battery into temperature of SOA

Keeping the battery within its SOA means not allowing voltage, current or temperature to go beyond a certain threshold. The SOA for this battery can be seen in Figure 2.4.

A BMS must not only detect when these values approaches their limits or violates them, but also have to validate how critical it is and take actions to bring inside the the SOA. Some BMSs simply shut down the battery current when current, temperature or voltage limits are met. This would be a simple, but not very functional way of doing it. If these variables are just barely violated for a short period, the BMS would unnecessary shutdown the ROV while being submerged. The ROV is designed to be buoyant, and the user could tow it in by its chord. However, there are more clever ways of handling this so unnecessary current interruption can be prevented. By gradually requesting a current draw reduction when voltage is approaching preset lower limit, the

voltage will rise and sudden shutdown can be prevented. This would cause the maximum thrust to be reduced, but it is a small price to pay compared to total shutdown. Alarming the user of low voltage, which would lead to reduced maximum thrust, a smart BMS could suggest to return to surface, lump back home and turn of unnecessary power consumers such as video stream and lights. Navigation would not be compromised as the ROV would be visible at the surface.

Space and cost limitations makes active thermal management difficult onboard the ROV. Installing coolers or fans would not be feasible, so current limitations is the only way of controlling the temperature.

This thesis propose to use state-of-power calculations as an model-predictive control law saturating the discharge current. By doing so, the battery will be kept within SOA in an optimal manner, compared to methods that do not consider the current states of the battery. This concept will be further explained in Chapter 8.

While the battery can detect and initiate protective actions for events within the battery system, there are some applications which require the battery to respond to external events. This could be an out of tolerance condition such as a high temperature in some other part of the application which requires the power to be shut off. In the case of an automobile accident for instance, an inertia switch should isolate the battery. In these situations the battery needs to incorporate a switch in the main current path which can be triggered by an external signal. For the ROV, taking in water be an example of accident that needs instantaneous actions. The ROV already has a internal pressure sensor which acts as a sensor measuring if the ROV is properly sealed. Using this, the BMS could immediately shut of power on pressure rise. Another possibility would be to include a humidity sensor. When humidity is over a certain threshold i.e. ROV leakage, a switch disconnect the battery to prohibit short circuit.

4.3.1 Cell balancing

Andrea (2010) defines a balanced battery pack as "*a battery pack in which, at some point in its cycle, all cells are at exactly the same SoC*". With this definition, the only cause of imbalanced cells are due to a different net current going in and out of the cells, or the coloumbic efficiency of the cell. The net current going in and out of a cell is:

$$i_{net} = i_{app} + i_{self-discharge} + i_{leakage} \tag{4.1}$$

where i_{app} is the battery-pack load current, $i_{self-discharge}$ is the rate of self-discharge, and $i_{leakage}$ is the current drawn from the cell that power the attached BMS circuitry. i_{app} will be the same for all cells in the pack, but $i_{self-discharge}, i_{leakage}$ might not. This would cause the SoC of cells to

diverge during discharge, and this imbalance will continue to grow 4.3

Other effects, as production tolerances, uneven temperature distribution and differences in total capacity does not cause imbalance (**?**). Different total capacities cause only a temporary imbalance that is corrected automatically when any cell returns to its original SoC (Fig. 4.2).

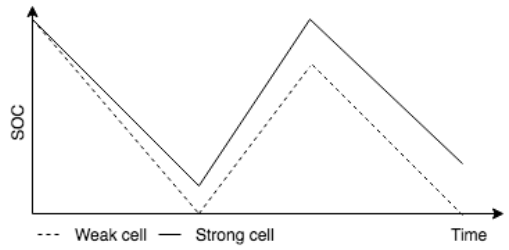

Figure 4.2: Battery-pack imbalance growing over time (Plett, 2016).

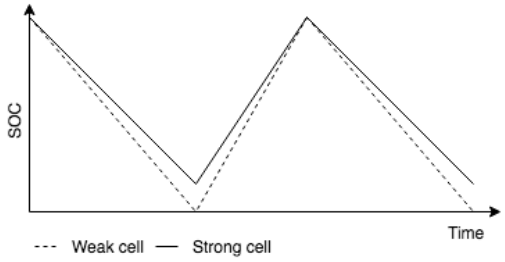

Figure 4.3: Difference in total capacity does not cause long-term growth in imbalance(**?**).

Different cell resistances will cause cell loaded terminal voltage to be different, but not their SoC (Plett, 2016). That is because during relaxation, both the cell with higher internal resistance and the one with lower internal resistance will converge to the same OCV, and thereof the same SoC.

Both these effects will indeed limit the performance of the battery pack, as the weakest cell will reach upper and lower limits on voltage and possibly temperature before other cells in the pack, but not cause imbalance. A BMS will never be able to correct these individual differences, but can use this information to prohibit further divergence.

There are mainly three ways of balancing a cell; balancing, distributed charging and redistribution. The conventionally idea behind the balancing is to remove charge from the the battery cell with the highest SoC, allowing the weakest cells to receive more charge during charging. In distributed charging the current is bypassed the strongest cells allowing the weaker to receive more charge. Redistribution is the most complicated, where the battery can balance itself by sending charge between strongest and weakest cell while being in use. Without going into details of the latter two, they are found to be inadequate for such a small scale system as on board the ROV.
Even though it seems that distributed charging and redistribution is superior to normal balancing, that has to be seen in terms of the application. The former two methods requires much more hardware with extra sets of wires going between each battery. The complications of such a setup would not be feasible for the ROV. Both because the ROV is meant to be a low-cost alternative to what the marked has to offer of ROV alternatives, and extra hardware, switches and development costs would not be not be justified. Further on, the extra hardware means more occupied volume and lower reliability compared to normal balancing (Andrea, 2010). These two methods are therefore

Table 4.1: Methods of cell balancing, adapted from (Andrea, 2010).

Method	**None**	**Balancing**	**Distributed Charging**	**Redistribution**
Method	N/A	Passive	Active	Active
Current transferred	None	Low:10mA-1A	Medium: 100mA-10A	High:1A-100A
Battery Energy Utilization	0-90%	ca 90%	100%	
Battery Capacity	Reduced over time	minimum cell cap.	Average cell cap	-
Pack SoC	N/A	Cell with least cap.	SoC of all cells	-
Cell SoC	all over the place	At 100% all cells have the same SoC	All cells always at same SoC	-
Duration	N/A	Some time during charging	During charging	Whenever in use

more often used at larger battery pack such as for HEVs, BEVs and larger energy-store battery packs.

Assuming that the battery is gross balanced from the manufacture, it is only small differences in SoC that needs to be taken care of; maintenance balancing. For that, normal balancing algorithms are best suited. Voltage and Final Voltage methods are the two most common ways of traditional balancing (Andrea, 2010). These methods are simple, but assumes that voltage measurements are a good indicator of SoC. As it will be seen later, this is not the case. By having a better and reliable SoC estimator, charge might be removed from cell (or PCM) with the highest SoC during the whole charge phase, allowing more charge into the weaker cells.

4.3.2 Charge control

The charging process is either controlled by the charger itself, or controlled by the BMS. The standard procedure for lithium-ion batteries is the classic constant-current constant-voltage (CC-CV). That means that the battery is charged with a constant current up to some preset voltage value, just below upper voltage limit. From there, the cells are charged at a constant voltage until the pack voltage reaches upper limit. This is a simple and safe algorithm to prevent over-voltage. (Chaturvedi et al., 2011). For more advanced BMS controlled charging, a CC-CV charging method is also the most commonly used, especially for lithium-ion batteries. The BMS has in general more information over each cell, which gives more control of the charging process. Many internal processes of the battery have an influence on the charge transfer capabilities, e.g. finite diffusion rate of lithium ions in the electrolyte, reduction/oxidation of materials other than the active material, and formation of resistive films on the active particle surface (Andrea, 2010). Therefore, manufactures gives preset current limits for charging, which for this battery is 1.5-4.5 A. Chaturvedi et al. (2011) presented an optimal charging strategy based on nonlinear model predictive control (NMPC) techniques to charge the battery in the fastest possible manner, while guaranteeing safety throughout the battery's life. That motivation was that charging limits are geared towards the CC/CV charging method, and hence are rather conservative, since they are specified for the complete lifetime of the battery (Chaturvedi et al., 2011). However, charging time is not considered to be critical for the ROV application compared to HEVs or BEVs. Also, it is computational expensive. Therefore, A CC-CV method controlled from the BMS is assumed to give the best overall solution.

4.4 Evaluation

In the evaluation block, the measurements are used to derive parameters that cannot be directly measured. These parameters can include State-of-Charge (SoC), Equal Series Resistance (ESR), total capacity, state-of-health (SoH) and State-of-Power (SoP). None of these parameters are strictly needed to protect the pack from hazardous conditions, but aids in operating the pack in an efficient manner. At the same time, indications of SoC and SoH level is very useful for the operator of the application. The main emphasize in this thesis lies in the evaluation block, and will therefore be discussed in greater detail in the Chapter 6,7 and 8.

4.5 Logging and Communications

Back-end communication and logging Communication with the external system is a vital part of a sophisticate BMS system. Most importantly, communication with the connected hardware is essential to request current reduction or interruption if the battery is getting close to its SOA. This type of communication is what can be referred to as back-end communication i.e. states of the battery that is not useful for the user, and therefore is hidden.

The only back-end communication that is needed between external system and the suggested BMS algorithm is the maximum allowed discharge power (SoP) estimate. SoP must be communicated to the computer in which allocates thrust. In this case, the computer is a Raspberry Pi. If the operator has enabled the limp-home functionality, the adapting saturation law is enabled. The Raspberry must use the communicated pack SoP to saturate the thrusters.

For diagnostic purposes, it might be useful to communicate individual voltage measurements together with temperature measurements to ease diagnostics of the BMS.

4.5.1 Front-end communication

Some of the information however, might be of interest to the operator, and how to choose relevant information depends on the intended user segment. Since this is a consumer based product, it can be assumed that low level details such as real time current, cell voltages etc. are not of interest. Displayed information regarding battery status could be held to a minimum, only displaying the most essential information. A suggestion of what this communication look like is:

- Pack SoC
- Runtime left in the battery
- Pack SoH

Either Pack SoC or the remaining run-time of the battery could be displayed to the operator at all time. A warning could pop up if the estimated SoH goes below 20% of nominal capacity.

Suggestions of what should be communicated to the external system and what should be displayed to the user has been discussed. How this communication is done has not. A traditional, but old fashioned way was to have dedicated wires, either analog or digital. This is costly and space consuming so not favourable onboard the ROV. CAN bus is the favoured communication method on large scale control systems because of its fast response and high security. The ROV however, is a small scale system. As of today, the BMS is connected to the microchip onboard (Ardiuno Mega 256) through a RS232 connection. The RS232 communication protocol is found sufficient for the ROV. In general, RS232 is frowned upon in the industry of BMS design (Andrea (2010)), as it is not balanced. This could be a problem for large battery packs because of electrically noisy environment. However, this is not a problem for the small battery on board the ROV.

Logging is essential for user to determine the overall health of the battery, but also for the SoC,SoH and SoP estimates. If any failures in the BMS happen, the log could also provide information prior to failure to see what went wrong, and therefore is a useful tool for diagnostics. A log may include:

- Cell SOH,SoC.
- Cell parameters.
- Index of worst-performing cell.
- Average cell series resistance.
- Average cell total capacity.
- Average bias estimate.

4.6 Requirements for a BMS on a low-cost ROV

The previous section discussed what functions a typical BMS needs to implement, brought in the light of the ROV application. There is a lot of literature on BMS for over water applications such as EVs,HEVs, AUVs etc. However, the battery, BMS and their requirements must be specified towards the applications they are used for. Levels of complexity and precision, and therefore also weight, costs and current draw are some of the parameters to consider when designing the BMS. Using the identified operation environment of the battery onboard the ROV (Tab.3.2) together with the basic knowledge of a general BM system, a performance requirement comparison between BEVs, HEVs, PE and ROVs can be seen in Table 4.2.

Table 4.2: Performance requirement comparison for different applications.

Characteristics	HEV	BEV	PE	ROV
SoC	Very precise	Precise	Crude	Precise
Predict available power	Yes	Yes	No	Yes
Cell balancing	Cont. req.	charge only	charge only	charge only
SOH	precise req.	precise req.	not req.	Optional
Cell balancing	precise req.	precise req.	not req.	req.
Handle temperature effect	req.	req.	not req.	req.

5

Battery Modeling

A simple BMS does not rely on a battery model. When voltage and temperature are approaching cutoff limits, the BMS simply disconnects the connections and shuts down the host. In order to ensure that the predefined limits of the SOA are withhold, conservative limits must be made. This is because the voltage drop upon large current demands in a low SoC condition exhibits very fast dynamics. The same goes for charging, with high currents at high SoC. This implies that for a short period of time, the BMS is not able to prevent under-or over voltage, as it lacks the capability of predicting the batterys voltage response upon loading. SoC estimation is also done in a crude way for BMS without a battery model, most of them relying on ampere-hour counting only (see Chapter 6). An accurate battery model is needed to improve both safety and efficiency of the battery. By modelling the voltage response of the battery, derived parameters such as State-of-Charge (SoC), State-of-Health (SoH) and State-of-Power (SoP) can be obtained.

In literature there is a wide variety of lithium-ion models that represents the dynamic behaviour of the battery, each with different degrees of complexity. The battery is, as mentioned before, a nonlinear system. Nonlinear models are in general more complex adding a lot of restrains and computational costs as the nonlinear systems are represented by complex partial differential equations (PDEs). Frameworks for handling linear systems however, are much more developed in the field of controls and easier to cope with. A common approach is therefore to simplify the dynamics to a linear system. This is done at the expense of accuracy of the model, as it no longer is able to capture all of the dynamic behaviour. However, the benefit of solving linear ODEs instead of complex nonlinear systems in terms of computational power and therefore requirements on equipment usually makes them much more suitable for online applications. That is, generally a simpler model will run faster, but at the expense of fidelity. This tradeoff is crucial to consider so that it fits the battery and its intended application. In the following sections the two most popular principles of battery models will be discussed; Electrochemical and Equivalent-Circuit models.

5.1 Electrochemical models

Electrochemical models (ECM) are based on highly nonlinear equations that represent the physical chemical reactions happening within the cell (Seaman et al. (2014)). The aim of these types of models is to capture as much of the key features of the battery behaviour and therefore achieve the highest accuracy possible. However, in order to describe the battery chemistry they introduce a high number of PDE's with a large number of unknown parameters. These must be solved simultaneously with high computational expense and enforces considerable requirements on memory.

EC models for lithium-ion batteries are usually founded on porous electrode theory, firstly introduces in 1975 by Newman and Tiedemann (1975). This theory introduces large sets of PDE's trying to explain every chemical action taking place, at both anode, cathode and separator. The theory of porous electrode is usually derived from Fick's law of diffusion of active material concentration, Ohm's law for electrical potential distributions, and the Nernst and Butler–Volmer equations(Seaman et al. (2014)). The PDE's must be defined at each positive and negative electrode as well as separator, and are coupled together with each other through boundary conditions, resulting in as much as 14 PDE's with 14 unknowns. Solving these PDE's are usually done by a finite difference technique approximating continuous change being constant within a discrete infinite small time interval, and representing the derivative through a Taylor expansion (Seaman et al. (2014)). The accuracy of this method of solving is depended on the number of discredited segments, and looses accuracy in regions of high non linearity due to linear approximation.

Simulating single charge/discharge with these PDE's might take hours to run, and therefore in recent years model reduction and various simplifications have been proposed in order to increase EC models efficiency and usability in real-time applications. Two different categories of simplifications can be found in the literature (Seaman et al., 2014):

- Model reduction while trying to maintain accuracy
- Neglecting some of the model properties possible loosing information

Subramanian et al. (2009) is one of the pioneers within battery modelling and has done extensive research trying to make EC models suitable for real-time application. By converting the PDEs into a simpler form they can be integrated faster using numerical solvers. The method of simplification is called Galerkin's method, where the idea is to find approximate numerical solution to a nonlinear PDE using a set of orthogonal basis functions which turns the PDE into coupled set of ODEs. According to Seaman et al. (2014), Subramanian et. al. managed to get the run time for a single charge/discharge simulation cycle down to 100 ms, which make it much more suitable in a real-time environment. However, in order to derive those simplification one needs extensive a

priori knowledge of behaviour of the system under various conditions making it less flexible than desired (Seaman et al., 2014).

5.2 Equivalent electric circuit models

Unlike the electrochemical models, equivalent electric circuit (EEC) models are not directly relateable to the physical reactions taking place, but rather try to model the response of the battery by the means of electric components. The effect of the parameters in common electric components used in these models, such as resistors and capacitors, are generally easier to understand for a control or electric engineer point of view compared to the parameters introduced in electrochemical models. In general, one can say that EEC models are easier to understand, is simpler in structure and therefore relaxes requirements for computational power. Variations of ECC models are thereof the preferred model for online applications. The simplest EEC model consist of an open circuit voltage element in a series with a resistor, also called the Rint model.

The real decaying exponential voltage response is modelled only as a step drop, with the terminal voltage V_l represented as:

$$U_l(t) = U_{oc}(SoC) - R_0 i_l(t) \tag{5.1}$$

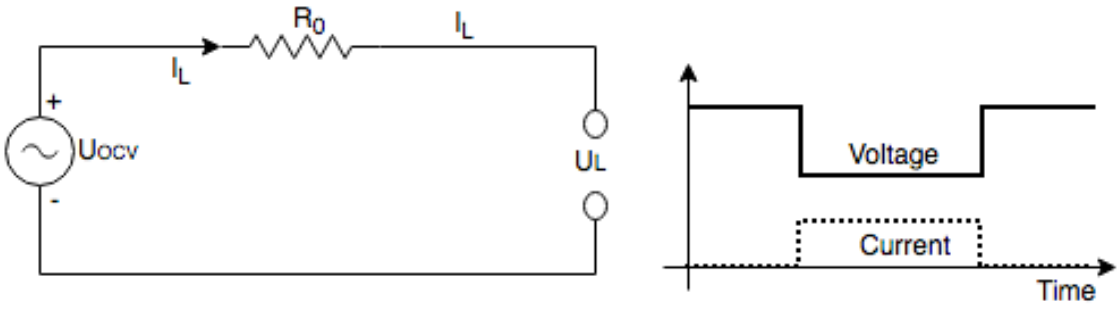

Figure 5.1: Electric circuit representation of the Rint model and illustration of dynamic voltage response

The Rint model, as shown in Equation 5.1, implements an ideal voltage source V_{oc} to define the battery open-circuit voltage, which is a function of the SoC. I_l is load current with a positive value at discharging and a negative value at charging. This uses the open circuit voltage $V_{oc}(SoC)$ and a resistor R to model the equivalent series resistance of the battery (Seaman et al. (2014)).

The Rint model is usually combined with the very basic, yet popular way of obtaining SoC estimates referred to in Table 6.1 as OCV-SoC mapping + Ah-counting.

5.2.1 Thevenin Models

Improvements to the single resistance model can be done by introducing different numbers of parallel RC circuits. These models with multiple RC parallel circuits can be divided into two types (Seaman et al., 2014); Thevenin models and impedance models. Thevinen models usually consist of a single resistor in series with pairs of parallel RC circuits. These type of models are capable of capture the time-dependent effect of battery recovery and charge depletion i.e. the batteries exponentially behaviour upon relaxation and loading. Charge depletion is an effect seen when one first begins to discharge a battery. At first there is a large drop in voltage. This rapid voltage change is restrained due to initially high concentration of active chemicals at both electrodes, and the voltage therefrom decreased gradually. Charge recovery on the other hand, is somewhat the opposite phenomena (Seaman et al. (2014)). Upon discharge the terminal voltage drops, but as the battery relaxes the terminal voltage increases exponentially up to its open-circuit voltage.

Hu et al. (2012) did a study on twelve different adaptions of the Thevenin model to validate their complexity, accuracy, and robustness under highly dynamical test cycles. The two batteries that the models where tested up against was a LiNMC and LiFePo battery. The study's conclusion was that for a LiNMC battery, the first-order RC Thevenin model gave the best combination of fidelity and complexity, giving an average of 7.9mV RMS error in voltage prediction for Hybrid Pulse Test (HPT). A 1. and 2. order RC model can be seen in Figure 5.2,5.4.

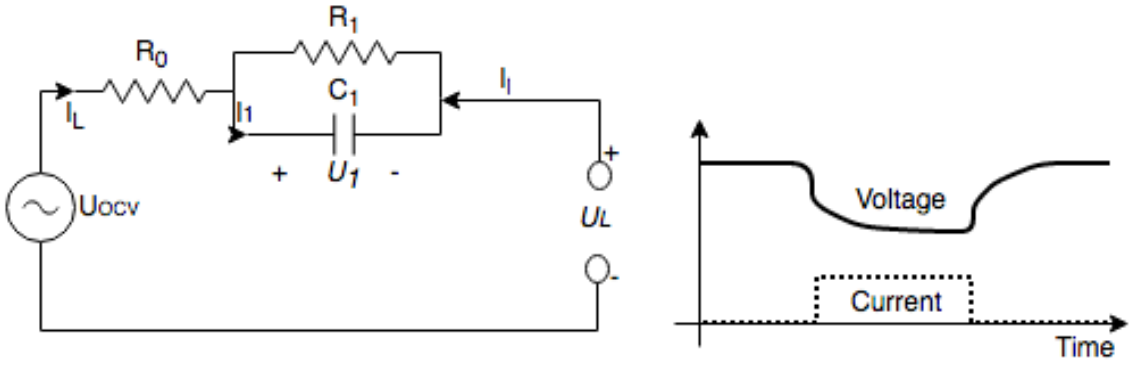

Figure 5.2: Electric circuit representation of the a 1. order model, with illustration of dynamic voltage response

.

R_i models the small initial voltage drop due to chemical processes and the bulk metal resistance in the sensors and terminals. The RC parallel network circuit R_1,C_1 models the charge depletion i.e. battery response to transient load events at a particular state of charge. This allows the model to more correctly emulate the actual behavior of a cell when suddenly loaded. R_1 in a typical lithium ion cell is in the order of few milliohms (10-50Ω). The time constant will be $\tau_1 = R_1 C_1$, which is

on the order of 1 minute (Andrea (2010)).

It should be noted that both Hu et al. (2012) and Andrea (2010) mentioned that adding a second RC parallel network would give better accuracy. This model can referred to as the dual polarization model (DP). By doing so, the polarization happening within the cell i.e. transient behaviour can be more accurately modeled, especially at in the range of 0-10% and 90-100% SoC. This is because the polarization effect are separated into two components separately; concentration polarization and the electrochemical polarization.

In general, the battery parameters of EEC models are obtained through measuring voltage response of the battery with piecewise constant loads. A common practice is discharge the fully charged battery with a constant current until the SoC has dropped by 10%, and then letting it rest for 30 minutes. While continuously measuring voltage, this is repeated until the SoC has reached 0%. Periodic discharge based on time intervals is also quite. If there is only one RC circuit, R_1, C_1 can be found manually by reading of the time constants of the exponential recovery in voltage. If there are multiple RC circuit, methods like least-square regression, Kalman Filter or other parameter identification tools can be used to best fit the measured data.

To make the model more robust in terms of ambient conditions, there has also been done research on incorporating temperature and c-rate effects into the battery parameters, with various methods proposed. Gao et al. (2002) introduces correction factors to the battery capacity and open circuit voltage of the battery that can be calculated from measurements or manufacturers' data sheets (Seaman et al., 2014). Verbrugge and Conell (2002) have the open circuit voltage, resistors, and self-discharge depend on temperature. The model of Baronti et al. (2010) has the resistors depend on temperature, and the model by Lam et al. (2011) has the resistors, capacitors, and usable capacity depend on temperature.

Zhang et al. (2010) uses a discharge-current-dependent charge storage capacitor to model the c-rate effect, which causes the capacity of the battery to diminish with increasing discharge current.

To include dependence's such as temperature and current draw, the parameter identification procedure has to be done for several temperatures and currents. This is extremely time consuming, both because there are more variables, but also because the battery needs to obtain temperature equilibrium with its surroundings throughout the whole pack. Further, it requires the operation to be done in a thermo-chamber so to keep the temperature constant. However, there are smarter ways of incorporating these effects through model observers (Chap. 6).

5.2.2 Impedance models

Impedance models one type of EEC model that uses impedance spectroscopy to obtain an ac-equivalent impedance model in the frequency domain and then use a somewhat more complicated equivalent network to fit the impedance spectra. The fitting process is difficult, complex, and nonintuitive (Vasebi et al., 2007). In addition, impedance-based models only work for a fixed SoC and temperature setting. The author has therefore chosen not to focus any further on these models, mostly due to lack of equipment to obtain model parameters.

5.3 Requirements of battery-model for a battery onboard ROV

To summarize, parameter identification for EC models are non-intuitive and they are generally not well suited for real time online applications due to complexity. Thenevin and its derived models has shown high fidelity and well balanced in terms of complexity and accuracy, and can be made to incorporate the effect of the variables that effect the battery's performance. It is not necessary to

Figure 5.3: Battery model comparison adapted from Dominico et al. (2013).

Batteries modeling

Model	Mathematical complexity	Identification	Required test for identification	Precision	Applications
Ah-counting + OCV	Very low	Basic	I/O measurements	Poor	SOC estimation, cell balancing
Equivalent circuit	Medium	Easy/ little difficult	I/O or EIS	Good	Pack design, thermal management, SOC and power estimation cell balancing, vehicle energy management, charge management
Electrochemical 0D	Medium-high	Difficult	Multi-level single-electrode	Good	Pack design, thermal management, SOC, SOH and power estimation, cell balancing, vehicle energy management, charge management
Electrochemical 1D - pseudo2D	High	Difficult	Multi-level single-electrode	Good/high	Pack design, thermal management SOC, SOH and power estimation, cell balancing, vehicle energy management, charge, fast-charging management

make a complex model that takes into account effects that are unlikely to happen in real operation of the battery. Because of the requirement on the ROV in terms of computational power, a rather simple model is needed. Also, it is preferable with a model that do not need extensive parameter identification and battery testing data. Therefore, some type of EEC model should provide the fidelity that is needed. As mentioned in the section above, these models can have their variables depended on both SoC, temperature and current draw. However, this complicates the testing data

gathering procedure a hole lot, which is not preferable. The requirements on accuracy for both SoC and SOH estimate are not as strict as for HEV or BEV either. This is because the number of cycles the battery in the ROV experiences are most likely much lower than that for a car. Also, the consequences of battery failure, even though that should not happen, are much cheaper and most likely not fatal for the user compared to in an EV, HEV etc.

According to the literature review, either 1. or 2. order parallel RC circuit model will be required to represent the exponential drop or increase upon loading.

5.4 Battery model for Blueyes Pioneer 1

From the literature review, the 1RC or 2RC model seemed to give the best combination of fidelity and accuracy. Because of the possible computational limits enforced by the raspberry Pi on board the drone, both 1RC and 2RC circuits tested to see if one RC parallel circuit was sufficient to model the dynamics. The parameter estimation algorithm used had trouble matching the measured voltage with the 1RC model output. Therefore, it was found necessary to implement the 2RC model.

From Kirchoff's and Ohm's law, the voltage across the RC parallel circuits and the terminal voltage can be expressed as:

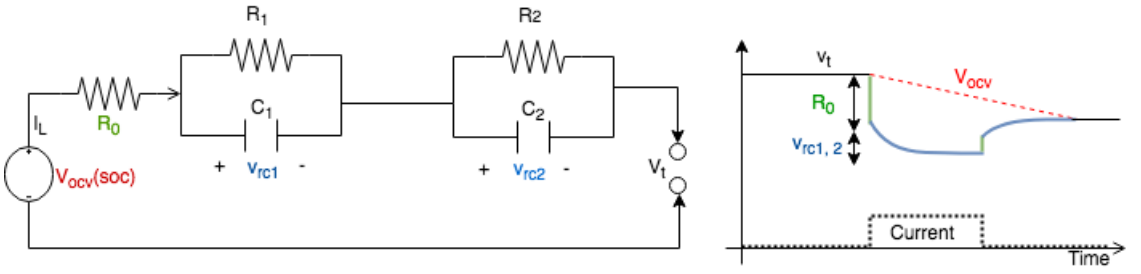

Figure 5.4: Electric circuit representation of the 2. order model, with illustration of dynamic voltage response

.

$$\dot{v}_{rc1}(t) = -\frac{1}{R_1 \cdot C_1} \cdot v_{rc1}(t) + \frac{1}{C_1} \cdot i(t) \tag{5.2}$$

$$\dot{v}_{rc2}(t) = -\frac{1}{R_2 \cdot C_2} \cdot v_{rc2}(t) + \frac{1}{C_2} \cdot i(t) \tag{5.3}$$

$$\dot{z}(t) = z(t_0) - \int_{t_0}^{t} \frac{1}{3600 Q_{tot}} \cdot i(t) \tag{5.4}$$

$$v_t(t) = h(z, i) = v_{oc}(z) - v_{rc1} - v_{rc2} - R_0 \cdot i(t) \tag{5.5}$$

where v_{rc1}, v_{rc2} is the voltage over the parallel circuits R_i, C_i, R_0 the series resistance, terminal voltage v_t, state-of-charge z and $v_{oc(z)}$, a nonlinear SoC-depended open circuit voltage function (Eq. 5.5).

This can be represented in a state-space representation, letting the states $x = [v_{rc1}, v_{rc2}, z]$, input $u = i$ and output $y = v_t$. This results in LTI state-and input matrix A, B, and a nonlinear output equation $h(x, u)$:

$$\begin{cases} x_t &= A \cdot x_{t-1} + B \cdot i_{t-1} \\ y_t &= h_t(x_t, i_t) \end{cases} \tag{5.6}$$

$$A = \begin{bmatrix} \frac{-1}{R_1 \cdot C_1} & 0 & 0 \\ 0 & \frac{-1}{R_1 \cdot C_1} & 0 \\ 0 & 0 & 0 \end{bmatrix} \tag{5.7}$$

$$B = \begin{bmatrix} \frac{1}{C_1} \\ \frac{1}{C_2} \\ \frac{-\Delta t}{Q_{tot} \cdot 3600} \end{bmatrix} \tag{5.8}$$

5.4.1 Training data

The voltage response for this model is a combination of the fast response represented by the R-RC-RC circuit, and the slower response of the OCV voltage element. To extract all the parameters in the proposed model a cell test is performed. In order to ease the separation of the fast and slow dynamics, two different experiments is conducted. During the charging/discharging, voltage, current, temperature of the cell is measured and recorded at 0.1hz for experiment *a* and 1hz for experiment *b*. These measurements can be seen in Figure 5.5-5.10.

The experimental setup is performed on a MACCOR 4200 computer based battery tester with the specifications listed in Table 5.1. The battery test bench was provided by Sintef Materials and Chemistry. Table 5.2 explains the two experiments conducted.

Table 5.1: Accuracy of sensors used in cell testing

Sensor	**Accuracy**
Current	$\pm$ 0.01 A
Voltage	$\pm$ 1 mV

Table 5.2: The procedure of the two lab experiments a and b:

Experiment a: Constant discharge

Action	Detail	Cutoff
1. Discharge	0.15 A	V = 2.5V

Experiment b: periodic discharge

Do step 1,2	while	V $\geqslant$ 2.5V
1. Discharge	1 A	C_{out} = 0.3Ah
2. Rest	1 hour	-

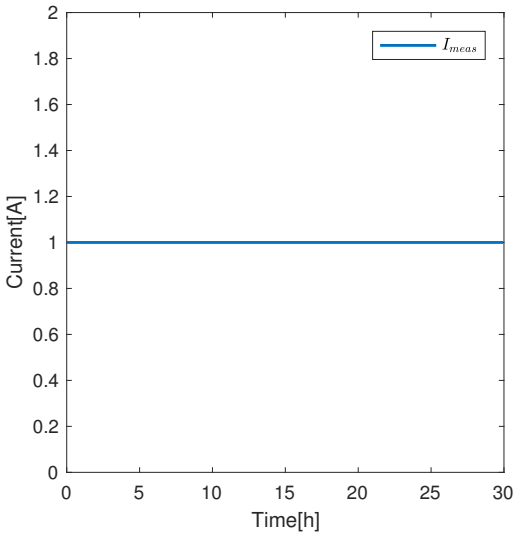

Figure 5.5: Experiment a: Discharge current.

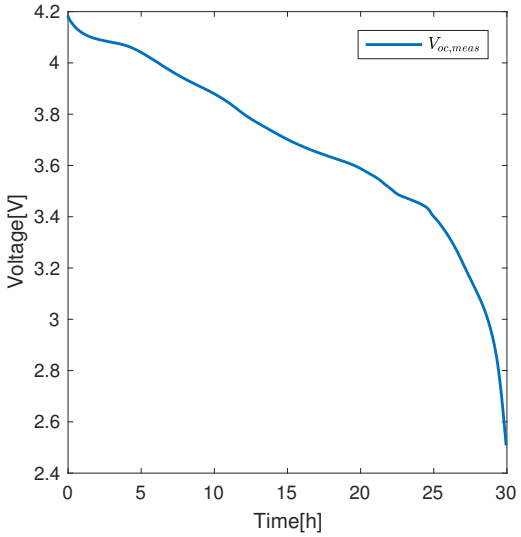

Figure 5.6: Experiment a: Voltage response.

Before the experiments explained in Table 5.2 were conducted, the cell was first charged up to its upper cutoff limit (4.2V) with 1.5A, and then constant voltage to ensure SoC reached 100%. From experiment a (Fig 5.6), the nominal capacity for the new cell matched manufactures specifications with Q_{nom} = 2.997Ah $\approx$ 3Ah. From Figure 5.8, the voltage drop is higher for lower SoC due to the increase in inner resistance, according to theory in Chapter 2.

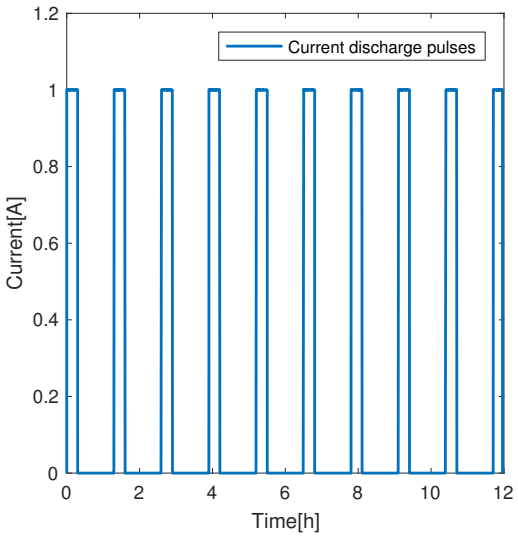

Figure 5.7: Experiment b: Discharge current.

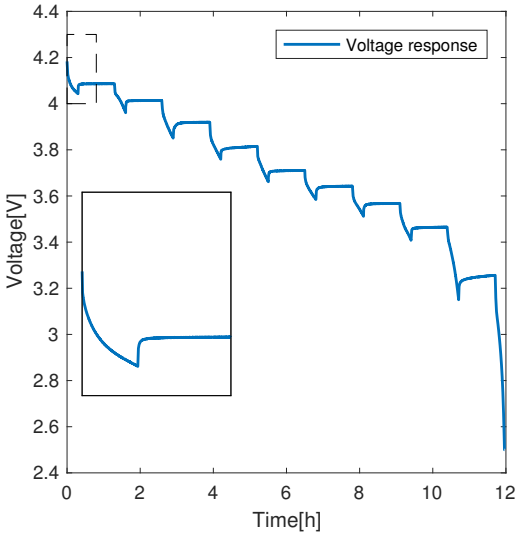

Figure 5.8: Experiment b: Voltage response.

5.4.2 Parameter estimation

The two cell tests a and b is then used to provide OCV-SoC relationship as well as the parameter R_i,C_i, in accordance with Figure 5.9

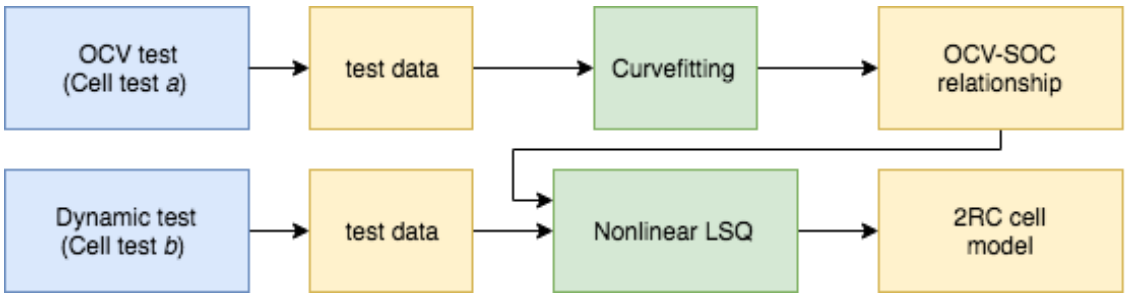

Figure 5.9: Procedure for determining parameters of the model

The OCV-SoC relationship was obtained with the curve fitting toolbox in Matlab. The function candidates are a linear $V_{oc,1}$ and two nonlinear function $V_{oc,2}$, $V_{oc,3}$. These represent different level of complexity, and its performance must be evaluated:

$$V_{oc,1} = k_1 \cdot z + k_0 \qquad z \in [0, 100] \tag{5.9}$$

$$V_{oc,2} = k_1 \cdot e^{k_2 \cdot z} + k_4 \cdot e^{k_4 \cdot z} \qquad z \in [0, 100] \tag{5.10}$$

$$\begin{aligned} V_{oc,3} = {} & k_0 - k_1/z + k_2 z + k_3 + \log z - k_4 \log(1 - z) \\ & + k_5 z^2 + k_6 z^3 + k_7 z^4 + k_8 z^5 \qquad z \in [0, 1] \end{aligned} \tag{5.11}$$

where k_i is constants and z is SoC. The optained constants k_i can be seen in A.2. The later two are nonlinear w.r.t. to the state x_3. For an EKF formulation, which will be explored later in the

thesis, it is necessary that

$$\frac{\delta V_{oc}}{\delta z} > 0 \quad \forall \quad z \quad \in [0, 1] \tag{5.12}$$

to ensure that observability is preserved when linearizing $V_{oc}(SoC)$. Figure 5.5 shows the measured data and the V_{oc} candidates. Figure 5.11 is a plot of $V_{oc,3}$ derivated with respect to SoC. Even though the derivative is close to zero at SoC = 0.9, (5.12) is met. This is also the case for the other two candidates.

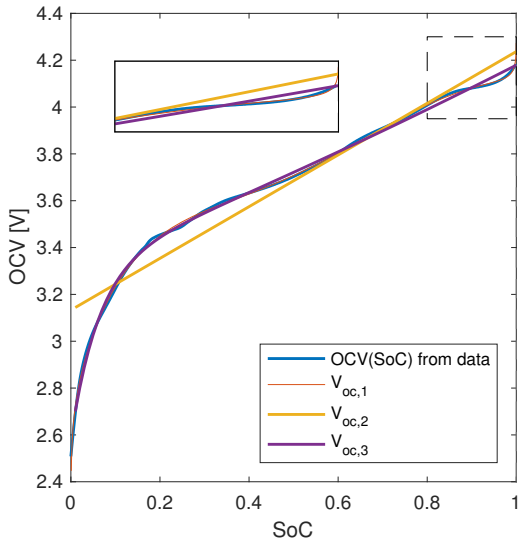

Figure 5.10: Experiment a: Voltage measured for constant 1/30C current to obtain SoC-OCV relationship.

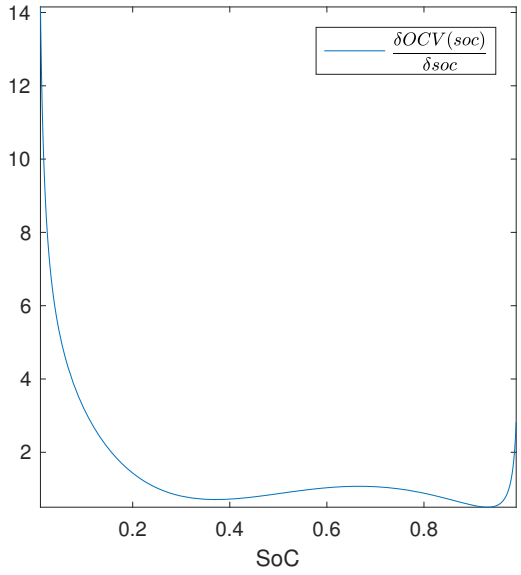

Figure 5.11: V_{oc} derivated with respect to SoC.

The parameters of RC circuit parameters $\beta = R_0, R_1, C_1, R_2, C_2$ is found in a nonlinear greybox modelling fashion with MATLAB Optimization Toolbox. Greybox-modelling is a type of modelling where the model structure is given, but the parameters are uncertain. Given current input and voltage response for each time step provided by lab experiment b, the parameters are adopting so that the sum of the squares of the deviations between measured voltage and model output is minimized.

$$\hat{\beta} = \text{argmin}_\beta \, S(\beta) \equiv \text{argmin}_\beta \sum_{i=1}^{m} [y_i - f(x_i, \boldsymbol{\beta})]^2. \tag{5.13}$$

Levenberg-Marquardt algorithm is used to find these parameters, which is an iterative trust-region based algorithm. It requires an fair assumptions for initial parameters in order to obtain global minimum. The initial parameters was found by studying measurement data. Reading of the instantaneous voltage drop, an initial estimate of the series resistor was found as

$$R_0 = \frac{v_{t,k} - v_{t,k-1}}{i_k - i_{k-1}} \tag{5.14}$$

Estimating the time constant

$$\tau_i = R_i \cdot C_i \tag{5.15}$$

of the exponential behaviour in the relaxation phase, and knowing that R_i should be in the magnitude of R_0, an initial guess of R_i, C_i is found. The benefit of having the parameters as a function of SoC is also explored. Theoretically, a small increase in resistance and time constants is expected as SoC reaches lower values. The voltage measurements is separated into 9 section, one for each discharge cycle. Then the parameter estimation algorithm is optimizing the parameters over each cycle. The inital states is assumed to be x_o = [0, 0, i]^T, where i goes incrementally from 10-90. This assumption can be relaxed as the battery has 1 hour relaxation between cycles i.e. the only present voltage is the open circuit voltage. The estimated parameters is presented in Table 5.3.

Table 5.3: Results of parameter estimation

SoC	R_0[mΩ]	R_1[mΩ]	C_1[F]	R_2[mΩ]	C_2[F]	τ_1[s]	τ_2[s]
-	9.49	14.83	6166.3	26.6	600	91.45	15.6
90	19.1	1.4931	5150.3	15.43	500	7.6	7.71
80	13.102	9.7644	5116.9	13.385	1490.1	49.9	19.9
70	18.151	25.755	5000	15.269	1500	128.8	22.9
60	14.181	12.902	5059.3	19.873	930.37	65.3	18.5
50	12.448	13.476	10900	14.554	1089.6	146.9	15.9
40	17.346	2.1202	13881	24.198	1498	29.43	36.5
30	7.4212	12.519	5000.3	18.579	1144.7	62.6	21.3
20	16.724	4.3921	8644.3	24.791	1356	37.9	33.6
10	21.2485	18.6	5014.4	14.69	967.54	148.64	17.1

From Table 5.3 it can be seen that estimation using the whole dataset is close to taking the average of the individual parameter over all SoC i.e. $\bar{\beta}_i(SoC) \approx \beta_i$. Further on, β_i shows no linear dependency on SoC. The increase in resistances and time constants are present, with overall higher resistances and time constants at lower SoC. It should be noted that the parameters where constrained under estimation, so that the algorithm would provide more consistent results. Lower and upper bounds were set so to insure that the first RC element had longer time constant than the other. However, as the values are unknown, the bounds could not be to strict to prohibit saturation of the parameters. The bound limits might cause dependencies in β_i that is not present.

5.4.3 Validation and Results

The root mean square error (RMSE) of the voltage response is used as a performance criteria for the open-loop 2RC model. RMSE has the benefit of being interpretable in the original units of the data, which for this case is voltage. Table 5.4 shows the RMSE between $V_{oc,i}(SoC)$ compared to data voltage data from experiment a, as well as RMSE for the complete model (5.2-5.5) with the

parameters identified in previous section (Table 5.3) combined with $V_{oc,3}$ function for experiment b.

Table 5.4: RMSE between the model and measured voltage.

Element	$V_{oc,1}$	$V_{oc,2}$	$V_{oc,3}$	2RC model*	2RC model**
RMSE[mV]	95.8	15.5	7.94	17	13.8

*Eq. 5.2-5.5 with $V_{oc,3}$ and fixed β. **$V_{oc,3}$ and β(SoC).

As expected, the linear $V_{oc,1}$ does not provide sufficient accuracy to represent the OCV. Both the nonlinear function $V_{oc,2}$, $V_{oc,3}$ are sufficiently good to model to relationship. However, studying the OCV in the range z = 90-100%, $V_{oc,3}$ better captures the exponential increase in OCV at the very end-condition. It can be important to capture this behaviour since it is so close to its maximum voltage limit at 4.2V. Therefore, $V_{oc,3}$ is the chosen open circuit voltage. The benefit of having β(SoC) is small (3.2mV), except SoC range from 0-5%. On one hand this is the most important range for which the model must be accurate. On the other hand, it is common practices to define a slightly higher cutoff limit than specified by manufacture to as an extra safety measure due to modelling error, aging effects and measurement noise. Therefore, it is not found necessary to make the variables depended on SoC.

Figure 5.12 shows the measured voltage and model output in Equation 5.5. In Figure 5.13, the error $e(t) = v_{t,meas} - v_t$ is plotted.

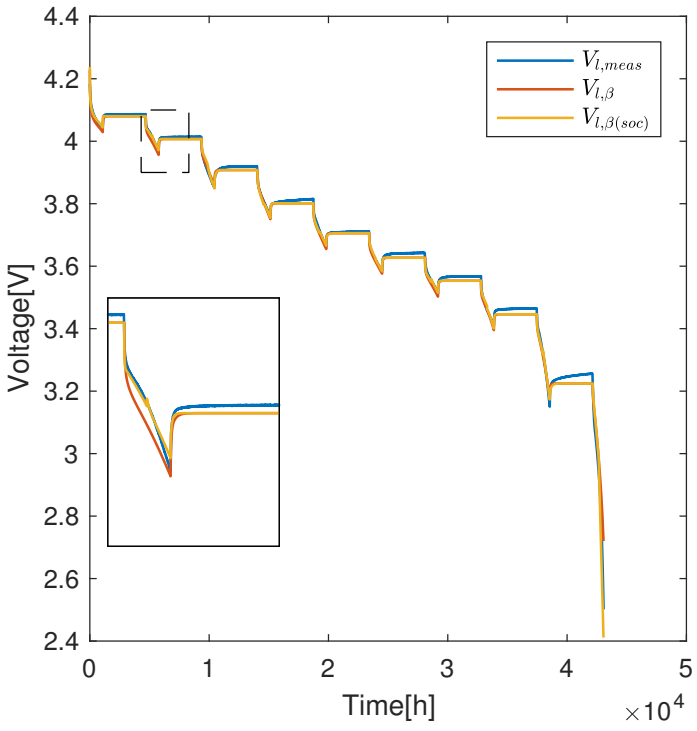

Figure 5.12: Model output terminal voltage v_t and measured terminal voltage $v_{t,meas}$.

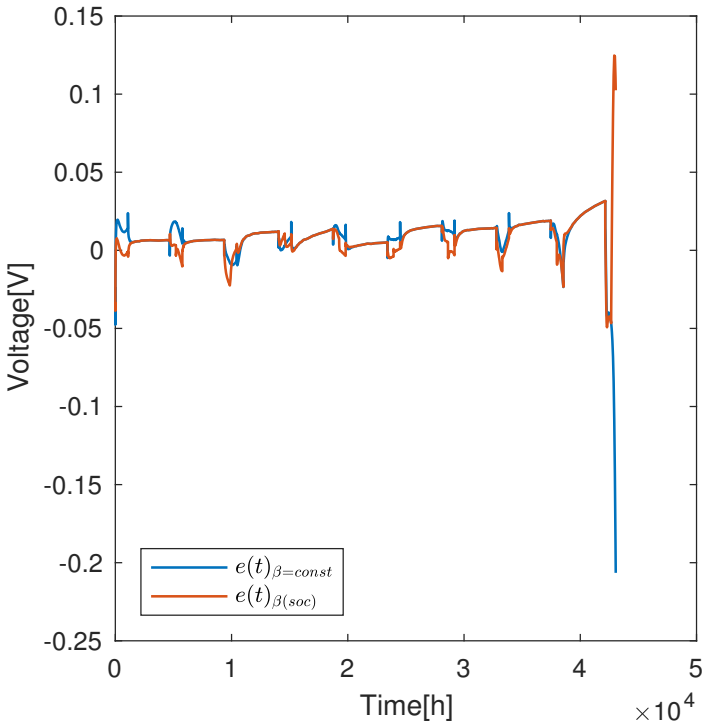

Figure 5.13: Error between v_t and measured terminal voltage $v_{t,meas}$.

5.5 Summary

The aim of this chapter was to find a suitable batter model to represent the voltage response of a battery cell. A conclusion of this chapter can be summerized as follows:

- The more complex $V_{oc,3}$ function is chosen to model the OCV-SoC relationship. $V_{oc,3}$ will be referred to as V_{oc} from this point on.
- Having the parameters β dependent on SoC did not provide any significant improvement. β is therefore set to be constant over SoC dimension.

Combing $V_{oc,3}$ with the β, the complete open-loop-model shows good performance for these specific conditions.

However, because of nature of an open-loop model, there is no robustness in terms of temperature, aging etc. This model is also incapable of estimating the initial State-of-Charge as it is build right now. The latter could be handled in a straightforward manner by assuming the first voltage measurement is the OCV, and do a OCV-SoC mapping. On the other hand, there are more elegant ways of incorporating this capability, which also opens up new possibilities in terms of measure-

ment noise and bias handling, online parameter estimation, SoH and SoP estimation etc. This will be further discussed in the next chapters where an Extended Kalman Filter (EKF) is introduced.

6

State-of-Charge Estimation

6.1 Methods of State of Charge estimation

The state of charge for a battery is a fuel tank equivalent of a fuel gauge. That is, it tells how much percentage of the capacity its left compared to a fully charged battery. There are various definition of SoC with various details. From a chemical point of view, SoC is defined from the lithium concentration stoichiometry as (Plett, 2016):

$$z_k = \frac{\theta_k - \theta_{0\%}}{\theta_{100\%} - \theta_{0\%}} \tag{6.1}$$

where $\theta = C_{s,avg,k}/C_{s,max}$ and C_s the average lithium concentration of the negative cathode. This is a precise, yet infeasable definition of SoC, because there are no sensors that can read C_s directly. Therefore it is a property that has to be estimated through other states that can be easily measured, such as voltage and current. The following definition of SoC is therefore used:

- A cell is fully discharged when its open-circuit-voltage reaches lower cutoff voltage v_{lim}^{dis}, specified from manufacture at a given temperature. SoC is then 0%.

- A cell is fully charged when its open-circuit-voltage reaches upper cutoff voltage v_{lim}^{chg}, specified from manufacture at a given temperature. SoC is then 100%.

In literature there are multiple ways for SoC-estimation, ranging from very basic to advanced and complex models. Table 6.1 summarizes some of these methods used for lithium-ion batteries. Offline estimation methods are not considered, as it is of no use for the ROV application.

Table 6.1: Comparison of the different methods of obtaining SoC-estimates

Method	Advantages	Disadvantages
AH-Counting	Very easy to implement, Accurate if if not recalibration points and noise free current measurements	Open-loop, sensitive to the current sensor precision, and uncertain to initial SoC
OCV-SoC Look-up Table	No need for initial SoC value.	Needs long rest time (current=0), Open-loop, sensitive to the voltage sensor precision, unsuitable for cells with flat OCV–SoC curves
OCV-SoC mapping + Ah-counting	Gets initial SoC from OCV-SoC mapping, use AH-counting for relative change, recalibrate SoC with OCV-SoC mapping at either end.	Still inaccurate estimates in SoC = 30-70%, must know actual pack capacity, depended on accurate SoC-OCV relation.
Model based estimation		
In general	More efficient usage of capacity, more accurate estimates.	Extensive laboratory data, increased complexity with parameter identification, model-dependent accuracy
OCV-SoC mapping + IR-compensation + Ah-counting	Closed-loop; Can give information about SOH, computationally inexpensive, good accuracy for short time intervals.	Large fluctuations in SoC estimate. Easy implementation
Extended Kalman Filter	Closed-loop; Best accuracy for weak observability compared to other observer designs	Affected by tuning, more computationally expensive than non-feedback methods, and highly depend on the model accuracy.
H_{inf} observer	Closed loop,Handles biased current sensor and perturbation in parameters well	Not as accurate as EKF for weak observability.
Fuzzy logic	Generic, good nonlinearity mapping approximation	Sensitive to the amount and quality of training data.
Neural networks	Generic, good nonlinearity mapping approximation	Sensitive to the amount and quality of training data.

Generally, the two most common ways of estimating SoC are either by voltage translation or current integration. Both techniques have their own limitations and advantages. By knowing the relationship between OCV and SoC (5.11) and measuring terminal voltage, SoC estimate can be obtained as $z = OCV^{-1}(v_{meas})$. This is a poor estimate, as the SoC depends on the OCV and not terminal voltage. Corrections can be made by modeling the inner resistance of the battery (OCV-SoC with IR-compensation) to compensate for the ohmic voltage as

$$z = OCV^{-1}(v_{meas} - iR_0) \tag{6.2}$$

This produces better results, but still misses the effects of diffusion voltage. That is why a model that incorporates at least one RC circuit is necessary. This was obtained in the previous chapter (5.2). Even with diffusion voltage modification, there is still not an good way of knowing these values in an open-loop. Lastly, there are areas of the OCV-SoC figure with poor observability i.e. $dV_{oc}(z)/dz \approx 0$ (80-90%), which can result in a poor mapping to SoC.
Looking at current methods of obtaining SoC estimates, coulomb counting i.e. current integration gives the relative change in charge compared to an initial SoC estimate

$$\dot{SoC}(t) = SoC(t_0) - \int_{t_0}^{t} \frac{1}{3600 \cdot Q_{tot}} \cdot i(t) \tag{6.3}$$

Given perfect current measurements and perfect initial SoC estimate, AH-counting would lead to exact SoC. This method is what is used in the last chapter to verify the models accuracy in terms voltage response. Stand-alone, this method has its major limitations. First of all, it must be recognized that neither capacity Q_{tot} or z_{t_0} are really known. There are therefore no feedback mechanism (e.g. voltage based) to correct this error over time, best case leading to a constant error. Also, this technique tend to drift, as it is integrating possibly noisy and biased current measurements.

Combinations of recalibrating SoC estimates from Ah-counting with voltage-based SoC methods is possible, but estimates will still be uncertain for SoC values where OCV-SoC relationship is flat. For further derivations on the non-model based SoC estimation teqniques (Tab. 6.1, 1-3), see Codecà et al. (2011).

Other reported methods for estimating SoC have been based on artificial neural networks (ANNs) (Chan et al., 2000) and fuzzy logic principles (Singh et al., 2004). The main advantage of the ANN-based methods, which makes them distinguishable from the other methods, is that they are capable of estimating SoC when the initial SoC is unknown. However, the implementation of these methods is relatively expensive and needs the training data of a similar battery (Vasebi et al., 2007), which may limit the application of these methods. In contrast, in fuzzy-based techniques, easy implementation is a great feature. Fuzzy logic and ANN-based methods are used to avoid

the need for a large number of empirically derived parameters required by the other methods, so these methods are best suited for portable equipment applications where precise predicting of SoC is not needed (Vasebi et al., 2007).

Recently, unscented and extended Kalman Filter techniques-based methods have been used to estimate SoC. Kalman filter is an intelligent and optimal method for estimating the state of a dynamic system; therefore many researches have used this predictive nature of KF to estimate SoC. What other factors than SoC is being estimated various in great deal for the EKF methods, and thereof also the respective battery model. Huria et al. (2013) implements a simplified EKF formulation with SoC as the only state in a feedback with a 1. order RC paralell network EEC model. The SoC estimate provided by AH-counting was only corrected every 10 minutes by the estimate provided by the EKF reducing computational requirements of a more advanced EKF formulation. The SoC estimation error was found to be within 4% of true SoC value. True value was assumed to be found by AH-counting with lab precise current sensor. Walder et al. proposed a combined online state and parameter identification through dual kalman filter proposition. The same method was suggested by Plett. In the former the main objective was to get as precise SoC estimate as possible, but Plett wanted to explore the possibilities of incorporating every aspect of estimation such as initialization, reliable SoC and SOH estimates, self discharge, dynamic power estimates and enhance the selection of cells that require equalization. The takeaways from Pletts research in the scope of this prestudy was the following; SoC error was within a few percent and it was more accurate than state-the-of-art current sensors combined with AH-counting (even EKF had much poorer sensors). The proposed method was computational expensive compared to a simpler method, but the paper concluded that an EKF approach had its advantages in the long term in that simpler methods had to add a lot of correction terms, such as temperature, cell aging etc., boiling it down to a spaghetti-heap of correction factors and special cases in order to get close to the same results. Fridholm et al. (2014) did a comparison test between the EKF, unscented KF and the H_{inf} observer to test for robustness in SoC estimates with a 1 RC ECC model. The paper concludes that for batteries with weak relation with between OCV and SoC, the EKF gave slightly better results than the H_{inf} observer, though given the right tuning. The authors did however report that the EKF came short of the H_{inf} observer for highly biased current measurements. The need for current bias estimation will therefore be explored later in this chapter.

The level of accuracy of SoC estimates for PE application are low as the power consumption is low and close to static. EVs,HEVs and ROVs however, have an operational profile characterized by high power peaks and highly dynamic loadings. Therefore, stricter requirement for precise SoC estimates are needed. It should be noted that SoC estimates are not necessary for operating the pack safely, but can aid in the work of doing so while also using the pack efficiently. By having a precise SoC estimate, we get

- Increased life expectancy: as we prevent overcharge- and discharge.
- Higher performance: Poor estimates would force the designer to be overly conservative to avoid under/over charge. By having good estimates, as well as a measure of how precise they are, one can more aggressively use the entire pack capacity and thereof also reduce costs and space of battery design.

Identified obstacles that the open-loop model from last chapter could not handle, and why an model-based observer such as EKF is proposed can be seen in the list below:

- Handle initialization of SoC estimate.
- Handle noisy current and voltage measurements.
- Handle biased current measurements.
- Handle temperature effects.

In this chapter the EKF algorithm is implemented in SIMULINK, and its capability to estimate SoC is evaluated through a sensitivity analysis on sensor noise and bias, temperature and aging.

6.2 Extended Kalman Filter

The EKF is based on the concept of least square estimation to obtain the observer gain K, where it minimizes the variance of the error dynamics. The EKF is the linear KF extended version for nonlinear systems. In contrast to the LKF, there are no guarantee of optimally or convergence, as it depends on the linearized equations ability to represent the system at each timestep k.

Without loss of generality we consider the nonlinear system:

$$\begin{aligned} \mathrm{x}_k &= f(x_{k-1}, u_{k-1}, v_{k-1}) \\ \mathrm{y}_k &= h(x_k, u_k, w_k) \end{aligned} \tag{6.4}$$

where v_k,w_k is assumed to white Gaussian, independent random process with zero mean and covariance matrix

$$E[v_k v_k^T] = R_k, \quad E[w_k w_k^T] = Q_k \tag{6.5}$$

representing the process and measurement noise, respectively. Using the 2RC battery model, it can be seen that the model is only nonlinear in its output equation $h(x_k, u_k, w_k)$. Further on, using $\hat{\beta}$ the system is time invariant. That means that (6.4) can be rewritten:

$$\begin{aligned} x_k &= A_k x_{k-1} + B_k u_{k-1} + \mathrm{v}_{k-1} \\ y_k &= H_k x_k + D_k u_k + w_k \end{aligned} \tag{6.6}$$

with the system matrices as:

$$A_k = e^{A\Delta t} = \begin{bmatrix} e^{\frac{-\Delta t}{R_1 \cdot C_1}} & 0 & 0 \\ 0 & e^{\frac{-\Delta t}{R_1 \cdot C_1}} & 0 \\ 0 & 0 & 1 \end{bmatrix} \tag{6.7}$$

$$B_k = \int_0^{\Delta t} e^{A\Delta t} = \begin{bmatrix} R_1(1 - e^{\frac{-\Delta t}{R_1 \cdot C_1}}) \\ R_2(1 - e^{\frac{-\Delta t}{R_2 \cdot C_2}}) \\ \frac{-\Delta t}{3600} i_k \end{bmatrix} \tag{6.8}$$

$$H_k = \frac{\partial h}{\partial x}\Big|_{\hat{x}_{k|k-1}} = \begin{bmatrix} -1 & -1 & \frac{\partial V_{oc,3}}{\partial SoC}|_{S\hat{o}C_{k|k-1}} \end{bmatrix} \tag{6.9}$$

$$D_k = -R_0 \tag{6.10}$$

where zero-order-hold (ZOH) method has been used to discretize the system (5.3-5.6). The recursive EKF algorithm for calculating the states, optimal feedback gain, state covariances and output voltage is listed in (6.11-6.19). For further derivations on Extended Kalman Filter, see (Simon, 2006).

Initialization

$$\hat{x}_{k=0} = X_0 \tag{6.11}$$

$$\hat{P}_{k=0} = E[(x(0) - \hat{x}(0))(x(0) - \hat{x}(0))^T] \tag{6.12}$$

Predictor

$$\bar{P}_k = A_k \hat{P}_k A_k^T + Q \tag{6.13}$$

$$\bar{x}_k = A_k \hat{x}_k + B_k \hat{u}_k \tag{6.14}$$

Corrector

$$K_k = \bar{P}_k {H_k}^T [H_k \bar{P}_k {H_k}^T + R]^{-1} \tag{6.15}$$

$$\tilde{y}_k = y_k - h(\bar{x}, u_k) \tag{6.16}$$

$$\hat{P}_k = (I - K_k H_k)\bar{P}_k (I - K_k H)^T + K_k R {K_k}^{-T} \tag{6.17}$$

$$\hat{x}_k = \bar{x}_k + K_k \tilde{y}_k \tag{6.18}$$

$$\hat{y}_k = h(\hat{x}_k, u_k) \tag{6.19}$$

When the algorithm is initilized with the states x_0 (6.11) and covariance matrix $\bar{P}_{k=0}$ (6.12), the a-priori estimates of covariance matrix $\bar{P}_k$ (6.13) and state $\bar{x}_k$ (6.14) can be found. Upon measurement update, the optimal Kalman matrix gain K_k is calculated (6.15). The residual $\tilde{y}_k$, that is the error between measurement and estimated output can be found (6.16), and used together with K_k to calculate a corrected (posteriori) state estimate $\hat{x}_k$ (6.18). The updated covariance matrix $\hat{P}_k$ (6.17) is found, as well as the output estimate $\hat{y}$ (6.19). Except of the initilization, these steps are performed at each time-step k.

6.2.1 Observability

The observability property for a linear discrete system is defined by (Simon, 2006) as a system in which

.. for any initial state x_0 and some final time k the initial state x_0 can be uniquely determined by knowledge of the input u_i and output y_i for all $i \in [0, k]$.

For the linear case, this definition deduces to the rank condition lemma of the observability matrix (Simon, 2006, p. 41):

$$rank(\mathscr{O}) = rank\left(\begin{bmatrix} H & HA & HA^2 & ...HA^{n-1} \end{bmatrix}^T\right) = n \tag{6.20}$$

where n is the total number of states. The requirement for the system to be local observable at x_0 is that rank($\mathscr{O}$) = n. That can easily be checked by ensuring det($\mathscr{O}$) $\neq 0$.

In the literature, it is common practice to simply equate the local observability of a nonlinear system with the observability of its linearised system (Zhao and Duncan). That is because observability for nonlinear systems are much more difficult to formalize (Simon, 2006). Cation should be taken when using the systems linearized version to conclude on weather the system is observable or not. That is because the rank condition lemma is only a sufficient, but not necessary condition for a nonlinear system to be locally observable at x_0. That means that a nonlinear system can be proved locally observable at every x_0 if the rank condition holds for its linearized version, but the converse does not hold.

The observability matrix for system is given as

$$\mathscr{O} = \begin{bmatrix} -1 & -1 & \frac{\delta V_{oc}}{\delta z}(z_0) \\ \frac{1}{\tau_1} & \frac{1}{\tau_2} & 0 \\ \frac{1}{\tau_1^2} & \frac{1}{\tau_2^2} & 0 \end{bmatrix} \tag{6.21}$$

which has full coloumn rank if and only if $\frac{\delta V_{oc}}{\delta z}(z_0) \neq 0$ and $\tau_1 \neq \tau_2$. If $\frac{\delta V_{oc}}{\delta z}(z_0) = 0$, it would not be possible to obtain any information on the open circuit voltage from the SoC estimates. This was however ensured in Section 5.4.2. The latter restriction is always ensured as $\tau_1 \neq \tau_2 =$ constant. The nonlinear system (Eq.6.7-6.10) is therefore locally observable.

6.2.2 Initilization

Adjusting R and Q, the filter can be tuned to produce the best estimate. Generally, a large R means low confidence in the sensors because R represents the uncertainty/noise in the sensor measurements. A fair estimate of R can be obtained by either knowing the sensor accuracy from manufacture or calculating the variance of the measured signal. A large Q on the other hand, represents high confidence in the model. Q is more difficult to get a good estimate of, and the discussion of finding Q is often left unexplained in the literature. Even though there have been developed methods to automatically find a guess for Q, common practice is try-and-error based the knowledge you have of the system and your model together with the desirable observer behaviour.

Assuming that the driving cycle obtained in Chapter 3 can represents a standard operational profile, the average current discharge is 0.65A per cell. That means that the ROV is completely discharged in $\frac{C_{nom}}{0.65A} = 4.6$ hours. The maximum change in SoC is 1. The maximum change in v_{rc1},v_{rc1} is found to be 0.18 and 0.06 respectively. These values are found by inspecting the states at the time interval where validation current is high. The maximum change per step in SoC and v_{rc1},v_{rc2}:

$$\begin{aligned} max(|dz|) &\approx \frac{1}{3600 * 4.6} h = 6.0e-05 \\ max(|v_{rc1}|) &\approx \frac{0.12}{3600 \cdot 4.6} h = 7.3e-05 \\ max(|v_{rc2}|) &\approx \frac{0.04}{3600 \cdot 4.6} h = 2.4e-6 \end{aligned} \tag{6.22}$$

where the sampling time h = 1s. The accurate lab voltage sensor had an accuracy of 0.01% FSR. The voltage sensor accuracy onbaord the drone is unknown, but can be assumed to be in the range of 1%, which gives 1%·4.2 = 0.042. The resulting Q and R (6.23) are unchanged unless specified:

$$\begin{aligned} \mathbf{Q} &= \cdot diag\{(max|dSoC|)^2, (max|v_{rc1}|)^2, (max|v_{rc2}|)^2\} \\ &= diag\{1.4e-8, 1.57e-09, 3.6e-7, 1.0e-09\} \\ \mathbf{R} &= \cdot 0.042^2 = 1e-3 \end{aligned} \tag{6.23}$$

The initial covariance $\hat{P}_0$ indicates how accurate and reliable the initial guess are. Assuming maximum initial error guess 0.1 for SoC, and that the remaining states are initialized close to its

correct value:

$$\begin{aligned}\hat{P}_0 &= diag(1e-5,\ 1e-5,\ 0.011e-5)\\ \hat{x}_0 &= [0,\ 0,\ SoC_{true}-0.01,\ 0.00949]^T\end{aligned} \tag{6.24}$$

6.3 Non-ideal sensors

6.3.1 Non-ideal current sensor

The two most common current sensors is either a Hall-effect sensor or a Shunt current sensors. Both type of sensors are often subject to a bias I_{bias} in their measurements.

$$I_{true,k} = I_{meas,k} - I_{bias,k} \tag{6.25}$$

For the former, the bias comes from the sensors dependency on magnetic circuity. The Shunt current sensor is inherently bias-free, but the electronics that amplify the voltage drop over the Shunt resistor may introduce a bias. Therefore, the sensors are calibrated upon installation to ensure that measured current is zero when the battery is at rest. However, the current bias is time-and temperature dependent, and an initial calibration will therefore only partially solve the problem. One way of handling this could be that the system reports to the BMS whenever the load is zero. The bias can then be identified and subtracted from the measurements. However, for this application this would not work because it is never a situation where the load is completely zero. The Ah-counting method is defenceless in terms of biased current measurements. The EKF however, is more robust in the sense that it uses voltage measurements as feedback for state estimation. Even so, the under-laying assumption of the EKF is that the noise is Gaussian with known mean. Since the bias is unknown, it could still introduce permanent SoC error if the accumulated Ah of the bias move SoC faster than the voltage measurement can correct. This can easily be handled by altering the states of the EKF formulation. Before introducing additional bias state, the ability of the EKF to handle biased current sensor is evaluated. Biased estimation is therefore not included in Chapter 6.

6.3.2 Non-ideal voltage sensor

The voltage sensor can also have a bias, but this is less intuitive to handle as there are no "true" readings. However, this is often not a problem as the bias is in order of a few milliohms, and therefore having a negligible effect on the SoC estimation.

6.3.3 Sensor Faults

Sensor faults are generally not a problem, as most of modern measurement chips have build in checksums to aid in the fault detection. If that it is not the case, some signal processing is needed. For voltage sensor fault, a solution could be to check the variance of difference between output voltage from the EKF and measured voltage:

$$e = y_{meas} - y_{ekf} \tag{6.26}$$

This would however require that the model is highly accurate for all conditions. This is naturally a desire for all modelling. The EKF will, as seen in figure 6.1, converge to the measured terminal voltage. However, upon loading small error peaks are present due to modelling errors and other unmodeled effects. Assuming that sensor fault would lead to i) voltage measurement drops to zero ii) frozen measurement, a simple variance test of the measurement signal is sufficient.

Current and temperature sensor faults are not that easy to detect. Current can jump drastically from one time step to the next, and variance tests are therefore not possible. Looking for covariance between two sensors is the only way to detect current sensor fault. For the temperature sensor, it is possible to include a temperature model describing the relationship between temperature and current together with heat transfer of ambient temperature. None of the above is regarded as necessity for such a small-scale system as the ROV.

6.3.4 Simulation

In order to better evaluate the effect of non-ideal measurements and to display the benefits of the EKF, the output and states will be compared to:

- An open-loop model as defined in Chapter 4, with non-noisy random generated current measurements. This process will be treated as the true process.
- An open-loop model as defined in Chapter 4, with noise/bias added to its measurements. This method will be compared to that of EKF observer.

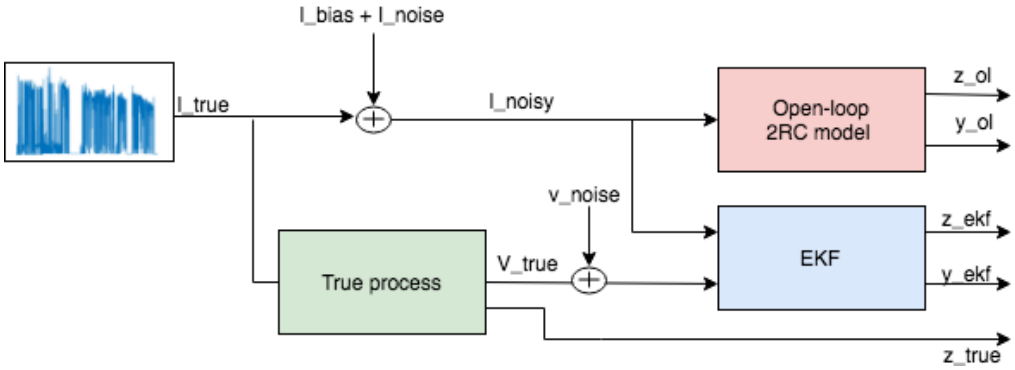

Figure 6.1: Scheme for testing noise handling of EKF

The robustness of SoC estimates provided by the EKF is compared to that of AH-counting, where the initial SoC is found through OCV-mapping of the first voltage measurement. Assuming 1% voltage accuracy of the sensor installed and that the drone will be initialized, in most cases, in a fully charged state, the initial error in SoC is found as 4%. Looking at 5.11, the worst initial SoC estimate through OCV-SoC mapping is at the point where $dV_{oc}/dt \approx= 0$ e.g. from 30-40% and 90-95%. Given sufficient time between the charge-and discharge cycle, the battery will often be initialized within the latter SoC region. This would lead to an initial error of 8% in SoC, and is the value that is assumed for the AH-combined method. Three different EKF's where initialized with 0-30% offset from true values:

Table 6.2: Initialization and noise characteristics.

Model	i_{bias}	I_w	V_w	SoC_{init}
True	0	0	0	95
OL	0.2	0.02	0.01	88
EKF_1	0.2	0.02	0.01	88
EKF_2	0.2	0.02	0.01	80
EKF_3	0.2	0.02	0.01	70

6.3.5 Simulation results

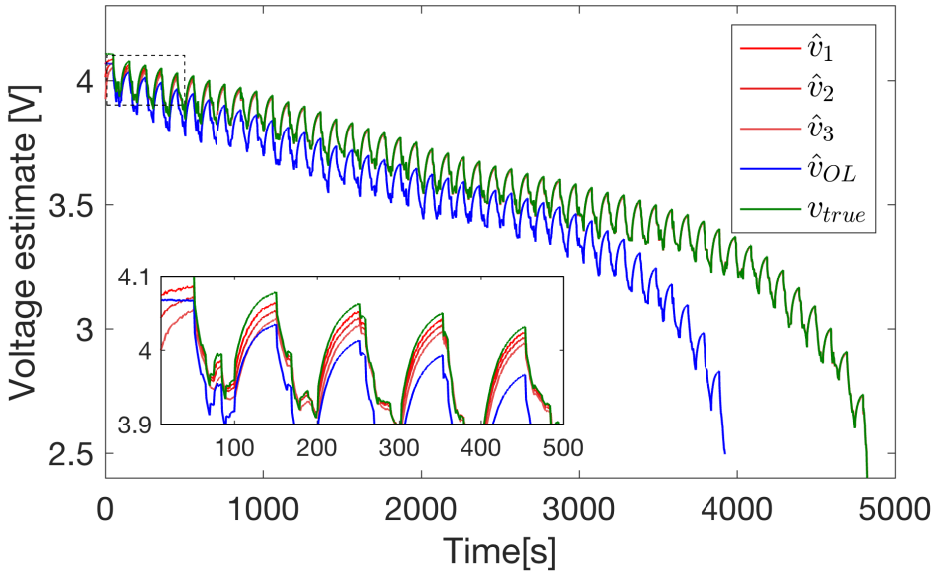

Figure 6.2: Output voltage response

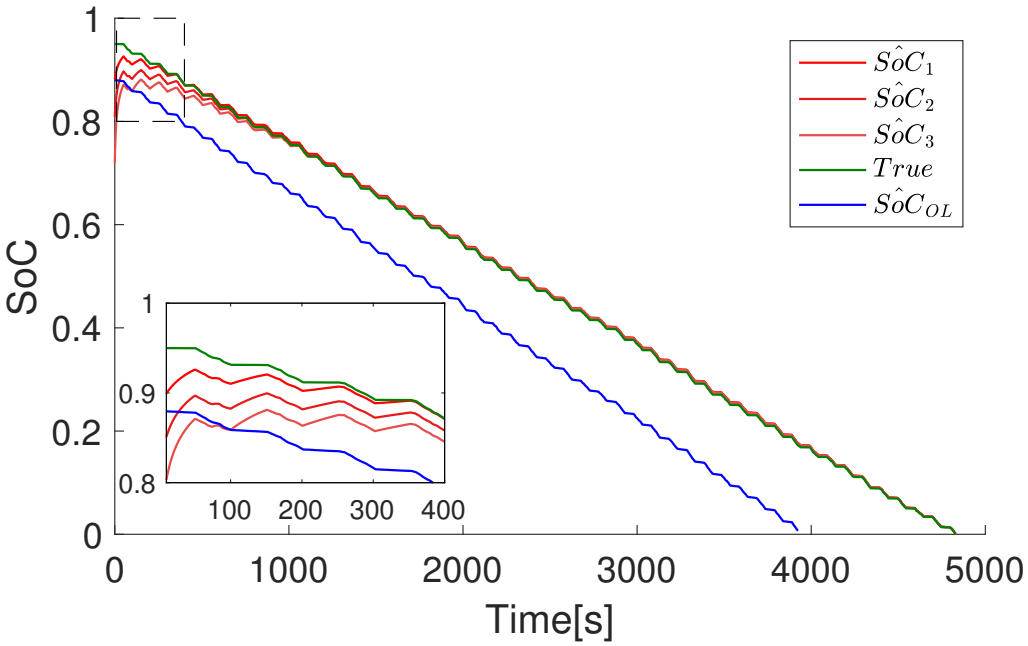

Figure 6.3: SoC estimates for the various initilizations.

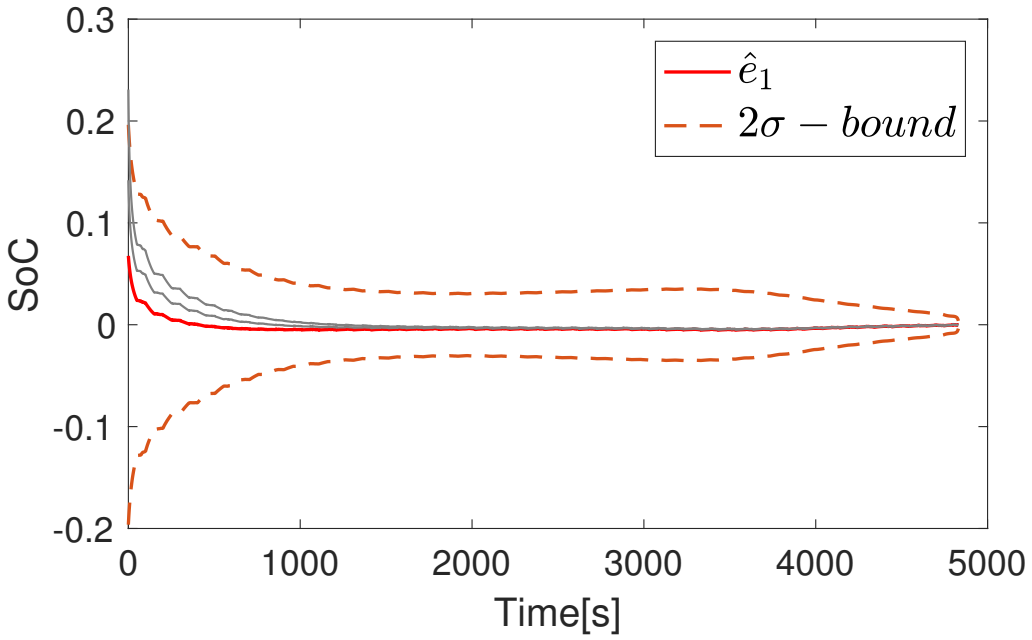

Figure 6.4: SoC estimates with confidence intervals. Case 1 highlighted in red.

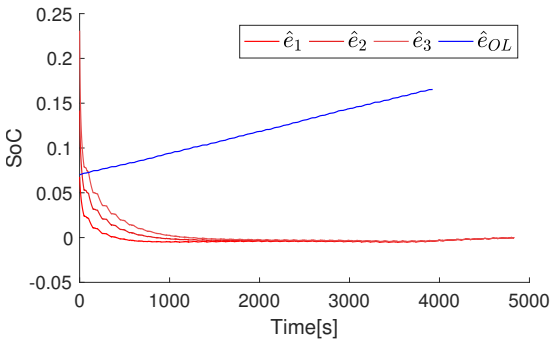

Figure 6.5: Error in SoC esimates.

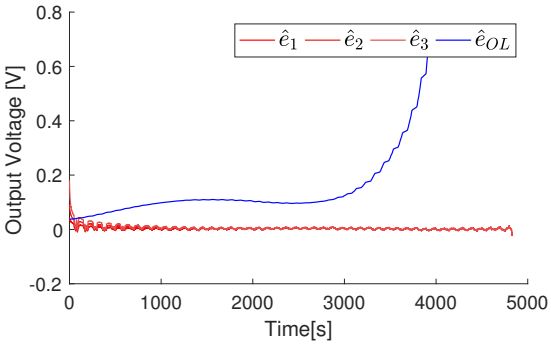

Figure 6.6: Error in output terminal voltage estimates.

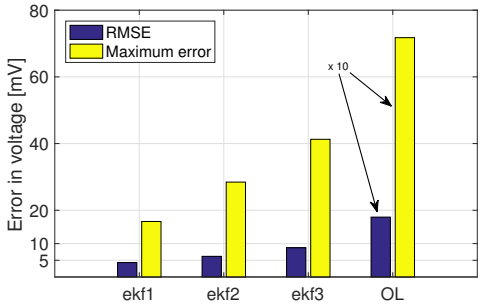

Figure 6.7: RMS and maximum error in output voltage for the various initilizations of EKF and the open loop model.

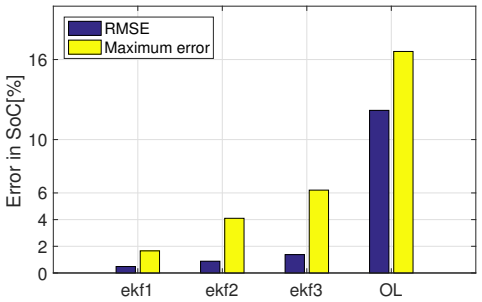

Figure 6.8: RMS and maximum error in SoC for the various initilizations of EKF and the open loop model.

6.3.6 Discussion

For all cases of initialization, both SoC and output terminal voltage v_t converge to true value (Fig.6.3,6.1). Time until convergences i.e. when values are within 5% of true value, is long for large initilization error in SoC. That is however not a real concern in real world application, as the EKF will get its initial SoC estimate from OCV-mapping of initial voltage measurement. Worst-case initialization of SoC is therefore $\approx 8\%$ e.g. case 1. Simply relying on AH-counting is not nearly sufficient when subjected to a biased current sensor, with an error of 26% after one single discharge cycle (Fig. 6.6). The EKF on the other hand, seems to handle the biased current measurements in a very natural manner. For SoC estimation only, the necessity of including estimation of biased current measurements is therefore not necessary.

In Figure 6.4, $\hat{SoC}$ for case 1 is highlighted together with its confidence intervals. The bounds are calculated from the diagonal elements in the state covariance matrix P:

$$95\% - conf.int. \approx 1.96 \cdot \sigma = 1.96\sqrt{P_{i,i}} \tag{6.27}$$

The confidence that the estimated SoC is close to true value increases as the innovation decreases. That can be seen by the decrease in $2\sigma - bound.$ At the end of simulation, the observer is 95% certain that the true value lies within $\pm 4\% \hat{SoC}$ (Fig. 6.4).

6.4 Robustness in temperature variations and aging

It should be noted that all the parameters of the model are in reality both a function of rapid changing conditions s.a. SoC, temperature, current rate, but also more slowly varying phenomenons as aging. Without going into details, online parameter estimation is one of the most common ways of indicating SoH i.e. level of aging in the cells. This will be further discussed in Chapter 8. Parameters dependency on the temperature and SoC are usually found through similar offline system identification that was performed in Chapter 5.4.2. The benefit of doing so, is that the distinction of the slowly varying effect on the parameters due to aging can be separated from temperature and SoC effects. This enables the opportunity to use the parameters estimates as an indication of SoH. However, the major drawback of this method is that it requires cell data on various temperature operating points, which in turn results in time-consuming cell testing and data gathering. This is a huge drawback for a companies as Blueye, who do not possess the resources required to perform such tests. Also, the choice of battery can change quickly as the drones are in a prototype phase, which makes extensive custom cell tests undesirable.

This paper will therefore explore the possibility of a joint state and parameter estimation, with

the aim of adapting SoC, temperature and other unmoddeled effects. X. et al. (2012) studied the sensitivity and performance of a state-estimating EKF with 1RC cell model where the effect of updating the parameters where evaluated. It showed that updating series resistance R_0 together with total capacity Q_{tot} had the greatest impact on SoC estimation performance. Therefore, a joint parameters-and state estimation EKF (JEKF) is therefore proposed.

6.4.1 Including series resistance estimation

The states is easily altered to $x = [v_{rc1}, v_{rc2}, z, R_0]^T$. Since there is no model for the dynamics of R_0, it is modeled as a random walk i.e.

$$R_{0,k} = R_{0,k-1} + v_{k-1} \tag{6.28}$$

where v_{k-1} is a random, fictitious white noise as the driving force of the state. The matrices then becomes:

$$A = \begin{bmatrix} e^{\frac{-\Delta T}{R_1 \cdot C_1}} & 0 & 0 & 0 \\ 0 & e^{\frac{-\Delta T}{R_1 \cdot C_1}} & 0 & 0 \\ 0 & 0 & 1 & 0 \\ 0 & 0 & 0 & 1 \end{bmatrix} \tag{6.29}$$

$$B = \begin{bmatrix} R_1(1 - e^{\frac{-\Delta T}{R_1 \cdot C_1}}) \\ R_2(1 - e^{\frac{-\Delta T}{R_2 \cdot C_2}}) \\ \frac{-\Delta t}{3600} i_k \\ 0 \\ \\ \end{bmatrix} \tag{6.30}$$

$$H_k = \frac{\partial h}{\partial x}\Big|_{\hat{x}_{k|k-1}} = \begin{bmatrix} -1 & -1 & \frac{\partial V_{oc,3}}{\partial SoC}|_{\hat{SoC}_{k|k-1}} & -i_k \end{bmatrix} \tag{6.31}$$

Note that there are no additional nonlinearites added with the proposed method. This is an additional benefit with respect to computational costs as state and input matrices still can be computed and stored offline.

6.4.2 Observability

The proposed observer is not observable using the linear observability rank test i.e. rank ($\mathscr{O}$) = ($\begin{bmatrix} H & HA & HA^2 & ... & HA^{n-1} \end{bmatrix}^T$) = n. This is only a sufficient condition for observability. Using Lee-derivatives (see A.2), proof of local observably is achieved. By induction, the Lie

derivatives are found to be:

$$dh = \begin{bmatrix} -1 & -1 & \frac{\delta V_oc}{\delta z} & -i \end{bmatrix} \tag{6.32}$$

$$dL_f^k h = \begin{bmatrix} -\frac{1}{(-1)^k} & -\frac{1}{(-1)^k} & 0 & 0 \end{bmatrix} \tag{6.33}$$

$$dL_g^k h = \begin{bmatrix} 0 & 0 & \frac{\delta^{k+1} V_oc}{\delta z^{k+1}} \frac{1}{(-Q_{tot})^k} & 0 \end{bmatrix} \tag{6.34}$$

$$dL_g L_f^k h = 0 \tag{6.35}$$

for all possible k. According to Theorem 1, the system is locally observable at a point x_0 if

$$(\mathcal{O}) = \begin{bmatrix} dh & dL_f h & dL_g h & dL_f^2 h & dL_g^2 h & dL_g L_f h & ... \end{bmatrix}^T \tag{6.36}$$

evaluated at x_0 has full rank. From (6.32-6.35), the system is observable given the following conditions: $\frac{\delta^{k+1} V_{oc}}{\delta z} \neq 0$, $\frac{1}{tau_1} \neq \frac{1}{tau_2}$ and $i \neq 0$. The former two conditions is already discussed (Ch. 5.4.2 The latter condition also holds because of the static current draw from electronic boards, video camera, lights etc. identified in Chapter 3.

6.4.3 Validation Data

The effect of temperature and aging are incomparable. Therefore, to test the robustness of the model, different data sets are preferable. Discharging the cell at a given, constant temperatures and logging current and voltage with lab-precise sensors, the robustness in terms of temperature can be assessed. This requires a temperature chamber to prohibit temperature variations in the cell. For aging, voltage, current, and inner resistance must be logged over hundreds/thousands of discharge/charge cycles under controlled environment in order to gathered good validation data. This takes several months to complete. The lack of equipment e.g. temperature chamber, as well as time, have made such extensive data gathering impossible.

The data obtained through drone operation (3.1-3.6) is therefore used as the final and ultimate robustness test w.r.t. temperature and aging. The charge- and discharge history nor cycle number of the battery is known, so the level of aging is unclear. What is known, is that the battery has been used in its prototype ROV P1 for over a year. Further, the battery benched in at total capacity $Q_{tot,pack} = 21.6A$ at 8A discharge current. Assuming same level of capacity fade for each cell yields 2.7Ah $Q_{tot}/cell$. For the JEKF, OL and AH-counting, Q_{tot} has been set to 2.7Ah. The implication of this assumptions are:

- All the cells within each PCM experience the same temperature, current draw and aging effect. That means that the same discharge current is assumed for each cell in the PCM
- Each PCM can be modeled as one single cell.

The JEKF and OL-model is initialized with 5% error in SoC. AH-counting with correct initialization serves as a reference.

6.4.4 Simulation Results

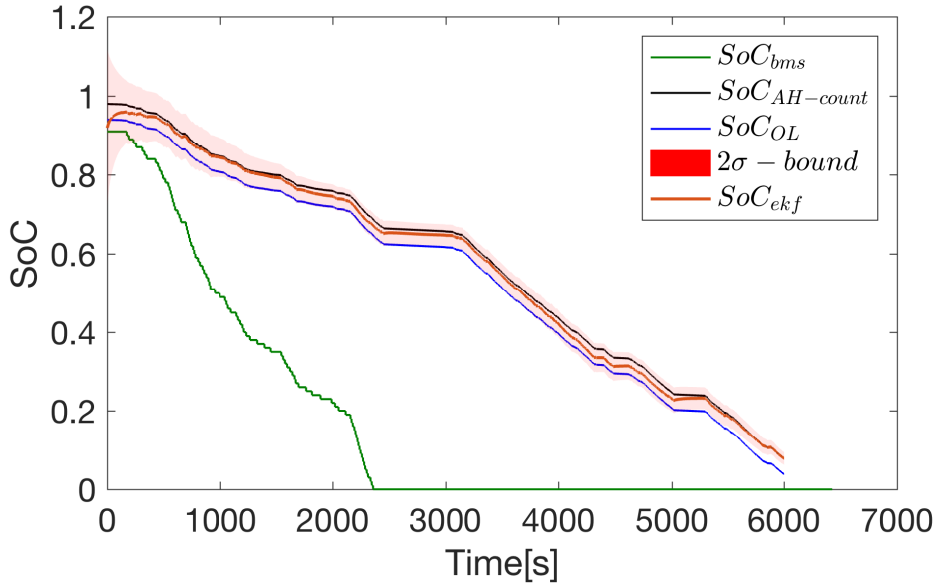

Figure 6.9: SoC estimates from the BMS onboard the drone compared to the estimates provided by the JEKF, OL and AH-counting.

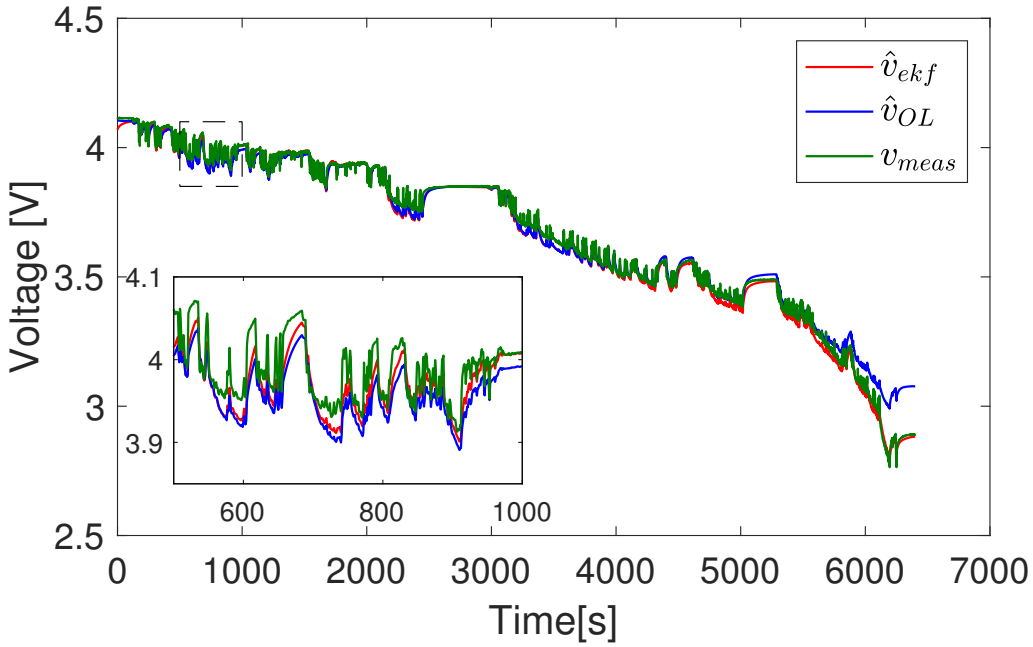

Figure 6.10: Measured voltage compared to output voltage from the open-loop-model and JEKF.

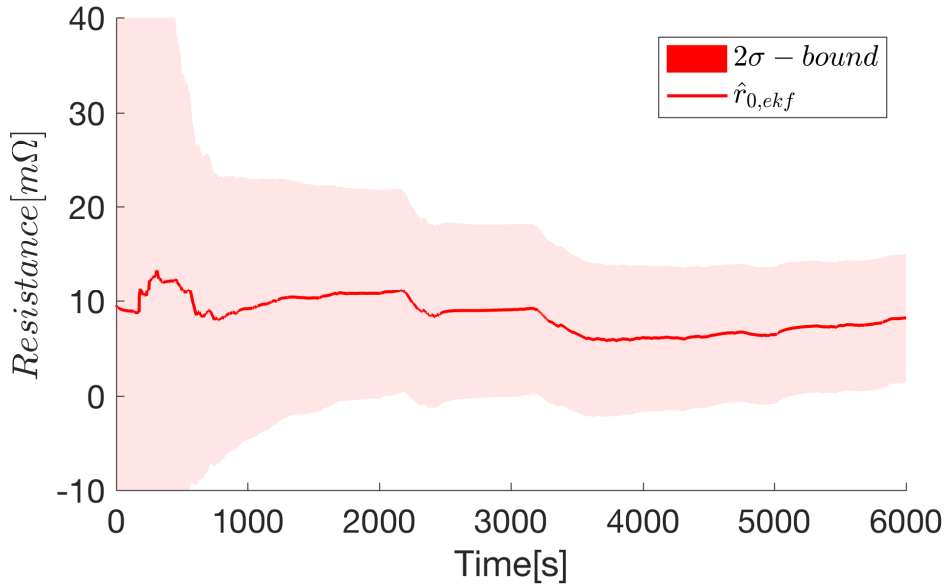

Figure 6.11: Estimated inner resistance with confidence bounds.

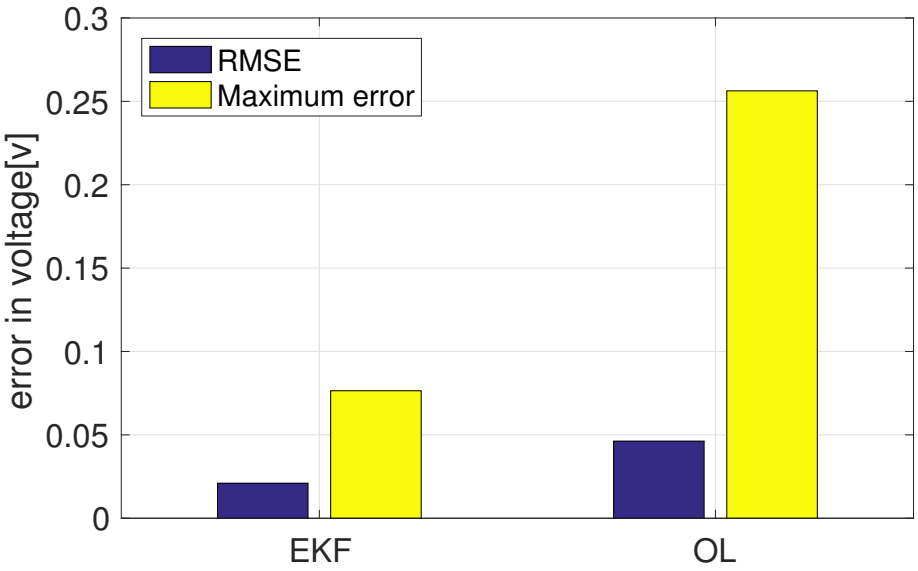

Figure 6.12: RMSE and maximum voltage error for the JEKF and open-loop model compared to measured voltage from drone operation.

6.4.5 Discussion

Performance of SoC estimates is difficult to validate. Comparing the estimate provided by the current BM system SoC_{bms} with the voltage readings, it is clear that the current system has 1) very poor performance 2) not calibrated correctly. The BMS estimates 0% SoC at t = 2345s. $v(t = 2345s) \approx 3.8V$ for all parallel connections. OCV is always higher than terminal voltage

for discharge. By definition, SoC = 0% at $OCV = v_{lim}^{dis}$ = 2.5V, which means the SoC estimate provided by the BMS is unquestionably inaccurate.

Using AH-counting with correct initialization as reference, the JEKF quickly converge to a more reasonable estimate. The confidence interval tightens at end-of-discharge as the JEKF relies more on voltage measurements than AH-counting. The OL- model never converge, but keeps the steady 4% error in SoC compared to SoC_{AH}. While it does not seem much, the implications for terminal voltage are large at end-of-discharge (Figure 6.10). The derivative of V_{oc}(SoC) is large at low SoC, so small errors in SoC leads to large errors in terminal voltage. The JEKF on the other hand tracks the measurements to the very end of operation. This can be seen as a sign that $\hat{SoC}_{ekf}$ are accurate?

The fluctuations in estimated inner resistance at the very beginning is due to deliberately wrong initilization of SoC (Fig. 6.11). The fluctuations throughout the rest of the cycle can be caused by a number of reasons. WHAT MORE TO SAY?. The confidence tightens, but large uncertainties in inner resistance is still present at end-of-discharge cycle. WHAT MORE TO COMMENT?
The RMSE and maximum error in terminal voltage for the EKF and OL-model can be seen in Fig. 6.12.

6.5 Summary

The standard EKF is sufficient to estimate SoC for a new cell. It handles non-ideal measurements in a natural manner. Because of the voltage-based feedback loop, biased current measurements had little effect on both SoC estimates and terminal voltage output (rms_{SoC} = 0.37% rms_v = 6.4mV). This is in huge contrast to the open-loop model, who did not cope with the non-ideal measurements. Keep in mind that these results are based on simulated data coming from the same model. The only difference is the non-ideal voltage and current measurements. This high level of performance is therefore not warranted in real application.

When testing for robustness in aging and temperature, some assumptions and adjustments where made that gave reasonable results (rms_v = 23mV). The measured pack total capacity was divided equally between 8 cells so to some extent take care of the decreased capacity. Estimation of series resistance R_0 was also added. While the SoC results is difficult to validate, it is clear that it outperformed the already installed BMS from LG. Given the tight confidence interval coupled with small error in terminal voltage at end-of-discharge, it performs well.

For this data the pack total capacity was measured before operation. This will not be possible in real application. Wrong Q_{tot} could lead to large errors in SoC estimates and terminal volt-

age. Therefore, some way of automatically updating Q_{tot} online is needed. This will be further explored in the next chapter (Chapter 7).

7

State-of-Health Estimation

7.1 Need for SoH estimation

Over time, the cell in a battery will age and its performance will degrade, in terms of lowered ability to store energy, lowered capability to deliver power and the compromise of safety. For applications that requires highly accurate SoC and SOP estimates, this loss of performance can be crucial to include. The level of degradation in performance is what is referred to as State-of-Health (SoH). The indicator of the battery health is often only given as a percentage of its nominal capacity Q_{nom} to its total capacity Q_{tot}:

$$SoH = \frac{Q_{tot}}{Q_{nom}} 100\% \tag{7.1}$$

even though battery aging affect more parameters than only the total capacity. The decrease in performance manifests itself through:

- Decrease in total capacity Q_{tot}
- Increased inner resistance, mainly through R_0
- Other cell parameters

The former two are the parameters that are most effectuated by the aging process (Plett, 2016), in which both are included in the model implemented in Chapter 6. Through (5.4), Q_{tot} directly influences the SoC estimation. The series resistance R_0 is represented in the output equation of the model (5.5). Increased R_0 leads to lower terminal voltage for a given discharge current. The decrease in Q_{tot} and increase in R_0 is commonly referred to as *capacity fade* and *power fade*. Other parameters, such as OCV relationship is also affected, but to less extend than the Q_{tot} and R_0 (Plett, 2016).

The need of health estimates is therefore evident. First, an illustrative and simplified explanation of the physical phenomena that takes place regarding capacity and power fade is discussed below

in Section 7.1.1. Then, state-of-the-art SoH methods is reviewed in Section 7.2. Lastly, methods of SoH estimation for the ROV application is discussed in Section 7.3, together with proof-of-concept simulation results (7.3.1). Biased current estimation is reintroduced in Section 7.4 to prohibit large fluctuations of total capacity estimates under biased current measurements. Lack of data from aged cells have made proper validation impossible, so all results are based on simulated voltage and current data.

7.1.1 Total capacity

The total capacity of the cell is equal to the minimum of the number of storage sites in the negative electrode, the number of storage sites in the positive electrode, and the amount of lithium that can be travel in between. For simplification, consider a cell with 16 storage cites in the anode and cathode structure and 9 lithium ions. For the ideal cell, Q_{tot} is the minimum of 16,16 and 9, which yields total capacity of 9 lithium ions.

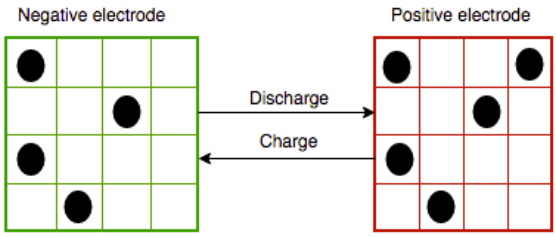

Figure 7.1: Ideal-cell operation (adapted from Plett (2016)).

The primarily reasons for capacity fade in an lithium ion battery is due to:

- Unwanted side reactions that consume lithium. This lithium could otherwise be used to charge/discharge the battery (Fig. 7.2).
- Structural deterioration of the electrode active materials that eliminates lithium storage sites (Fig. 7.3).

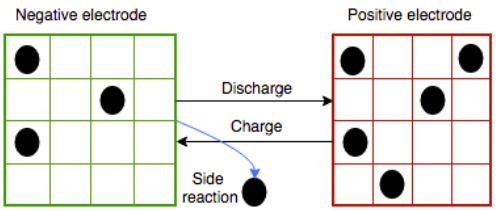

Figure 7.2: Capcity loss due to side reaction (adapted from Plett (2016)).

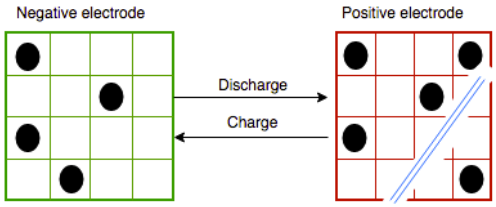

Figure 7.3: Capacity loss due to structural deterioration (adapted from Plett (2016)).

7.1.2 Equivalent series resistance

The main reasons for increased R_0 is due to the same mechanisms as for total capacity (Fig. 7.2-7.3). The side reaction form resistive films on the surface of the active material particles that impede the ionic conductivity (Plett, 2016). Structural deterioration severs electronic pathways between particles and decreases the electronic conductivity (Plett, 2016).

7.2 Methods of SoH estimation

The SoH estimation methods mainly include durability model-based open-loop methods and battery model-based closed-loop methods. The durability models describe the increase of solid-electrolyte interface (SEI) film resistance and changes in capacity fade and internal resistance. This will not be further explained, as it includes electro-chemical modeling, which was considered infeasible for this application (see Chapter 4). For the latter, methods like least-squares regression, Kalman Filtering and fuzzy logic is used to identify capacity and internal resistance (Zoua et al., 2015).

Table 7.1 below summarizes the methods of found in SoH estimation, with their respective advantages and disadvantages.

In the HEV's and EV's research community, the most common SoH methods are through a version of the least square estimator or EKF observers. Plett (2016) compared different methods of a recursive least square estimators, including weighted least square (WLS), total least square, weighted total least square(WLTS) and approximated weighted total least square (AWTLS). Dual/joint EKF was also explored in the research. In joint estimation, the states and parameters are combined in a single high-dimension vector, whereas the in the dual method EKFs are used for state estimation and parameter estimation. This can require more computational power compared to the dual EKF method if it is a large set of states/parameters. Based on literature review and the identified requirements (Chapter 3.6), two SoH estimation methods will be further discussed;

- Estimating Q_{tot} individually for each PCM by the means of an JEKF. Q_{tot} estimates is calculated every timestep i.e. every second

- Measuring $Q_{tot,p}$ by integrating charge current, and having a seperate KF for Q_{tot}. Q_{tot} estimates is only calculated at end-of-charge cycle.

Table 7.1: Comparison of the different methods of obtaining SOH estimates. Some content is adopted from Zoua et al. (2015).

Method	Advantages	Disadvantages
Durability mechanism	Comprehensive understanding	Complex, need accurate parameters
Durability external characteristic	Simple and easy	Based on a large number of experiments
DC resistance	Simple	Not accurate, disturbance sensitive
AC impedance	Accuracy	Complex, offline
DEKF/JEKF	Once EKF for SoC estimation is implemented, easy to add SOH estimation	Sensitive to model accuracy
WTLS/AWTLS	Accuracy	Computationally more expense
Fuzzy logic	Accurate	Slow convergence
Sample entropy	Simple	Need large amount of data
Discharge voltage	Easy	Inaccurate
Adaptive estimation	Precise	Given accurate model

7.3 Total capacity estimation through JEKF

The established joint EKF proposed in Chapter 6 already estimates R_0. The powerfade of the aging cells is therefore already handled. It is therefore natural to extend this approach to also include Q_{tot} estimation. This can be done in the same manner as (6.28), with

$$Q_{inv,k} = Q_{inv,k-1} + n_{k-1}^{Q_{inv}} \tag{7.2}$$

where Q_{inv} is the inverse of total capacity and $n_k^{Q_{inv}}$ is fiction noise source that allow the adaption of true cell capacity. The states are extended to x = $[v_{rc1} \quad v_{rc2} \quad SoC \quad r_0 \quad Q_{inv}]$, with the state and input matrices as:

$$A_{=} \begin{bmatrix} e^{\frac{-\Delta T}{R_1 \cdot C_1}} & 0 & 0 & 0 & 0 \\ 0 & e^{\frac{-\Delta T}{R_1 \cdot C_1}} & 0 & 0 & 0 \\ 0 & 0 & 1 & 0 & \frac{-\Delta t}{3600} I_k \\ 0 & 0 & 0 & 1 & 0 \\ 0 & 0 & 0 & 0 & 1 \end{bmatrix} \tag{7.3}$$

$$B_k = \begin{bmatrix} R_1(1 - e^{\frac{-\Delta T}{R_1 \cdot C_1}}) \\ R_2(1 - e^{\frac{-\Delta T}{R_2 \cdot C_2}}) \\ 0 \\ 0 \\ 0 \end{bmatrix} \tag{7.4}$$

$$H_k = \frac{\partial h}{\partial x}\Big|_{\hat{x}_{k|k-1}} = \begin{bmatrix} -1 & -1 & \frac{\partial V_{oc,3}}{\partial SoC}|_{S\hat{o}C_{k|k-1}} & I_k & 0 \end{bmatrix} \tag{7.5}$$

Note that Q_{inv} is not directly observable in the output equation, which makes the sensitivity of terminal voltage on Q_{inv} low. This state combination is in the remaining of this chapter referred to as $JEKF_2$.

7.3.1 Simulation results

True capacity fade is modeled as linear slope with 0.013 Ah per discharg cycle. A bias of 0.1Ah to current measurements. Total capacity results are shown in this subsection to highlight the necessity of including bias current estimation when estimating Q_tot.

Table 7.2: Initialization of the EKF_2 States and parameters

Model	$R_{0,init}$	SoC_{init}	$Q_{inv,init}$	states
True	R_{nom}	95	3 Ah	-
EKF_2	$R_{nom}\cdot$ 0.7	88	2.85 Ah	$[v_{rc1}\ v_{rc2}\ z\ R_0\ Q_{tot}]^T$

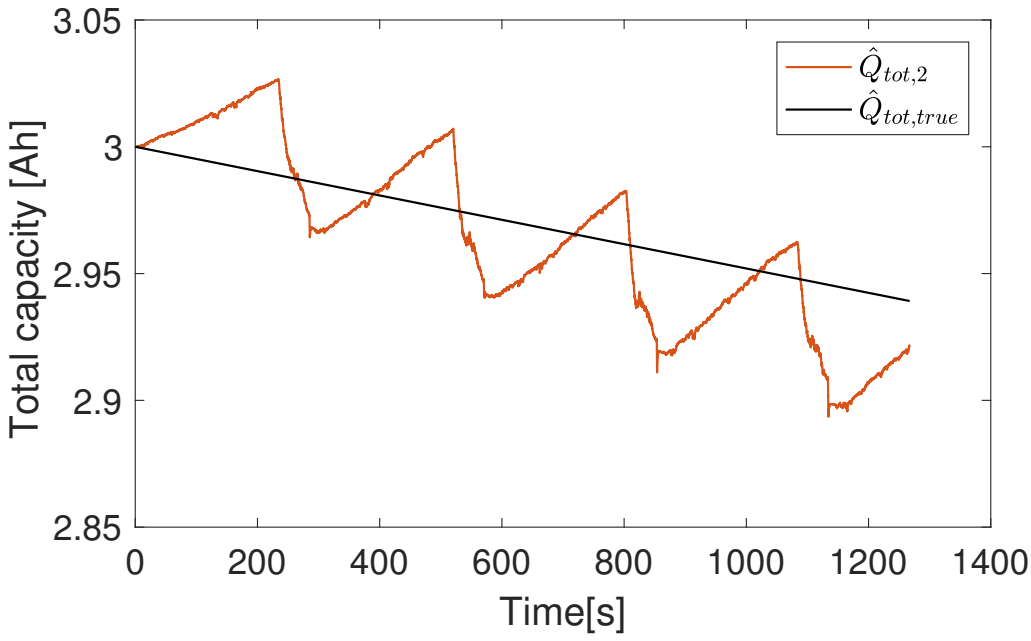

Figure 7.4: Total capacity estimation over 4 cycles with added i_b = 0.1Ah.

It is clear that the observer is unable to differentiate between the effect of biased current measurements from capacity fade. JEKF$_2$ strives to match the estimated output with terminal voltage measurements, and is doing so by adjusting Q$_{tot}$ The reason for this is that Q$_{tot}$ and I_b mainly influences the output terminal voltage through the SoC equation, and is doing so in the same manner.

$$SoC_k = SoC_{k-1} - \frac{(i_{meas} - i_b)\Delta t}{3600} Q_{inv} \tag{7.6}$$

The possibility of adding a bias estimator to eliminate large fluctuations in $\hat{Q_{inv}}$ is therefore investigated.

7.3.2 Adding current bias estimation

Current bias estimation i_b can be added in the same manner as for total capacity i.e. a random walk:

$$i_{b,k} = i_{b,k-1} + n_{k-1}^{i_b} \tag{7.7}$$

where i$_b$ is the estimated current bias of the current sensor and $n_k^{i_b}$ is fiction noise source that allow the adaption of true measurement bias. The states are extended to
x$_k$ = [v_{rc1}, v_{rc2}, SoC, r_0, Q_{inv}, i_b], with the state and input matrices as:

$$A_k = \begin{bmatrix} e^{\frac{-\Delta T}{R_1 \cdot C_1}} & 0 & 0 & 0 & 0 & R_1(1 - e^{\frac{-\Delta T}{R_1 \cdot C_1}}) \\ 0 & e^{\frac{-\Delta T}{R_1 \cdot C_1}} & 0 & 0 & 0 & R_2(1 - e^{\frac{-\Delta T}{R_2 \cdot C_2}}) \\ 0 & 0 & 1 & 0 & \frac{-\Delta t}{3600} i_k & \frac{\Delta t Q_{inv}}{3600} \\ 0 & 0 & 0 & 1 & 0 & 0 \\ 0 & 0 & 0 & 0 & 1 & 0 \\ 0 & 0 & 0 & 0 & 0 & 1 \end{bmatrix} \tag{7.8}$$

$$B_k = \begin{bmatrix} R_1(1 - e^{\frac{-\Delta T}{R_1 \cdot C_1}}) \\ R_2(1 - e^{\frac{-\Delta T}{R_2 \cdot C_2}}) \\ 0 \\ 0 \\ 0 \\ 0 \end{bmatrix} \tag{7.9}$$

$$H_k = \left.\frac{\partial h}{\partial x}\right|_{\hat{x}_{k|k-1}} = \begin{bmatrix} -1 & -1 & \frac{\partial V_{oc,3}}{\partial SoC}|_{\hat{SoC}_{k|k-1}} & I_k & 0 & \hat{r_0}_{k|k-1} \end{bmatrix} \tag{7.10}$$

This is in the remaining of this chapter referred to as $JEKF_3$.

7.3.3 Observability

Using Theorem 1, neither $JEKF_2$ nor $JEKF_3$ has been prooved observabable. The Lie-derivative for $JEKF_3$ is calculated, and by the means of induction the observability matrix is given as:

$$dh = \begin{bmatrix} -1 & -1 & \frac{\delta V_{oc}}{\delta z} & i_b - i & 0 & r_0 \end{bmatrix} \tag{7.11}$$

$$dL_f^k h = \Big[\tfrac{1}{-(-\tau_1)^k},\ \tfrac{1}{-(-\tau_2)^k},\ -(iQ_{inv} - Q_{inv} i_b)^k \tfrac{\delta^{k+1} V_{oc}}{\delta z^{k+1}},\ 0, (-1)^k (i - i_b)(iQ_{inv} - Q_{inv} i_b)^{k-1} \tfrac{\delta^k V_{oc}}{\delta z^k},\ \ldots\ (-1)^k k Q_{inv} (iQ_{inv} - Q_{inv} i_b)^{k-1} \tfrac{\delta^k V_{oc}}{\delta z^k} + \tfrac{1}{-C_1(-\tau_1)^{k-1}} + \tfrac{1}{-C_2(-\tau_2)^{k-1}} \Big] \tag{7.12}$$

$$dL_g^k h = \begin{bmatrix} 0 & 0 & 0 & 0 & 0 & 0 \end{bmatrix} \tag{7.13}$$

$$dL_g^k F h = \begin{bmatrix} 0 & 0 & 0 & 0 & 0 & 0 \end{bmatrix} \tag{7.14}$$

for all positive integers k$\in \mathbb{Z}_+$. Inputting $k \geqslant 5$, the set of vectors in the observability matrix is not independent anymore. Thus, the rank condition for local observability is not met as rank O = 5 < 6 = n number of states of the system.

The same conclussion is made for $JEKF_2$. Physically, it is because the total capacity is not observable through the output equation i.e. through terminal voltage measurements. However, as we will see in later in Section 7.5.1, they still provide good results given the right tuning.

7.4 Capacity estimation with event-based linear Kalman Filter

Since the decrease in capacity is a very slow process it might be justified not estimating Q_{tot} at every time-step (every second). A seperate event-based linear Kalman Filter is suggested. This Kalman filter is used to estimate the battery capacity when the battery transitions from charging to discharging.

The battery degradation is modeled by decreasing capacity. In this example, the cells capacity is set to decrease 0.013 Ah per discharge-charge cycle. Since the degradation rate of capacity is not known in advance, Q_{tot} is modeled as a random walk:

$$Q_{tot,c} = Q_{tot,c-1} + n_{c-1}^{Q_{tot}} \tag{7.15}$$

where c is the number of discharge-charge cycles and $n_{c-1}^{Q_{tot}}$ the process noise. The simulation is set to run between $z \in$ (0.1,0.95). This information is used to obtain a synthetic measurement. Denote $c \in C$ as the timestep at end of each charge cycle, C total number of discharge cycles and

j = 1....J, where J is the total number of timesteps within each charge-cycle. Then,

$$Q_{tot,c}^{meas} = Q_{tot,c} + v_c = \sum_{i=1}^{J} \frac{i_{meas,j} - \hat{i}_{b,j}}{\Delta z_c} \tag{7.16}$$

where v_q is the measurement noise, $\hat{i}_{b,k}$ the estimated biased coming from the JEKF and Δz_c the change in z over the charge-cycle i.e. Δz_c = 0.95-0.1 = 0.85. In state-space form;

$$x_c = Q_{tot,c} = A_Q x_{c-1} + w_{Q,c-1} \tag{7.17}$$

$$y_c = Q_{tot,c}^{meas} = C_Q x_c + v_c \tag{7.18}$$

where A_Q, C_Q = 1; The total decrease in Q_{tot} for a full charge-and discharge cycle is 0.013Ah. The process noise covariance Q is therefore set set to;

$$Q_c = \begin{cases} 0.013^2 = 0.00017 & \text{for } c \in C \\ 0 & \text{else} \end{cases} \tag{7.19}$$

The time-varying Q prohibits state prediction between measurements, making Q_{tot} estimates constant in between consecutive cycles. In practice, this means that measurements are updated at the end of every discharge cycle. These estimates are then fed into the JEKF which estimates SoC and the other parameters. The measurement covariance R_c is difficult to estimate, since it depends on the accuracy of the bias estimates coming from the JEKF, and is therefore tuned thereafter.

The states of the JEKF is adjusted since Q_{tot} estimation is now performed in the LKF. The JEKF below, with R_0 and i_b estimation, is referred to as $JEKF_4$ in the remaining of this chapter.

$$A_k = \begin{bmatrix} e^{\frac{-\Delta T}{R_1 \cdot C_1}} & 0 & 0 & 0 & R_1(1 - e^{\frac{-\Delta T}{R_1 \cdot C_1}}) \\ 0 & e^{\frac{-\Delta T}{R_1 \cdot C_1}} & 0 & 0 & R_2(1 - e^{\frac{-\Delta T}{R_2 \cdot C_2}}) \\ 0 & 0 & 1 & 0 & \frac{\Delta t}{3600 \hat{Q}_{tot,c}} \\ 0 & 0 & 0 & 1 & 0 \\ 0 & 0 & 0 & 0 & 1 \end{bmatrix} \tag{7.20}$$

$$B_k = \begin{bmatrix} R_1(1 - e^{\frac{-\Delta T}{R_1 \cdot C_1}}) \\ R_2(1 - e^{\frac{-\Delta T}{R_2 \cdot C_2}}) \\ -\frac{\Delta t}{3600 \hat{Q}_{tot,c}} \\ 0 \\ 0 \end{bmatrix} \tag{7.21}$$

$$H_k = \frac{\partial h}{\partial x}\Big|_{\hat{x}_{k|k-1}} = \begin{bmatrix} -1 & -1 & \frac{\partial V_{oc,3}}{\partial SoC}|_{S\hat{o}C_{k|k-1}} & -I_k & \hat{r_0}_{k|k-1} \end{bmatrix} \tag{7.22}$$

7.4.1 Observability

The observability rank condition from Theorem 1 is used to check the observability of $JEKF_4$:

$$rank(\mathscr{O}) = rank\left(\begin{bmatrix} dh \\ L_f dh \\ L_g dh \\ L_f^2 dh \end{bmatrix}\right) \tag{7.23}$$

$$= rank\begin{bmatrix} -1 & -1 & \frac{\delta V_{oc}}{\delta z} & -i & 0 \\ 0 & 0 & 0 & i_b & r_0 \\ \frac{1}{\tau_1} & \frac{1}{\tau_1} & \frac{i_b}{Q_{tot,c}}\frac{\delta V_{oc}}{\delta z} & 0 & \frac{1}{Q_{tot,c}}\frac{\delta V_{oc}}{\delta z} + \frac{1}{C_1} + \frac{1}{C_2} \\ 0 & 0 & 0 & 0 & 0 \\ 0 & 0 & -\frac{i}{Q_{tot,c}}\frac{\delta V_{oc}}{\delta z} & 0 & 0 \\ 0 & 0 & 0 & 0 & 0 \\ -\frac{1}{\tau_1} & -\frac{1}{\tau_2} & \frac{i_b^2}{Q_{tot,c}^2}\frac{\delta^2 V_o c}{\delta z^2} & 0 & \frac{2i_b}{Q_{tot,c}^2}\frac{\delta^2 V_o c}{\delta z^2} + \frac{1}{C_1\tau_1} + \frac{1}{C_2\tau_2} \end{bmatrix} \tag{7.24}$$

$$= 5 \tag{7.25}$$

The system is therefore locally observable at all points x_0 given an additional condition that $i, i_b \neq 0$ simultaneously.

7.5 Simulation

Simulation results are shown for error in terminal voltage, error in SoC, estimated Q_{tot}, R_0 and i_b over 38 charge/discharge cycles (10000 min) for the four proposed JEKFs. The figures in the left column shows the evolution of the respective state/outputs over all discharge cycles, and figures in the right over one single discharge-charge cycle.

Table 7.3: Initialization of the EKF's states and parameters

Model	$R_{0,init}$	SoC_{init}	Q_{init}	states
True	R_{nom}	95	3 Ah	-
$JEKF_1$	$R_{nom}\cdot$ 0.7	88	2.85 Ah	$[v_rc1\ v_rc2\ SoC\ R_0]^T$
$JEKF_2$	$R_{nom}\cdot$ 0.7	88	2.85 Ah	$[v_{rc1}\ v_{rc2}\ SoC\ R_0\ Q_{tot}]^T$
$JEKF_3$	$R_{nom}\cdot$ 0.7	88	2.85 Ah	$[v_{rc1}\ v_{rc2}\ SoC\ R_0\ Q_{tot}\ I_{bias}]^T$
$JEKF_4$	$R_{nom}\cdot$ 0.7	88	2.85 Ah	$[v_{rc1}\ v_{rc2}\ SoC\ R_0\ I_{bias}]^T$

7.5.1 Simulation results

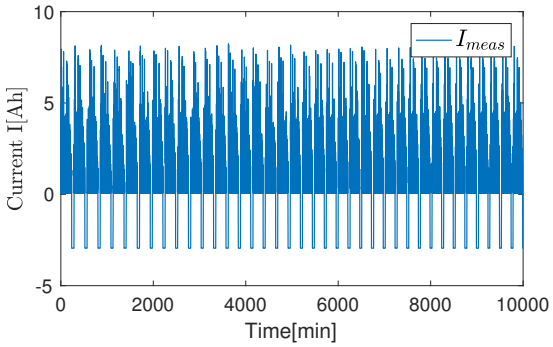

Figure 7.5: Current profile

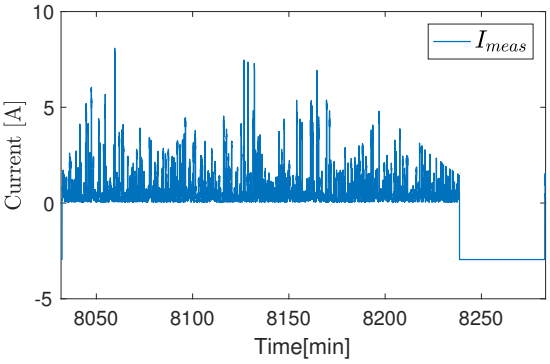

Figure 7.6: Current profile for one discharge-charge cycle.

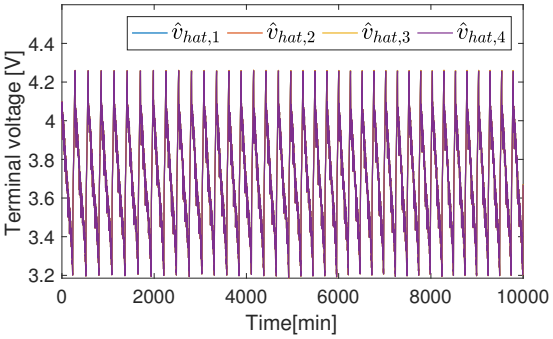

Figure 7.7: Terminal voltage v_t for all JEKFs.

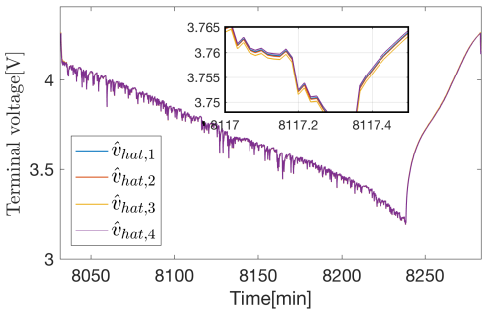

Figure 7.8: Terminal voltage v_t for all JEKFs.

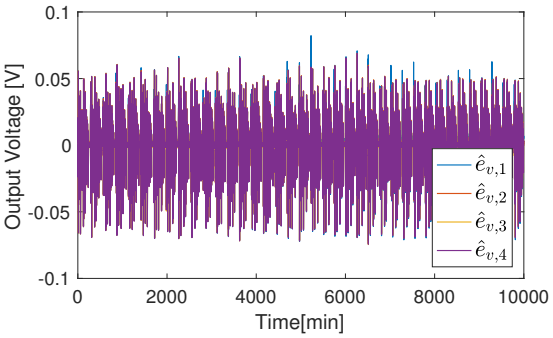

Figure 7.9: Error in terminal voltage v_t.

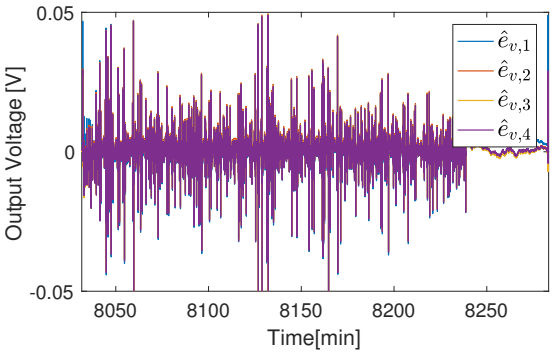

Figure 7.10: Error in terminal voltage over one discharge-charge cycle.

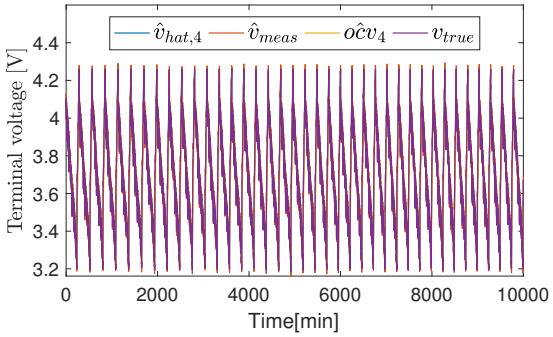

Figure 7.11: Terminal voltage for $JEKF_4$ v_t.

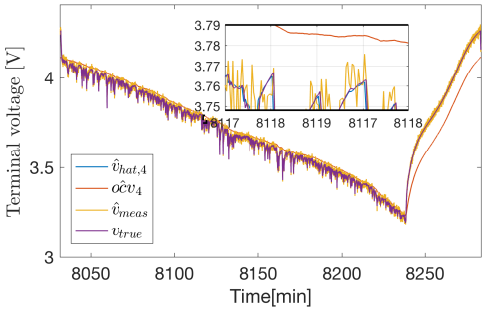

Figure 7.12: Terminal voltage for $JEKF_4$ v_t.

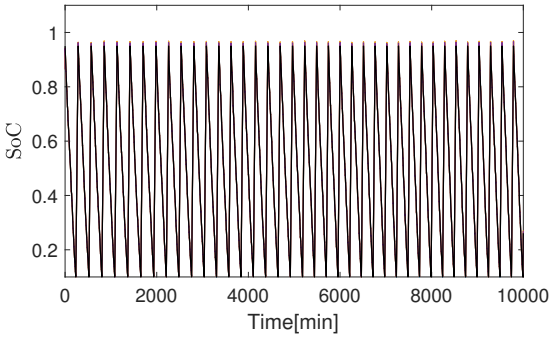

Figure 7.13: SoC for all JEKF.

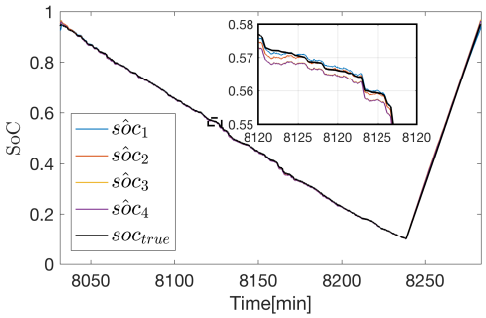

Figure 7.14: SoC for all JEKF.

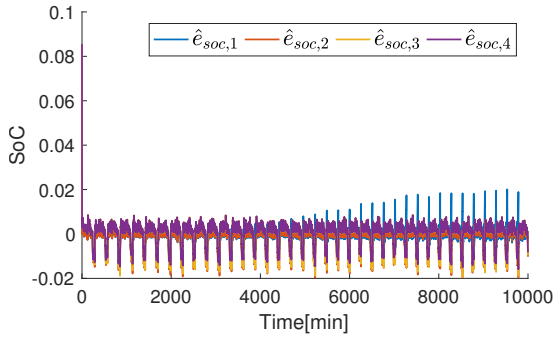

Figure 7.15: Error in SoC estimates

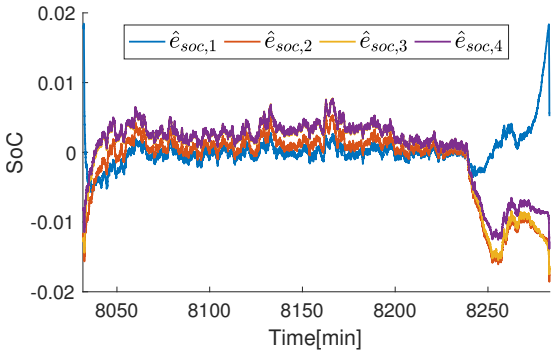

Figure 7.16: Error in SoC estimates.

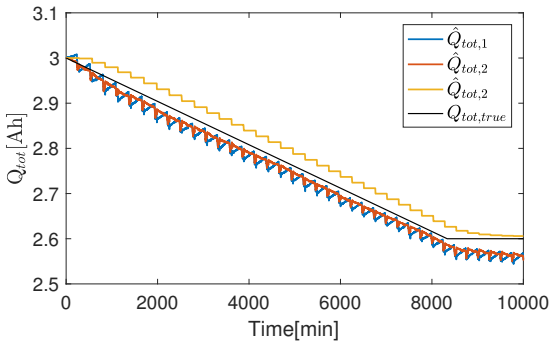

Figure 7.17: Total capacity Q_{tot} estimates.

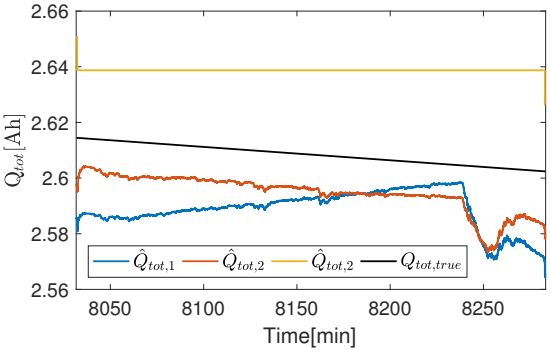

Figure 7.18: Total capacity Q_{tot} estimates.

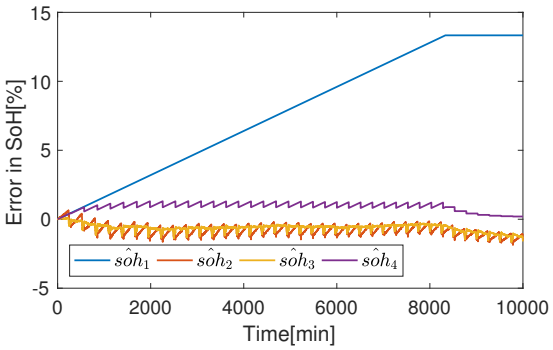

Figure 7.19: Error in SoH.

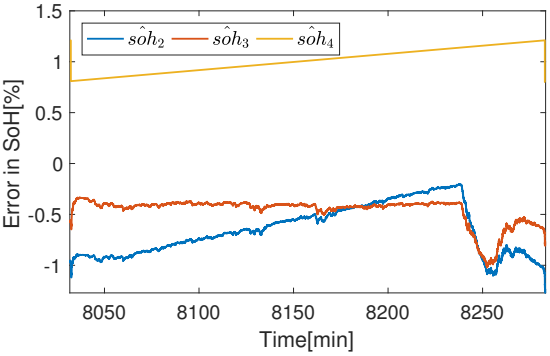

Figure 7.20: Error in SoH.

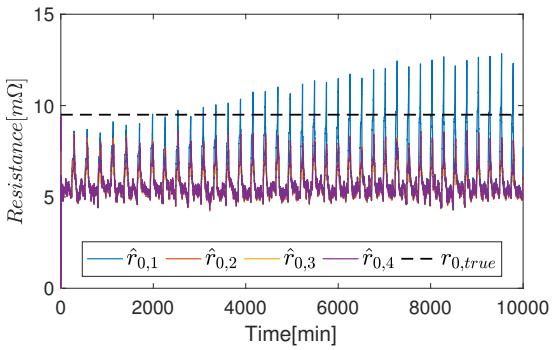

Figure 7.21: Series resistance R_0 estimates.

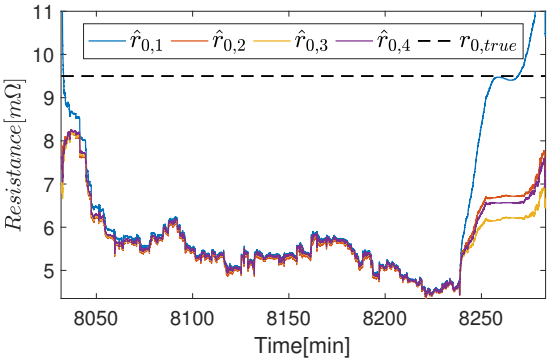

Figure 7.22: Series resistance R_0 estimates.

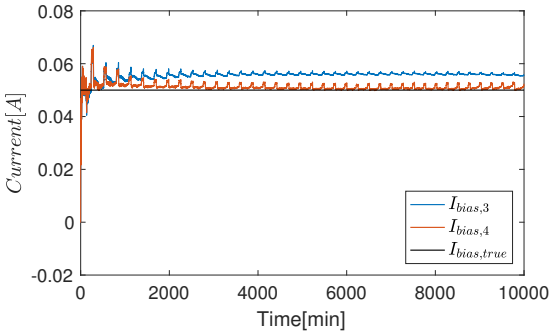

Figure 7.23: Current bias i_b estimates.

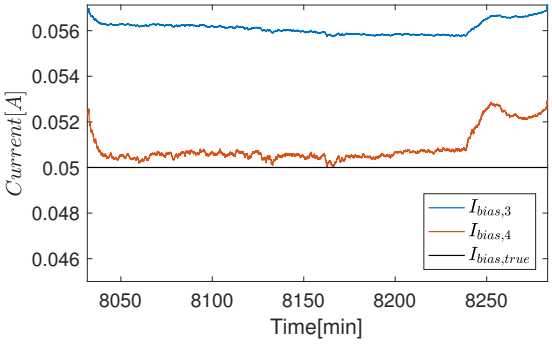

Figure 7.24: Current bias i_b estimates.

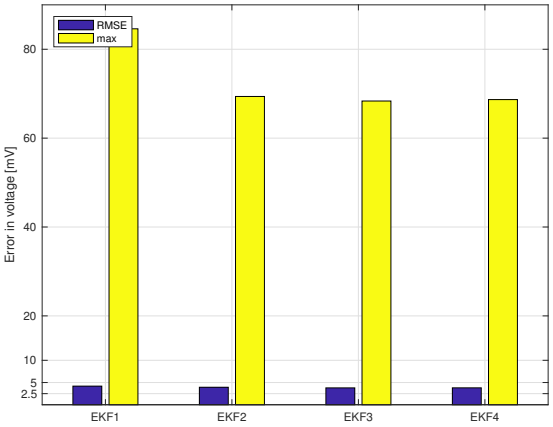

Figure 7.25: RMSE in voltage.

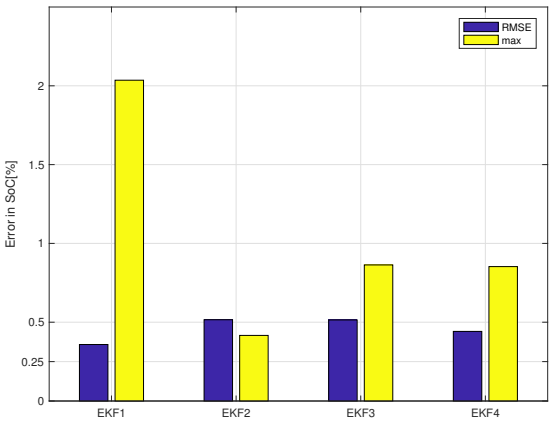

Figure 7.26: RMSE in SoC estimates.

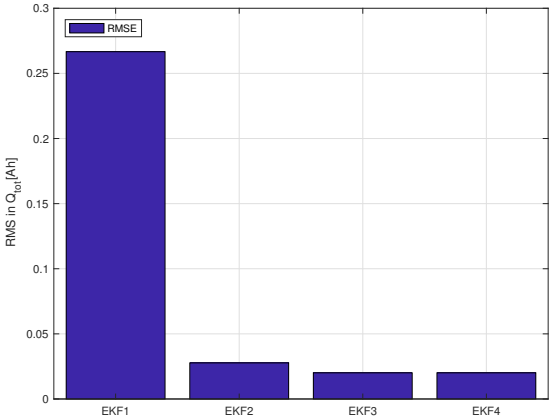

Figure 7.27: RMSE in Q_{tot} estimates.

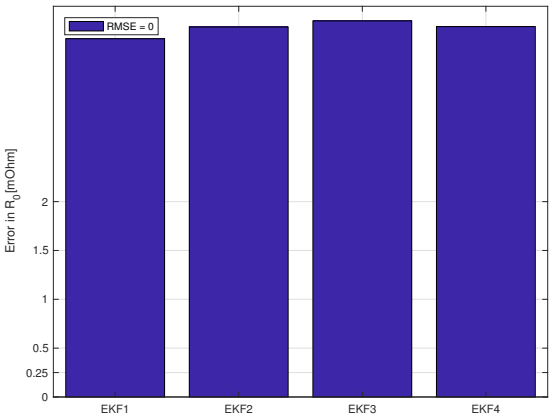

Figure 7.28: RMSE in R_0 estimates.

7.6 Summary

Key findings can be summarized as follows: All JEKFs performance well, even with biased current measurements and a 13% decrease in total capacity. The RMSE of terminal voltage is about 5 mV for all JEKFs. The noise is filtered out smoothly (7.12) and no large spikes is observed in

the open-circuit voltage. The error is fluctuating at the dynamic discharge cycles but goes to zero at the more constant charge cycles.

For SoC estimation, the observer without capacity as a state ($JEKF_{1,4}$) gives sightly less error than those with including Q_{tot}($JEKF_{2,3}$). The reason $JEKF_1$ performs so well is because of the low measurement noise R. This results in a large kalman gain, which makes the observer adjust its a-priori AH-counted SoC estimate so to quickly minimize the residual of output voltage. Put in other words, the observer is tuned to use voltage-based SoC estimation compered to AH-counting. In fact, it is only at SoC ranges with little observability ($dV_{oc} \approx 0$) e.g. 90-95% that the four SoC estimates differ in any significant way. That is because those observers that update its total capacity have a better model of SoC and thereof more precise estimates at those SoC ranges. Estimating Q_{tot} for the sake of SoC estimation performance only is therefore not justified, given that voltage sensors have accuracy of >1% FSR and that the OCV-SoC function is still valid. According to literature these assumptions can be relaxed.

All observer estimating Q_{tot} tracks true decrease of total capacity. For $JEKF_{1,2}$, which estimates Q_{tot} at every timestep, the estimates are more fluctuating between charge and discharge, but has the same RMSE as the estimates provided by the linear kalman filter. Even so, the linear kalman filter has the benefit of converging to true capacity when the decrease is set to zero (t = $\approx$ 8100 min). The former two on the other hand overshoots. This might be due to the weak observability that capacity estimation introduces. Separating capacity estimation has therefore the benefit of not being updated at all timesteps, stronger observability of the other states while maintaining performance.

8

State-of-Power Estimation

The aging of the battery will severely increase if the battery is operated outside its SOA. It is therefore important to ensure that the limits on current, voltage, SoC and temperature are not violated. The SoP is the estimation of these limits with respect to the input current. The simplest way is to let the current rate be decided by the power consumers, only restricted by simple logic. If the battery is at high SoC, the current is only restricted by the current limits imposed by the battery manufacturer. As SoC approaches zero, high loads might cause the voltage to reach and exceed its lower voltage limit. If the measured voltage is below lower limit, the discharge current is set to zero and the drone shuts down. That means that full power is available until a sudden shutdown. Also, this method is crude in the way that is extremely reliant on the measurements, and therefore also sampling time. If the sampling time is to big compared to the dynamics of the battery, the voltage is allowed, for a small period of time, to fall below its lower limits since the BMS is not aware of the violation before voltage measurements are updated. Lastly, this crude method leads to poor effective capacity because of the immature shutdown of the drone. For these reasons, the necessity of an SoP estimator rises. The question that the SoP estimator wants to answer is:

- What is the maximum discharge/charge current $I_{l,min}$,$I_{l,max}$ or maximum discharge/charge $P_{l,max}$,$P_{l,max}$ that makes the battery voltage reach its lower/upper cutoff voltage V_{lim}^{max}, V_{lim}^{max}.

The battery model lets us predict voltage response V_k based on current input I_k. By running the model with the constant current $I_k = I_{k+l}$ from current time t_k =k to t_{k+l} = t_k+kl, and estimate of V_{k+l} is found. Various methods of obtaining $I_{l,max}$ has been proposed by prior research. Hu et al. (2014) compared two iterative algorithms; bisection search and levenberg–Marquardt algorithm. These solvers was necessary because the authors wanted to investigate the implication of updating the parameters within the prediction interval $k + l$, which leads to non-trivial explicit solution of the optimization problem. However, in this section we will assume constant parameters over the prediction interval i.e. R_0 Q_{tot} constant over the prediction horizon $k + l$. This assumption can be relaxed given a fairly small time interval $k + l$. In the coming sections three different power constraints is implemented and combined. These are based on the work of Sun et al.(2014).

8.1 Constrains for SoP calculations

8.1.1 SoC constrained power prediction

Design limits on SoC at time t_{k+l} can be set so that SoC limits are not violated:

$$0 \leqslant SoC_{lim}^{min} \leqslant SoC_{k+l} \leqslant SoC_{lim}^{max} \leqslant 1 \tag{8.1}$$

$SoC_{lim}^{min,max}$ should then be set in accordance to the accuracy of the SoC estimation, which extend the motivation of having an accurate SoC estimator. The JEKF formulation enables the use of uncertainty of the states through its covariance matrix P. Using the σ_{soc} uncertainty bound provided by the EKF in Chapter 6, the maximum current $I_{max,l}^{soc}$ that is allowed at timestep k to ensure with 95% probability that $SoC_{lim}^{min} \leqslant SoC_{k+l}$, can be found be rearranging the model equations:

$$I_{max,l}^{soc} = \hat{Q}_{tot} \cdot \frac{(soc_k - \sigma_{soc}) - soc_{min}}{\Delta t \cdot l} \tag{8.2}$$

By for example setting SoC_{lim}^{min} = 10%, current will be reduced when there is more than 5% probability that SoC$\leqslant$0.1.

8.1.2 Voltage constrained power prediction

Assuming an sufficiently small prediction interval l, the parameters can be assumed to be constant $\beta_{k+l} = \beta_k \in [t_k, t_{k+l}]$. This assumption can be relaxed as temperature, aging or SoC is close to constant over prediction interval. Given this assumption, the output voltage at sampling time $k+l$ can be written:

$$\begin{aligned} x_{k+l} &= Ax_{k+l-1} + Bu_{k+l-1} \\ y_{k+l} &= h(x_{k+l}, u_{k+l-1}) \end{aligned} \tag{8.3}$$

Assuming constant current over the prediction horizon, (8.3) can generally be written as:

$$x_{k+l} = A^l x_k + (\sum_{j=0}^{l-1} A^{(l-1-j)} B) u_k \tag{8.4}$$

To find the maximum current $I_{max,l}^{v}$ restricted by voltage limits v_{lim}^{min}, the output voltage v_{k+l} must equal v_{lim}^{min}. Reformulated with (8.4), (8.3) can be stated as:

$$V_{oc}(z_{k+l}) - v_k^{(rc1)} A_{1,1}^l - v_k^{(rc2)} A_{2,2}^l - I_{max,k}^{v}(R_{0,k} + (\sum_{i=1}^{2}(\sum_{j=0}^{l-1} A_{i,i}^{(l-1-j)}) B_{i,i})) - v_{lim}^{min} = 0 \tag{8.5}$$

where i is the index of the matrices A, B. Again, under the assumption that the time interval is small, $V_{oc}(z+l)$ can be approximated with a taylor expansion:

$$
\begin{aligned}
V_{oc}(z_{k+l}) &= V_{oc}(z_k + \Delta z) \\
&= V_{oc}(z_k + \frac{I^v_{max,l} \cdot \Delta t}{\hat{Q}_{tot}}) \\
&= V_{oc}(z_k) + \frac{I^v_{max,l} \cdot \Delta t}{\hat{Q}_{tot}} \cdot \frac{\delta V_{oc}(z_k)}{\delta z}\Big|_{z=z_k}
\end{aligned}
\tag{8.6}
$$

Inserting (8.6) in (8.5), and solving w.r.t. $I^v_{max,l}$, we can get the computational approach to predict peak current from the kth sampling time to the $(k+l)$th sampling time by:

$$
I^v_{max,k} = \frac{V_{oc}(z_k) - v_k^{(rc1)} A^l_{1,1} - v_k^{(rc2)} A^l_{2,2} - v^{min}_{lim}}{\frac{\Delta t}{Q_{tot}} \cdot \frac{\delta V_{oc}(z_k)}{\delta z}\Big|_{z=z_k} + R_{0,k} + (\sum_{i=1}^{2}(\sum_{j=0}^{l-1} A_{i,i}^{(l-1-j)})B_{i,i})}
\tag{8.7}
$$

8.1.3 Current constrained power prediction

The last constrains on the maximum current is explicitly expressed from the battery manufacture as the peak current limit $I^{I_{max}}_{lim}$:

$$
I^I_{max} \leqslant I^{max}_{lim}
\tag{8.8}
$$

which for this battery is I^{max}_{lim} = 20A.

Now that all the constraints for discharge current are calculated, the peak current limits with all limits enforced are calculated as

$$
I^{dis}_{max,k} = \min\,(I^I_{max},\ I^v_{max},\ I^z_{max})
\tag{8.9}
$$

where $I^{dis}_{max,k}$ is the maximum current with all limits enforced. Then the peak power capability estimation based on the dynamic model can be calculated as follows:

$$
P^{dis}_{max,k} = \min\,(P^{max}_{lim},\ V_{k+l},\ I^{dis}_{max})
\tag{8.10}
$$

where $P_{max,k}$ is the maximum power allowed at timestep k and P^{max}_{lim} is the peak power limit enforced by battery manufacture. Predicted terminal voltage at timestep k+l given maximum current I^{dis}_{max} can be expressed as:

$$
\begin{aligned}
V_{k+l} &= V_{oc}(z_k - \frac{i_{k+1} L \Delta t}{C_{nom}}) - V_{rc1,k} e^{\frac{-\delta t}{\tau_1}} - i_k(R_0 + R_1(1 - e^{\frac{-\Delta t}{\tau_1}}) \\
&= V_{oc}(z_k) - v_k^{(rc1)} A^l_{1,1} - v_k^{(rc2)} A^l_{2,2} - v^{min}_{lim} \\
&- I^{dis}_{max}(\frac{\Delta t}{C_{nom}} \cdot \frac{\Delta V_{oc}(z_k)}{\delta z}\Big|_{z=z_k} + R_0 + R_1(1 - A_{1,1}) \sum_{j=0}^{l-1} A_{i,i}^{(l-1-j)})B_{i,i})
\end{aligned}
\tag{8.11}
$$

then,

$$P_{max}^{dis} = \min\left(P_{max}, V_{k+l} \cdot I_{max}^{dis}\right) \tag{8.12}$$

8.2 Results

Using the data obtained from ROV operation, simulation of SoP can be seen in the figure below (Fig. 8.2). The current measurements are pack measurement. Assuming equal current draw of all cells in parallell gives $I_{meas,cell} = 1/8 I_{meas,pack}$. The voltage measurements are done for at each parallell connection. Assuming same voltage over parallel connection due to self balance in voltage $V_{meas,pcm} = V_{meas,cell}$. The limits of $V_{min}lim$ and soc_{lim}^{min} can be user-defined so to prelong both lifetime of the battery. Estimated P_{max}^{dis} (SoP), and which of the constrains are being used, are plotted together (Fig.8.2) for the different lower limits (Tab. **??**), as well as estimated maximum current I_{max}^{dis} (Fig.8.1).

Table 8.1: User-defined lower limits for SoC and voltage.

-	SoC_{lim}^{min}	$V_{lim}min$	I_{lim}^{max}	Time window l
Case 1	0.05	3.0V	20A	50
Case 2	0.05*	3.0V	20A	50
Case 3	0	3.0V	20A	50

*With uncertainty bounds on SoC constrain.

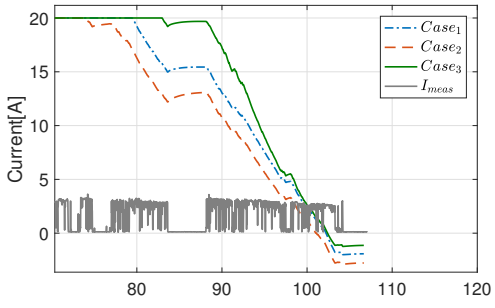

Figure 8.1: Maximum discharge current for limits case$_{1,2,3}$, and measured current.

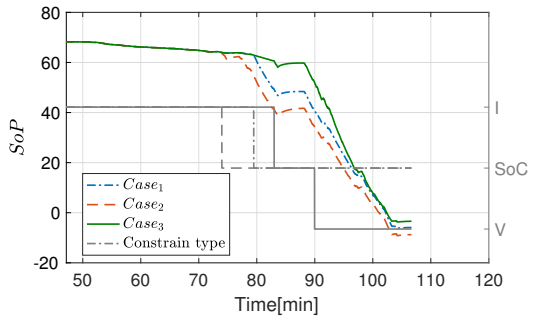

Figure 8.2: Maximum discharge power and the respective constraints for the case$_{1,2,3}$.

8.2.1 Pack power prediction

To extend this power prediction methodically to a battery pack, simple modification can be done to include the parallel and series connections. Letting $N_p = j$ cells in paralell within the PCM and

N_s = *i* PCM in the battery, the overall pack maximum discharge current and power, $I^{dis}_{max,p}$, $P^{dis}_{max,p}$ are found as:

$$I^{dis}_{max,p} = N_p \min\left(I^{I}_{max,i},\ \min_i I^{v}_{max,i},\ \min_i I^{z}_{max,i}\right) \tag{8.13}$$

$$P^{dis}_{max,p} = \min\left(N_s N_p P^{max}_{dis},\ \sum_{i=1}^{N_s} I^{dis}_{max,k} V^{(i)}_{k+l}\right) \tag{8.14}$$

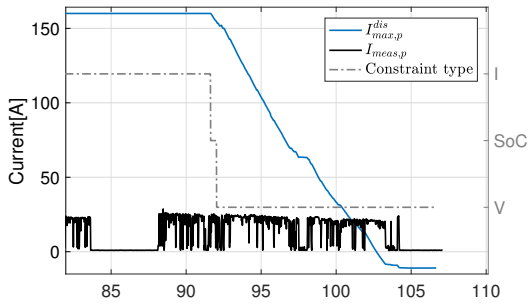

Figure 8.3: Maximum PCM discharge current based on limits $case_2$.

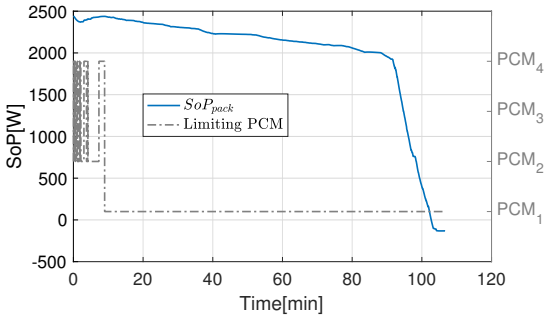

Figure 8.4: Maximum pack discharge power for limits case$_2$.

8.3 Power management using SoP estimates

The possibility of using SoP as an adapting control law is explored in this section. The adaptive SoP estimates can be used as a saturation parameter on the loads, and in that way easily implement a "limp-home" functionality. "Limp-home" functionality is a general description of a functionality that, when enabled, reduces the load. Generally, the benefit of load shedding for a battery is twofolded:

- Extend battery run-time: It is clear that lower loads leads to longer run-time, as less charge is removed from the battery. This relationship is however not linear. An extra benefit of saturating the load at low SoC is that the rate-varying discharge capacity Q_{rate} gets closer to total capacity Q_{tot}. This means that is possible extract more charge out of the same battery at lower rates.

- Safety against over-and under charge/discharge.

This functionality could be implemented with simple logic. By simple logic it is meant that the discharge rate is reduced by a predefined number as SoC approaches SoC^{dis}_{lim}. This is however far from optimal since it does not consider the current states of the battery. Instead, the adaptive SoP

predictor can be used in feedback, saturating the discharge rates. The schematics of this strategy is illustrated below.

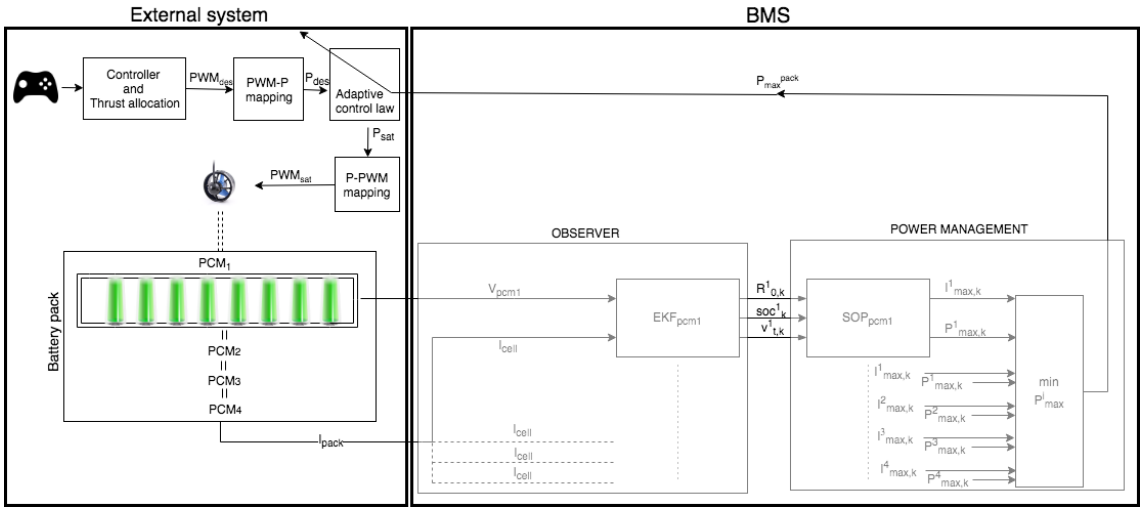

Figure 8.5: Illustration of BMS system flow.

The controller-and thrust allocation calculates the pwm signals pwm_{des} for the thrusters based on the desired actions of the operator. The voltage of the PCMs $\text{v}_{pcm,i}$ and pack current I_{pack} is then measured and communicated to the BMS. It is assumed equal distribution of current within each PCM. A JEKF then estimates the internal states and parameters for each PCM. $R_{0,k}, Q_{tot}, v_{rc1,k} v_{rc1,k}$ and soc_k is then given to the power management evaluator block, where SoP for each PCM is calculated based on defined limits $SoC_{lim}^{min}, I_{lim}^{max}$ and v_{lim}^{min}. From there, $P_{max,p}^{dis}$ is easily found taken the minimum of $P_{max,i}^{dis}$. This is communicated to the external system against the desired power P_{des}:

$$P_{sat} = \begin{cases} \{P_{max} r_i, P_{max} r_i, P_{max} r_i\}, & \text{if } P_{max,p} \leqslant \sum_{i=1}^{3} P_{des,i} \\ \{P_{des,1}, P_{des,2}, P_{des,i}\} & \text{else} \end{cases} \tag{8.15}$$

where r is power ratio between P(pwm):

$$r_i = \frac{P(pwm_i)}{\sum_{i=1}^{3} P(pwm_i)} \tag{8.16}$$

In order to keep the thrust ratio between the thrusters, it is necessary to map the desired pwm signal to desired power ($\text{pwm}_{des} \rightarrow \text{P}(\text{pwm}_{des}) \rightarrow \text{P}_{sat}$) instead of maximum power to maximum pwm signal ($\text{P}_{max,p} \rightarrow \text{pwm}_{max}$). This gives an additional mapping back to pwm-signal pwm_{sat} before going into the thrusters. For illustration, say $\text{P}_{max,p}$ = 100, pwm_{des} = {40 60 80} and P(pwm_{des}) = {60 100 180}. r(pwm) = {22 30 44} while r(P(pwm_{des})) = {0.17 0.29 0.53}. This is due to the nonlinear relationship between pwm-signal and power.

8.3.1 PWM-Current-Power mapping

The thrusters being used onboard Pioneer 1 is BlueRobotics t200. Performance data from BlueRobotics t200 are available online (BlueRobotics) and used for pwm-current-power mapping. The data A.1 is stored in computationally efficient look-up table. Linear interpolation is used for voltage values outside of 12-16V.

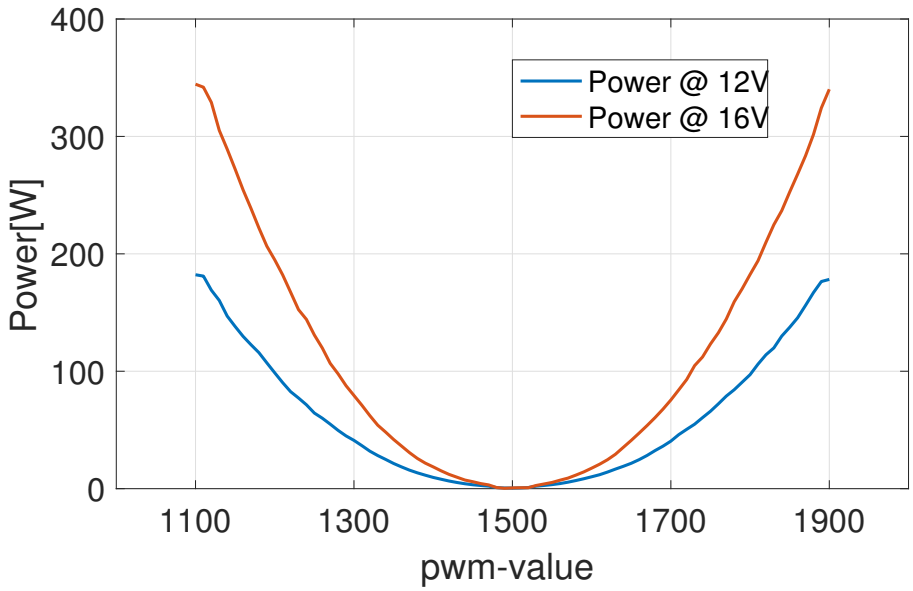

Figure 8.6: Mapping between power and pwm signal.

8.3.2 Results

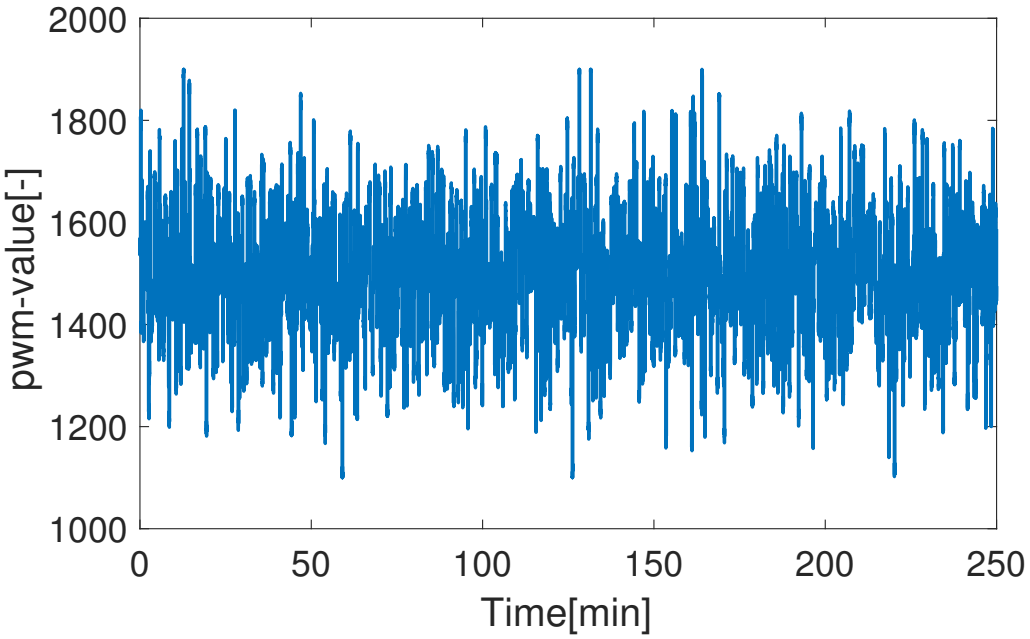

Figure 8.7: pwm-signal used as input to one thruster.

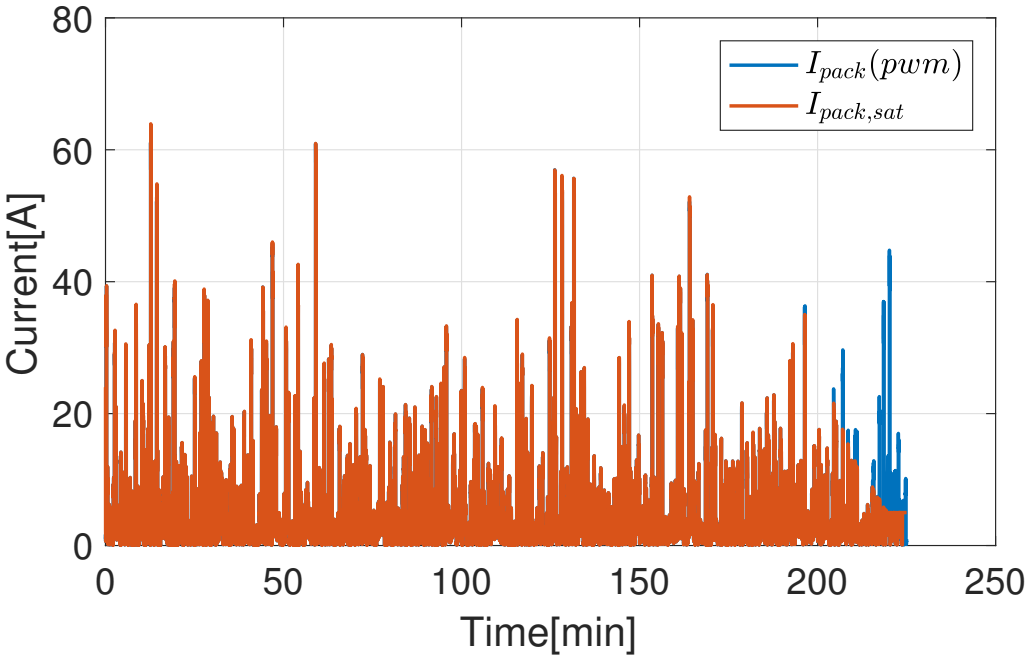

Figure 8.8: The effect of SoP feedback on discharge current.

The main input to the system is the pwm signal(Fig.8.7). First, $P_{max,p}$ is only limited by the maximum discharge rate (Fig. 8.9). At t = 200 min, the states of the battery are closing in on lower limits, and the maximum available power drops drastically. The pwm signals are then saturated

and the corresponding pack discharge current is reduced (Fig. 8.8), so to not violate the constraints and increase battery runtime. The increase in battery runtime can be seen on in resulting terminal voltage (Fig. 8.10). The extended battery time for this simulation was 258 seconds. The cost of this extended time is less available power. This is a feature that needs to be balanced properly to ensure that $P_{max,p}$ is large enough to properly operate ROV.

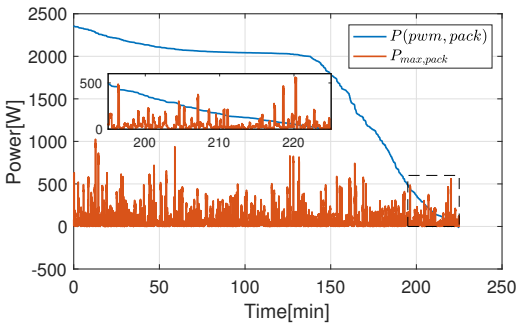

Figure 8.9: Maximum allowed pack discharge power and pack power from pwm-signal.

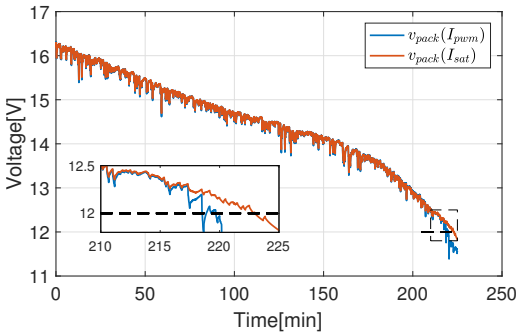

Figure 8.10: The effect of SoP feedback on terminal voltage.

For 8.7-8.10, the prediction horizon l = 100s. By tuning the prediction horizon, the tradeoff between extended battery runtime and available power can be tuned.

It is clear that longer prediction intervals gives lower maximum power estimates, and thereof also longer battery runtime. The accuracy of the predictions is depended on the length of the interval. Longer prediction intervals stretches the assumption that the parameters stays constant over the prediction horizon.

8.4 Summary

By defining limits on voltage, SoC and current, an estimate of maximum allowed discharge current can be found. This is what is referred to as SoP. Accuracy of SoP estimates are depended on the accuracy of estimated parameters in the JEKF and the length of the prediction horizon. Extending from a cell level to battery pack level was done in a straightforward manner, again assuming equal current distribution within each PCM.

A limp-home functionality using SoP estimates have been simulated. The prediction horizon of SoP estimates was increased to limit power at an earlier stage, by that prolonging battery life time. This adaptive control law saturates the pwm-signals from the operator to the thrusters, making the thrusters draw less power.

9

Conclusion

The operational profile for ROV has been characterized and its power consumers identified. It showed a highly dynamic current profile with maximum measured current draw of 39 A. Higher discharge currents (up to 69 A) can theoretically occur when the vertical thruster is activated and boost-function enabled.

The literature review of battery models revealed that either a 1RC or 2RC EEC model would provide the required level of accuracy, complexity of implementation and computational cost. The nonlinear least-square algorithm had problems fitting the data to 1RC model, so an extra RC cicrcuit was added. The estimation results showed the parameter's expected dependency on SoC. The effect of including this dependency and thereof also complexity was however not found necessary as the RMSE of output voltage only decreased $\approx$ 3.2mV. Accurate open-circuit-voltage function $v_oc(soc)$ has a bigger impact on both SoC and open-circuit voltage convergence, especially for biased current measurements. Simplification of OCV-SoC relationship should therefore be avoided. The open-loop model with $V_{oc,3}$ and constant parameters β fitted the voltage response from lab data well with RMSE of 17.5mV.

All of the proposed JEKF's performed well in terms of SoC estimation, even for biased current measurements, decreasing total capacity and noisy voltage measurements. For the assumed level of noise and bias on voltage and current sensors, capacity estimation, and therefore SoH estimation, it is not found necessary for reliable SoC estimates. This is due to the voltage-feedback mechanism of the EKF through the obtained OCV-SoC relationship. Should the OCV-SoC relationship change drastically over time, this conlussion might be questioned. If so, the observer must be tuned to rely more on the ah-counted a-priori SoC estimate. Capacity estimation would then be important to maintain accuracy of SoC estimates. According to literature review however, the OCV-SoC relationship is not heavily influenced by aging effects and reliable SoC estimates would be obtained without capacity estimation.

SoH estimates is however useful in itself giving the operator an indication of when the battery is due for replacement. For SoH estimation through total capacity estimation, a separate linear

Kalman filter running only at end of discharge cycle is suggested. This might be justified because of the operational profile of the ROV, which utilizes close to full SoC range. Since total capacity is such a slowly varying process, there is little reason to estimate it every timestep i.e. every second. The JEKF was in general extremely sensitive to tuning of Q and P_0, especially to ensure reasonable results for parameters estimation. This is an additional argument for seperation of Q_{tot} estimation.

A novel approach of using SoP as a model-predictive control law saturating maximum power of the battery has been explored. While the accuracy of the SoP estimates are not validated, the concept showed great potential. This is a feature that should be considered implemented independently of chosen SoC/SoH estimator.

The findings can be summarized in the following keypoints:

- To solely operate a battery pack safely, simpler methods will suffice. But to operate the battery pack efficiently and aggressively, accurate SoC are needed.
- Overall, all Joint Extended Kalman Filters showed great robustness and performance.
- For State-of-Charge (SoC) estimation only, the benefit of parameter estimation is low, even with biased current measurements.
- SoC performance is slightly improved adding total capacity estimation.
- Total capacity estimation was used as a measure of State-of-Health (SoH), which gave reasonable results for ideal measurements.
- The sensitive of capacity on voltage measurements is low, so adding bias estimation is necessary for highly biased current measurements.
- The concept of using State-of-Power (Sop) estimates for gradual load-shedding was tested and should be implemented independently of choice of SoC- and SoH estimator.

10

Future work

Lack of equipment and time made extensive validation of temperature and aging effects impossible. Data-gathering from operations was time consuming and limited due to multiple malfunctioning of the ROVs. Even though the end solution with combined SoC, SoH and SoP estimation showed great potential, more extensive validation is necessary to ensure precision for more extreme situations. A future direction might be summarized as:

- Further evaluation of robustness by more extensive data gathering. Data from lab-test on various temperatures from a fresh and aged cell would aid in the way of separating the two effects, and therefore the conclusion on robustness. Had there been less malfunctioning with the ROVs, a more systematic approach of data gathering from operations could be done. This would be preferable to better map out different driving profiles. Statistical tools could then be used to categorize these profiles and maybe conclude on a standard driving profile for ROV application.
- The choice of BMS hardware and communication with already existing Arduino and Raspberry Pi, and evaluate the computational cost of the JEKF observer compared to the choice of hardware. The already installed microprocessors might be overloaded, so a separate microprocessor for BMS functions only might be necessary.
- Implement of the algorithms on an embedded system and final validation.

Bibliography

D. Andrea. *Battery Management Systems for Large Lithium-Ion Battery Packs*. Artech House, 2010.

F. Baronti, Fantechi G., E. Leonardi, R. Roncella, and R. Saletti. Electrochemical and thermal characterization of battery modules commensurate with electric vehicle integration. *Annual Conference on IEEE Industrial Electronics Society*, pages 2329–2333, 2010.

Battery University. Types of battery cells, 2016. URL http://batteryuniversity.com/learn/article/types$_o f_b attery_c ells$.

BlueRobotics. Performance charts t200. Technical report. Accessed: 2017-14-05.

I. Buchmann. Science and applications of mixed conductors for lithium batteries, 2011. URL http://batteryuniversity.com/learn/article/types$_o f_l ithium_i on$.

C.C. Chan, E.W.C. Lo, and S. Weixiang. The available capacity computation model based on artificial neural network for lead–acid batteries in electric vehicles. *Journal of Power Sources*, 2000.

N.A Chaturvedi, Christensen.J, J. Ahmed, R. Findeisen, and A. Kojic. Optimal charging strategies in lithium-ion battery. *American Control Conference*, 2011.

F. Codecà, S. M. Savaresi, and V. Manzoni. The mix estimation algorithm for battery state-of-charge estimator- analysis of the sensitivity to measurement errors. *American Control Conference*, 2011.

D.D. Dominico, Y. Creff, E. Prada, P. Duchene, J. Bernard, and V. Sauvant-Moynot. A review of approaches for the design of li-ion bms estimation functions. *Oil Gas Science and Technology - IFP Energies nouvelles*, 2013.

B. Fridholm, M. Nilsson, and T. Wik. Robustness comparison of battery state of charge observers for automotive applications. 2014.

L. Gao, S. Lie, and R.A Dougal. Dynamic lithium-ion battery model for system simulation. *IEEE Transactions on Components and Packaging Technologies*, pages 495–505, 2002.

Garche, J. et.al. Encyclopedia of electrochemical power sources. 2009.

X. Hu, S. Li, and H. Penga. A comparative study of equivalent circuit models for li-ion batteries. *Journal of Power Sources*, 198:359–367, 2012.

X. Hu, R. Xiong, and B. Egardt. Model-based dynamic power assessment of lithium-ion batteries considering different operating conditions. *IEEE Transactions on Industrial Informatics*, pages 1948–1959, 2014.

T. Huria, M. Ceraolo, J. Gazzarri, and R. Jackey. Simplified extended kalman filter observer for soc estimation of commercial power-oriented lfp lithium battery cells. *SAE Technical Paper*, 2013.

L. Lam, P. Bauer, and Kelder E. Electrochemical and thermal characterization of battery modules commensurate with electric vehicle integration. *Telecommunications Energy Conference (INTELEC)*, pages 1–9, 2011.

LG LG chem: Mobile battery division. Technical information of 18650hg2 (3.0ah). Technical report, LG, 2016.

D. Linden and T. B Reddy. Ch 14: Lithium-ion batteries. In *Handbook of Batteries, 3rd edition*. McGraw-Hill, 2002.

C. Messina. Lithium-ion cylindrical cells vs. prismatic cells. http://www.relionbattery.com/blog/lithium-cells-should-i-go-cylindrical-or-prismatic, 2015.

J. Newman and W. Tiedemann. Porous-electrode theory with battery applications. *AIChE Journal*, 21:25–41, 1975.

G.L Plett. Extended kalman filtering for battery management systems of lipb-based hev battery packs pt. 1-3. *Journal of Power Sources*, 134.

G.L. Plett. *Battery Management Systems: Equivalent-Circuit Methods*. Artech House, 2016.

A. Seaman, T.S Dao, and J. McPhee. A survey of mathematics-based equivalent-circuit and electrochemical battery models for hybrid and electric vehicle simulation. *Journal of Power Sources*, 256:410–423, 2014.

Dan Simon. *Optimal State Estimation: Kalman, H, and Nonlinear Approaches*. John Wiley Sons, inc, 2006.

P. Singh, C. Fennie jr., and D. Reisner. Fuzzy logic modelling of state-of-charge and available capacity of nickel/metal hydride batteries. *Journal of Power Sources*, 2004.

V.R Subramanian, V. Boovaragavan, and V.D Diwakar. Toward real-time simulation of physics based lithium-ion battery models. *Electrochem. Solid-State Lett.*, 10:A255–A260, 2009.

F. Sun, R. Xiong, and H. He.

A. Vasebi, M. Partovibakhsh, and S.T.B Mohammad. A novel combined battery model for state-of-charge estimation in lead-acid batteries based on extended kalman filter for hybrid electric vehicle applications. *Journal of Power Sources*, 174:30–40, 2007.

Mark W. Verbrugge and Robert S. Conell. Electrochemical and thermal characterization of battery modules commensurate with electric vehicle integration. *Journal of The Electrochemical Society*, 149:495–505, 2002.

G. Walder, C. Campestrini, S. Kohlmeier, M Lienkamp, and A. Jossen. Functionality and behaviour of an dual kalman filter implemented on a modular battery-management-system.

Hua X., S. Li, Peng H., and Sun F. Robustness analysis of state-of-charge estimation methods for two types of li-ion batteries. *Journal of Power Sources*, page 209–219, 2012.

J. Zhang, S. H. Ci, and Sharif M. Alahmad. An enhanced circuit-based model for single-cell battery. *Applied Power Electronics Conference and Exposition (APEC)*, pages 672–675, 2010.

S. Zhao and S. R. Duncan.

Y. Zoua, X. Hub, M. Hongmin, and S.E Lic. Combined state of charge and state of health estimation over lithium-ion battery cell cycle lifespan for electric vehicles. *Journal of Power Sources*, 273:793–803, 2015.

A

Appendix 1

A.1 Thruster data from BlueRobitics

Table A.1: Performance data on thrusters (BlueRobotics) -

@12V			@16V			
PWM	Power[W]	current[A]	Thrust[N]	Power[W]	current[A]	Thrust[N]
1100.0	182.2	15.4	-6.6	344.5	21.5	-9.0
1110.0	181.0	15.2	-6.6	341.9	21.4	-8.9
1120.0	169.1	14.2	-6.3	329.0	20.6	-8.7
1130.0	160.3	13.5	-6.1	305.1	19.1	-8.4
1140.0	147.0	12.4	-5.8	289.1	18.1	-8.2
1150.0	138.1	11.7	-5.6	272.2	17.0	-8.0
1160.0	129.7	10.9	-5.2	254.6	15.9	-7.6
1170.0	122.6	10.3	-5.2	238.7	14.9	-7.3
1180.0	115.9	9.7	-5.0	222.1	13.9	-7.0
1190.0	107.2	9.0	-4.8	206.6	12.9	-6.7
1200.0	98.7	8.3	-4.3	194.9	12.2	-6.4
1210.0	90.3	7.6	-4.0	182.1	11.4	-6.2
1220.0	82.6	6.9	-3.9	167.4	10.5	-6.0
1230.0	77.2	6.5	-3.7	152.5	9.5	-5.6
1240.0	71.4	6.0	-3.5	144.2	9.0	-5.2
1250.0	64.4	5.4	-3.2	130.9	8.2	-5.0
1260.0	60.0	5.0	-3.1	119.8	7.5	-4.8
1270.0	55.0	4.6	-2.9	106.7	6.7	-4.4
1280.0	49.6	4.2	-2.7	97.8	6.1	-4.2
1290.0	44.9	3.8	-2.5	87.7	5.5	-3.9
1300.0	41.1	3.5	-2.4	79.4	5.0	-3.6
1310.0	36.6	3.1	-2.2	71.0	4.4	-3.3

1320.0	32.0	2.7	-2.0	62.2	3.9	-2.9
1330.0	28.2	2.4	-1.8	54.1	3.4	-2.7
1340.0	24.9	2.1	-1.7	48.2	3.0	-2.5
1350.0	21.5	1.8	-1.5	41.9	2.6	-2.3
1360.0	18.5	1.6	-1.3	36.3	2.3	-2.0
1370.0	15.8	1.3	-1.1	30.7	1.9	-1.7
1380.0	13.5	1.1	-1.0	25.8	1.6	-1.5
1390.0	11.5	1.0	-0.8	21.8	1.4	-1.4
1400.0	9.6	0.8	-0.7	18.6	1.2	-1.1
1410.0	8.0	0.7	-0.6	15.2	0.9	-1.0
1420.0	6.5	0.6	-0.5	12.2	0.8	-0.8
1430.0	5.3	0.4	-0.4	9.8	0.6	-0.6
1440.0	4.2	0.3	-0.3	7.4	0.5	-0.4
1450.0	3.3	0.3	-0.2	5.9	0.4	-0.2
1460.0	2.7	0.2	-0.1	4.3	0.3	-0.1
1470.0	2.2	0.2	-0.1	3.2	0.2	-0.1
1480.0	0.9	0.1	0.0	1.0	0.1	0.0
1490.0	0.6	0.1	0.0	0.3	0.0	0.0
1500.0	0.5	0.0	0.0	0.6	0.0	0.0
1510.0	0.6	0.1	0.0	0.8	0.1	0.0
1520.0	0.9	0.1	0.0	0.8	0.1	0.0
1530.0	2.1	0.2	0.1	2.7	0.2	0.1
1540.0	2.7	0.2	0.2	4.0	0.2	0.2
1550.0	3.5	0.3	0.3	5.3	0.3	0.4
1560.0	4.3	0.4	0.4	7.2	0.5	0.6
1570.0	5.5	0.5	0.5	9.0	0.6	0.8
1580.0	6.9	0.6	0.6	11.5	0.7	0.9
1590.0	8.4	0.7	0.8	14.2	0.9	1.1
1600.0	10.1	0.8	0.9	17.4	1.1	1.4
1610.0	11.9	1.0	1.0	20.8	1.3	1.6
1620.0	14.1	1.2	1.2	24.6	1.5	1.9
1630.0	16.7	1.4	1.4	29.3	1.8	2.1
1640.0	19.0	1.6	1.5	35.2	2.2	2.4
1650.0	21.6	1.8	1.6	41.1	2.6	2.8
1660.0	24.7	2.1	1.9	47.4	3.0	3.1
1670.0	28.3	2.4	2.1	53.8	3.4	3.4

1680.0	32.4	2.7	2.3	60.5	3.8	3.7
1690.0	36.2	3.0	2.5	67.7	4.2	4.0
1700.0	40.5	3.4	2.8	75.5	4.7	4.3
1710.0	46.0	3.9	3.1	84.2	5.3	4.6
1720.0	50.5	4.2	3.3	93.0	5.8	4.9
1730.0	54.9	4.6	3.5	104.8	6.5	5.3
1740.0	60.5	5.1	3.9	112.2	7.0	5.6
1750.0	65.9	5.6	4.1	123.2	7.7	5.9
1760.0	72.2	6.1	4.3	132.8	8.3	6.2
1770.0	78.8	6.7	4.7	144.5	9.0	6.7
1780.0	84.3	7.1	4.8	159.2	9.9	7.0
1790.0	90.7	7.7	5.0	170.2	10.6	7.4
1800.0	97.1	8.2	5.2	182.4	11.4	7.6
1810.0	106.0	8.9	5.5	194.1	12.1	7.7
1820.0	114.0	9.6	5.9	209.8	13.1	8.3
1830.0	119.9	10.1	6.1	224.8	14.1	8.7
1840.0	130.0	10.9	6.5	236.8	14.8	8.8
1850.0	137.4	11.6	6.5	252.6	15.8	9.2
1860.0	145.5	12.2	6.6	267.8	16.7	9.7
1870.0	156.1	13.1	7.0	283.5	17.7	10.1
1880.0	167.0	14.0	7.4	301.6	18.9	10.6
1890.0	176.4	14.8	7.7	324.3	20.3	10.8
1900.0	178.2	14.9	7.8	340.2	21.3	11.2

Table A.1: MyTableCaption

A.2 Curvefitting constants for OCV-functions

Table A.2: Constants k_i from $V_{oc,i}$ curvefitting:

-	k_0	k_1	k_2	k_3	k_4	k_5	k_6	k_7	k_8
$V_{oc,1}$	0.011	3.131	-	-	-	-	-	-	-
$V_{oc,2}$	3.314	0.0023	-0.73	-0.1619	-	-	-	-	-
$V_{oc,3}$	3.13	-2.3e-07	4.591	0.098	0.032	-15.82	26.95	-19.9	5.04

B

Appendix B1: Observability of Nonlinear System

Consider a general system:

$$\dot{x} = f(x) + \sum_{i=1}^{m} u_i g(x) \tag{B.1}$$

$$y = h(x) \tag{B.2}$$

Suppose that h(x) = [h1(x) . . . hp(x)]^T is a p- dimensional vector function on X and its j'th component h_j(x) is a real-valued smooth function. Denote the gradient of h_j as dh_j , i.e.,

$$dh_j = \begin{bmatrix} \frac{\delta h_j}{\delta x_1} & \frac{\delta h_j}{\delta x_2} & \dots & \frac{\delta h_j}{\delta x_n} \end{bmatrix} \tag{B.3}$$

then the Lie derivative of h_j is defined by

$$L_f h_j = dh_j \cdot f = \sum_{i=1}^{n} f_i \frac{\delta h_j}{x_i} \tag{B.4}$$

where $f(x) = \begin{bmatrix} f_1(x) & \dots & f_n(x) \end{bmatrix}^T$ The following theorem (Zhao and Duncan) gives the corresponding rank test for nonlinear system:

Theorem 1 *System B.2 is locally observable at $x_0 \in X$ if there are n linearly independent rows in the set*

$$(dL_{zs} \quad L_{zs}1 \quad \dots L_{z1}h_j)(x0) \tag{B.5}$$

where $s > 0, z_k \in \{f, \quad g_1 \quad \dots, g_m\}$ for k = 1,...s, j = 1,...,p and with s = 0, the expression is defined as equivalent to $dh_j(x_0)$.

That is, the system is locally observable at x_0 if the rank condition is satisfied:

$$rank\mathcal{O} = rank \left(\begin{bmatrix} dh \\ dL_f h \\ dL_g h \\ dL_f^2 h \\ dL_g^2 h \\ dL_g L_f h \\ \vdots \end{bmatrix} \right) = n \tag{B.6}$$

C

Appendix C1: Simulink Model

C.1 Full model

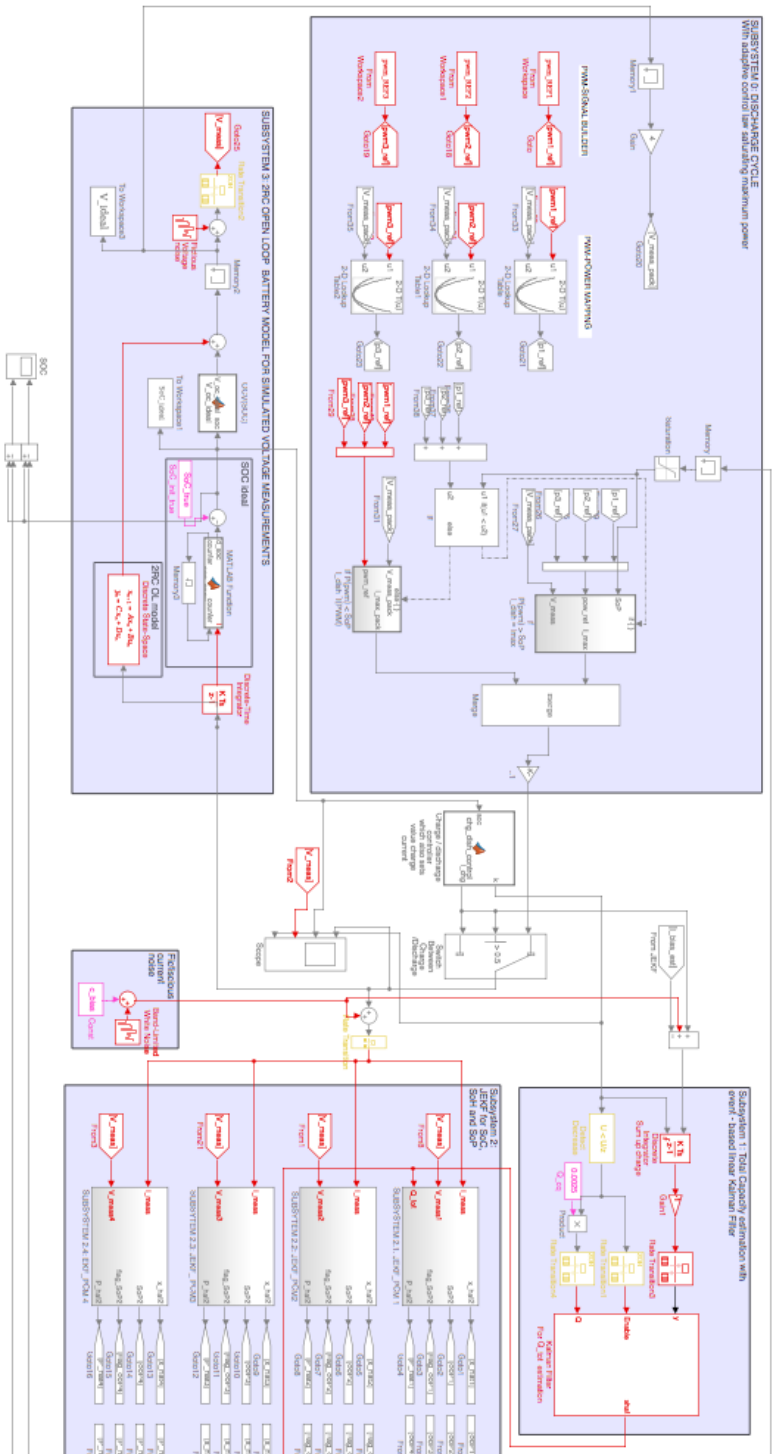

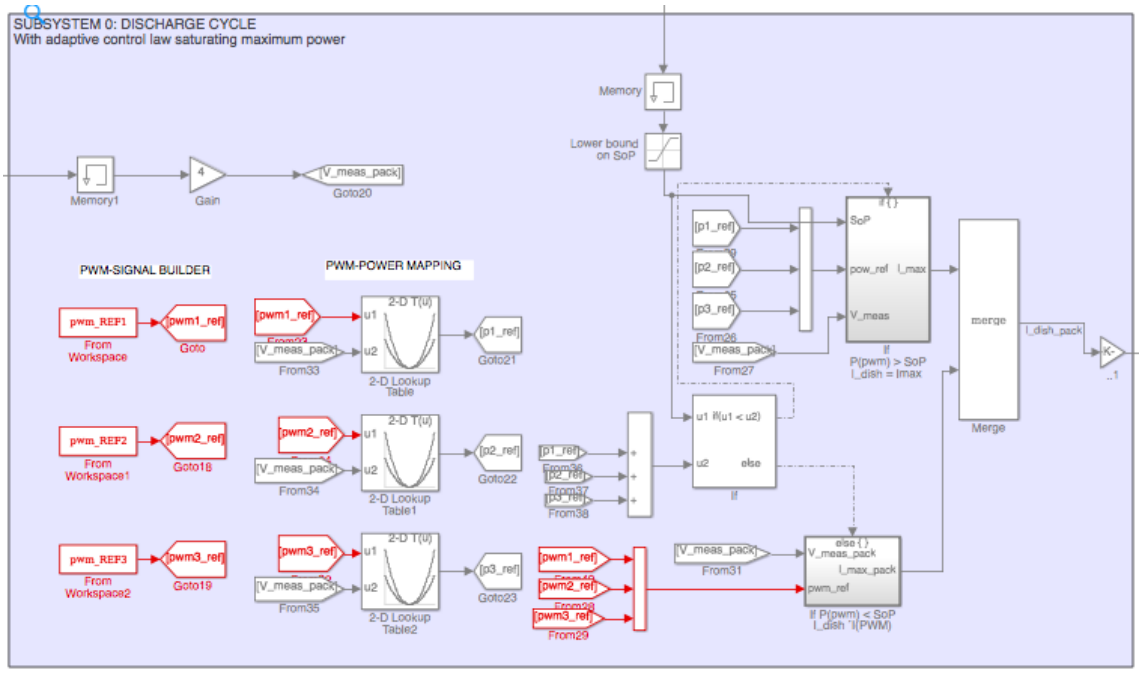

Figure C.2: Subsystem 0.

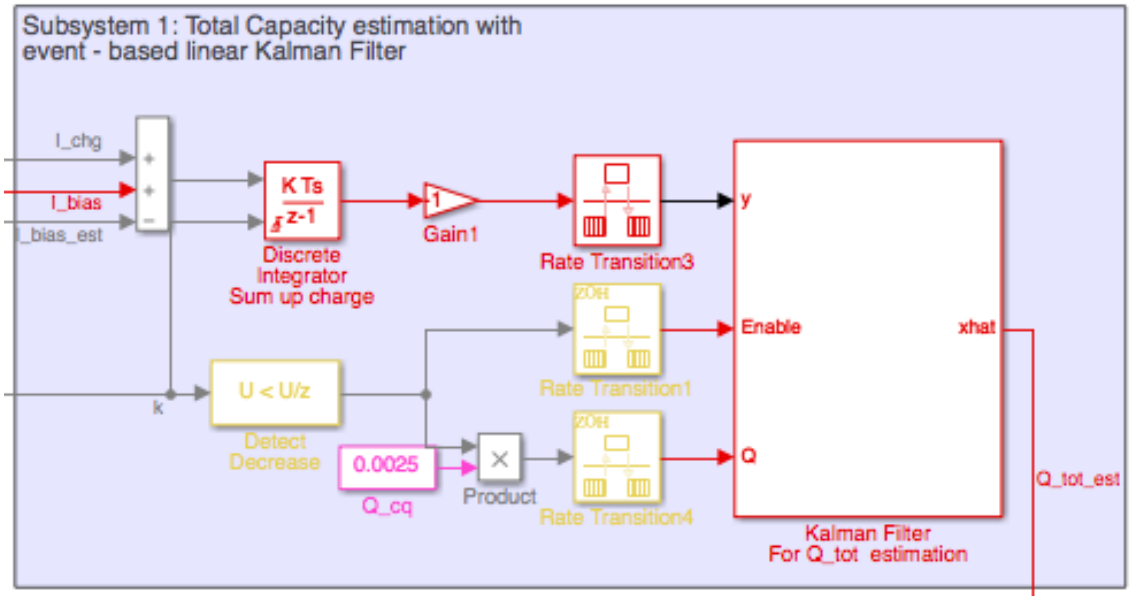

Figure C.3: Subsystem 1.

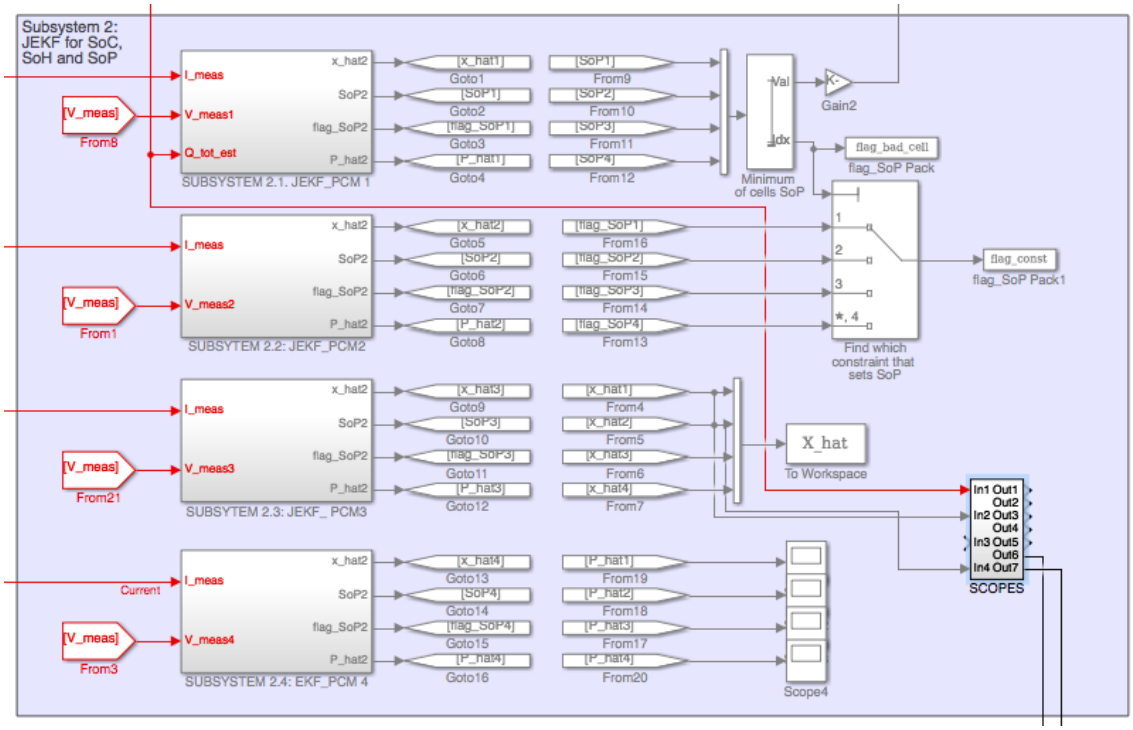

Figure C.4: Subsystem 2.

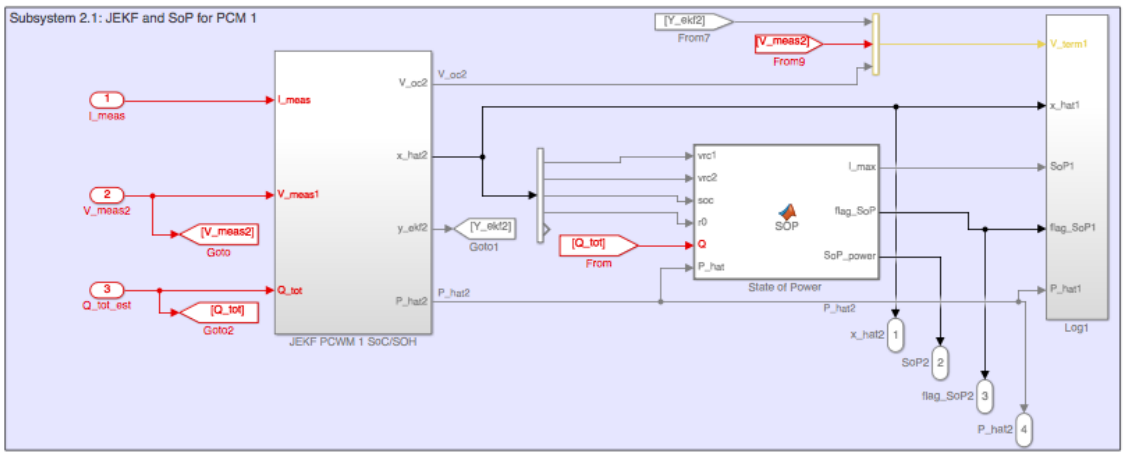

Figure C.5: Subsystem 4.